STUDIES IN MOLECULAR RECOGNITION: HYDROPHOBIC BINDING OF WATER-SOLUBLE GUESTS BY HIGH SYMMETRY, CHIRAL HOSTS

Thesis by

Timothy Jon Shepodd

In Partial Fulfillment of the Requirements

for the Degree of

Doctor of Philosophy

California Institute of Technology

Pasadena, California

1988

(Submitted February 4, 1988)

To my family.

Acknowledgements

Many people deserve thanks for their special friendship during my stay at Caltech. The members of the Dougherty group/Killer Potatoes, are a wonderful group of scientists/softball players. This thesis would not exist without the teamwork provided by all of you. Special thanks go to Mike Petti, who was a partner in this project from its conception; to Frank Coms, who shared many afternoons at trackside; to Dave Stauffer who proofread this thesis; and to Dennis Dougherty, who was always a patient, supportive advisor and friend.

I must acknowledge the incredible, if somewhat unorthodox, Shepodd family and Lisa for their unfailing love and support. Thanks also to Dave Wheeler for many hours of assistance with the special NMR experiments, and to Eric Ginsburg for sharing many long runs up into the mountains.

Finally, I must thank the National Institutes of Health, the W. R. Grace Fellowship program, and Howard Scrap Metal Co. for financial support.

Abstract

A new class of high-symmetry, water-soluble receptors has been synthesized. The enantiomerically pure hosts are D_2-symmetric and are synthesized in 8 steps with an overall yield of 5-10%. An asymmetric Diels-Alder reaction between di-(+)-menthyl fumarate and 2,6-di-*t*-butyldimethylsiloxyanthracene leads to two diastereomeric Diels-Alder adducts that are elaborated to the key intermediates: (+)- and (–)-2,6-dihydroxy-11,12-dicarbomethoxy-9,10-ethenoanthracene. A number of hosts are synthesized from these intermediates when they are connected by variable linker units. These hosts possess chiral cavities (receptor sites) surrounded by an array of substituted aromatic rings.

The ability of these hosts to complex water-soluble guests with different sizes, shapes, and degrees of preorganization has been quantified by NMR. The electron-rich hosts have a general affinity for electron-deficient guests. Hosts **P** and **M** show a moderate hydrophobic-type attraction towards a variety of aromatic and aliphatic guests (3-4 kcal/mol). Host **P** shows an added attraction towards trimethylammonium (TMA) substituted guests. In almost all cases studied, NMR-shift patterns indicate that when the host-guest complex forms, the polar TMA group lies deepest within the electron-rich, yet hydrophobic, receptor.

Hosts **P** and **M** have a strong attraction towards adamantyltrimethylammonium iodide (ATMA). $\mathbf{P}_R$ and $\mathbf{P}_S$ have binding

affinities of 6.6±0.2 kcal/mol with ATMA and bind the guest, encapsulated within the receptor site, in one guest orientation. $\mathbf{M}_R$ and $\mathbf{M}_S$ have binding affinities of 5.5±0.2 kcal/mol with ATMA and bind the guest in a non-specific fashion, yet they demonstrate a preferred attraction towards the TMA group of the guest.

Aromatic-linked hosts $\mathbf{P}_R$, $\mathbf{P}_S$, $\mathbf{M}_R$ and $\mathbf{M}_S$ show an enhanced ion-dipole attraction towards charged quinolinium-type, flat aromatic guests as compared to neutral ones ($\mathbf{P} \approx 1$ kcal/mol and $\mathbf{M} \approx 2$ kcal/mol). Host **C**, with aliphatic linkers, does not experience an enhanced attraction to the charged flat guests.

Hosts $\mathbf{P}_R$ and $\mathbf{P}_S$ demonstrate enantioselective binding with certain guests. For one case, a simple model for the cause of the enantioselectivity is presented.

List of tables: Page

List of schemes: Page

List of figures: Page

List of graphs: Page

Nomenclature

The chiral compounds in this thesis are denoted in one of two ways. The two enantiomers of compound **X** are listed as **(+)-X** and **(–)-X** according to the sign of their optical rotations, or where appropriate, the enantiomers are identified as $\mathbf{X}_R$ and $\mathbf{X}_S$ where the *R* and *S* refer to the absolute configuration at the bridgehead carbons (9,10-carbons). Racemic mixtures are identified as **±X**, and *meso* compounds are identified as $\mathbf{X}_{meso}$. A simple **X** is used when a general reference to the set of different **X** molecules is needed.

CHAPTER 1

Introduction and Background

The study of intermolecular interactions is widespread throughout organic chemistry.[1,2] Molecules interact continuously. Understanding the forces involved when molecules approach each other is a vital part of predicting everything from the simplest to the most complex reactions. One area of current interest is the study of molecular recognition, specifically molecular recognition in water.[3] Molecular recognition is the basis for information transfer in chemical systems. As one molecule interacts with another in a non-random fashion, specific information can be transferred or specific chemical reactions can occur. The forces that drive molecular recognition are fundamentally important. The results of many recognition events lead to the highly organized (localized low entropy) systems that make up our present surroundings.

This thesis describes our work, which consists of synthesizing a new class of water-soluble macrocyclic host molecules having hydrophobic receptor sites, and studying the ability of these hosts to bind and orient various guest molecules within their cavities. Our goal is to understand the details of the binding event — the details of molecular recognition in water. An idealized host-guest system and the equations that describe the host-guest equilibrium are shown in Figure 1.1.

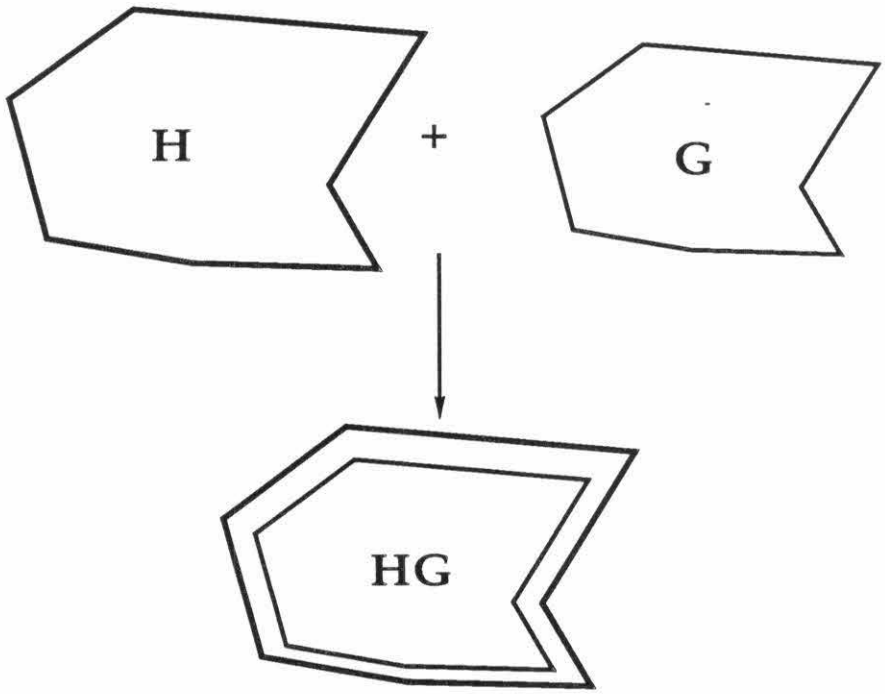

Figure 1.1: A schematic of host (H) and guest (G) coming together to form host-guest complex (HG).
The association constant (K_a) is defined as

$$K_a = \frac{[HG]}{[H] \cdot [G]}$$

The binding affinity – $\Delta G°$ is defined as

$$-\Delta G° = RT \cdot \ln K_a$$

Exactly how and why does the guest enter the binding cavity or receptor region of the host? How strongly is the guest held and what orientation does the host impose or the guest prefer? Eventually, can we thoroughly understand the forces that control these interactions and go on to design systems with predictable binding behavior? These are the questions we address.

One familiar example of host-guest chemistry is enzymatic chemistry in living systems. Often, studies in molecular recognition are directed towards the syntheses of artificial enzymes.[4] Enzymes recognize substrates in their receptor sites where specific transformations occur. Many important forces drive these binding events, including opposite charge (electrostatic), charge-dipole, hydrogen-bond, π-stacking and van der Waals attractions, as well as free energy changes due to the net differences in the solvent environment that result upon binding. Among these, the strong attractive forces between opposite charges and strong dipoles are best understood. Designing receptors with charges positioned to maximize strong electrostatic interactions complementary to those of a given guest is conceptually simple. Early work on systems that bind ions established the field of host-guest chemistry.[5] Cram and others[6] made crown ethers,

molecules with rings of oxygen atoms that are used as effective and selective hosts. Crown ethers bind water-soluble cationic guests in organic solvents within the rings of high electron density created by the oxygen lone pairs. Much thorough experimentation and many innovative syntheses have created a good understanding of host-guest systems driven by strong electronic attractions. In contrast, the weaker forces, which cause binding in water, are much less understood.

The binding event in water involves the host presenting a new environment to the guest that is more thermodynamically favorable than that of the bulk aqueous medium. Water is a unique solvent, and interacts with solute molecules in many ways. If water is reorganized upon binding, then the free energy of the system changes. Classic hydrophobic binding is the result of hosts and guests seeking out environments more favorable than that of the water. The other weak attractive forces mentioned above also collectively contribute to the driving force for binding. Optimizing exactly the design features that maximize hydrophobic host-guest interactions requires that we look at the details of the binding event.

We must consider *all* intermolecular interactions, especially weak ones, because as a host receptor site binds a guest of limited water solubility,

attractions are built up from a combination of sterically enforced dipole and induced-dipole interactions as well as changes in the solvation shell surrounding the host and guest. Electrostatic and strong dipole attractions are also important where they exist. Single instances of these stronger and longer-ranged electrostatic forces often have bigger influences upon the free energy of binding than a collection of weaker forces.[3]

A tight fit between host and guest is also important, because selectivity increases as the steric demands necessary for the guest to gain the benefits of residing in the binding site become more strict. In theory, for idealized hydrophobic binding, a guest that fits tightly within a host binds strongly when weak van der Waals contacts are maximized and when highly structured water that is organized around the hydrophobic surfaces of the guest and host is displaced.

In practice, a variety of other, stronger forces such as π-stacking and dipolar interactions also influence hydrophobic binding. When we understand the potential attractive and repulsive forces involved with binding, we will be closer to accurately predicting strong binding affinities. As the research in this group proceeds, we hope to sort out and understand more of the details necessary to design efficient, selective receptors for

specific guests.

Many researchers have observed that water-soluble hosts with hydrophobic cavities can bind other organic molecules as guests within these cavities. Cyclodextrins, commercially available water-soluble cyclic oligosaccharides[7], have been shown to effectively bind hydrophobic guests within their non-polar cavities. Much elegant work has been done with cyclodextrins, including interesting enzyme mimics made by Breslow[8,9] and others.[10,11] Cyclodextrins are convenient as hydrophobic receptors; however, they are only available in three sizes (α, β and γ; 6, 7 and 8 saccharide units) or synthetically modified versions thereof.[12] We concentrate on studies involving fully synthetic hosts possessing cavities that can be modified with fewer restrictions. We feel strongly that rational host syntheses lead to greater flexibility during subsequent generations of improved host design.

Many techniques have been used to explore the binding event, but proof of hydrophobic guest inclusion by a water-soluble host was given by Koga.[13] The crystal structure of durene as a guest with Koga's fully synthetic host (Figure 1.2) was solved and showed the durene to be at the center of the receptor site. Most host-guest crystals are host-guest alternate, not inclusion

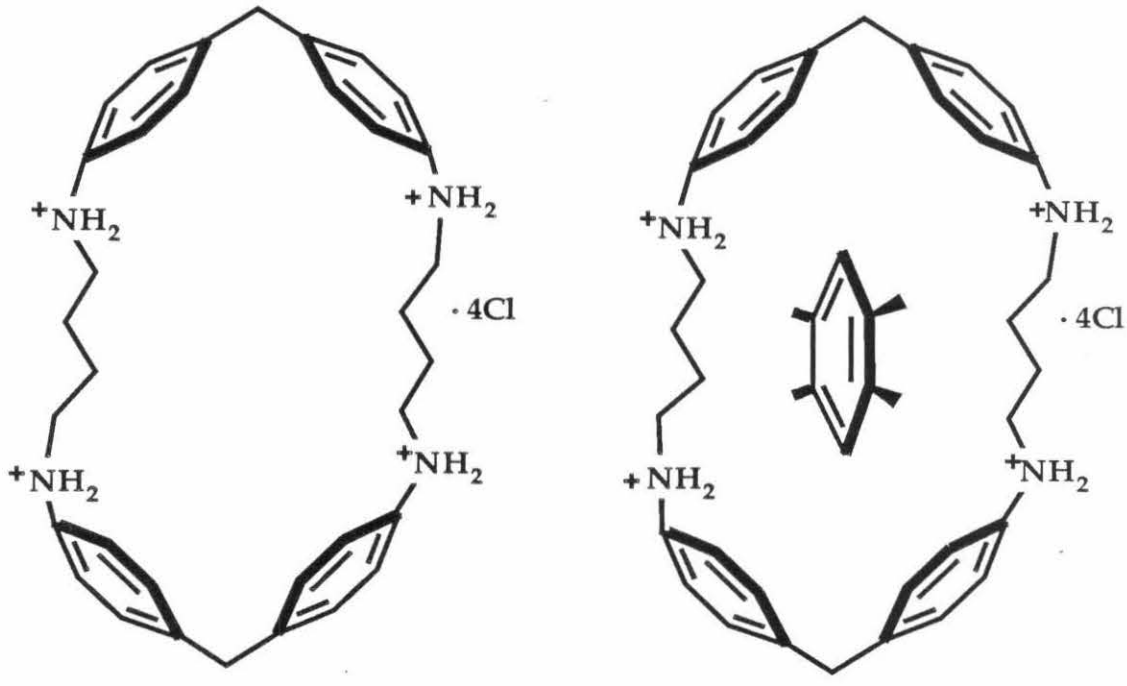

Figure 1.2: A schematic of Koga's macrocycle (left), and of the macrocycle·durene complex (right). The durene guest lies in the binding plane which splits each of the two diphenylmethane units.

complexes.[14,15] Other inclusion complexes crystallize from organic solvents,[16,17] but not from water. Koga's result unambiguously proves that a synthetic host can extract a hydrophobic guest out of bulk water into a specific position within its receptor cavity.

Koga made many significant contributions to the field. He studied the effects of varying host structure upon K_a.[18,19] Binding studies with fluorescent guests sodium 1-anilinonaphthalene-8-sulfonate (ANS) and sodium 2-*p*-toluidinylnaphthalene-6-sulfonate (TNS), as well as with a variety of substituted naphthalenes and other guests showed distinct trends. Hosts with more rigid and larger hydrophobic surfaces (*trans*-1,4-dimethylenecyclohexyl > $(CH_2)_8$ > $(CH_2)_6$) formed more stable host-guest complexes.[20] Koga ascribed this to the increased hydrophobic nature of the receptor sites. Other experiments, using NMR,[21] demonstrated specific guest orientations within the receptor site. For aromatic guests, the observed orientations are similar to that found in the crystal structure mentioned above. Koga argued that these specific shift patterns rule out random, fluid, micellar type binding.[21] Negatively charged aromatic guests (aryl sulfonates) have K_a's of 10^3–10^5. Only weak unquantified

complexation is observed[20] with aliphatic anions and aromatic cations. Clearly, in Koga's systems, host interactions between aromatic π-systems and oppositely charged guests contribute to the formation of more stable host-guest complexes.

Koga also made an optically pure chiral molecule that was the first totally synthetic host to show diastereomeric differentiation while binding single guest enantiomers in water.[22] Though he reports no K_a's for those experiments, his spectra show chemical shift differences for diastereomeric host-guest complexes as we have seen in our studies.

Other researchers have taken different approaches to designing water-soluble hosts with hydrophobic receptors. Tabushi[23-25] demonstrated that his macrocycles, tetramer paracyclophanes with amine, ammonium or sulfonium units, could bind a variety of small organic molecules. Tabushi also showed that his hosts could selectively enhance the ester cleavage rates of guest esters.[22,26] Furthermore, he has also made substituted cyclodextrins that perform specific enantioselective transformations.[10]

In these early studies, Koga emphasized exploring the details of the binding event while Tabushi began exploring the catalytic capabilities of a

synthetic host. Both researchers used many similar techniques to study the binding event. Many of these early quantitative binding results utilized the fluorescence enhancement technique. This technique involves measuring changes in fluorescence of molecules that have environment-sensitive spectra. As guest molecules leave the polar water environment and enter the non-polar cavity of the host, the net fluorescence changes with percentage guest bound. These data are solved for K_a values using a Benesi-Hildebrand analysis.[27] Fluorescence enhancement can also be used to determine the K_a's for a large range of guests including those for non-fluorescent molecules by using inhibition studies. This technique remains a powerful tool for determining K_a's.

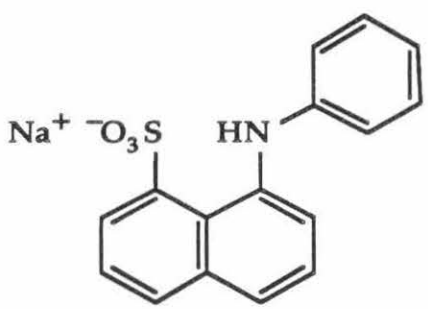

ANS

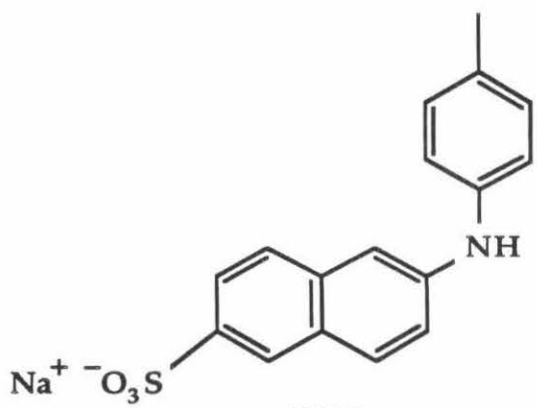

TNS

Diederich has also made many contributions to this field. His

spiropiperidinium-based macrocycles and macrobicycles (Figure 1.3) are effective hosts for non-polar arenes in water[28-33] and even in organic solvents.[34,35] Diederich also used fluorescence techniques to show that his hosts are effective at binding ANS and TNS type guests.[28] These fluorescence experiments are run at low concentrations where aggregation is not a problem. Diederich was the first in the field to emphasize the importance of operating below the critical micellar concentrations (CMC) of his hosts.[28] Our own related control experiments are discussed in detail later.

Diederich measured CMC's with both NMR[28,32] and light scattering[30] techniques. The values he obtained from the two techniques agree. His various hosts have CMC values in the 10^{-5}M – 10^{-3}M range, and follow a consistent trend; as the relative polar to non-polar areas of the host increase in size and number, the CMC rises. Performing binding experiments below the CMC of the hosts helps ensure that 1:1 host-guest complexation is being observed. For hosts with low CMC's, fluorescence techniques are ideal because of their sensitivity. Only 10^{-6}M guest and 10^{-5} M – 10^{-4}M host are necessary.

NMR experiments were used to study Diederich's hosts that had higher

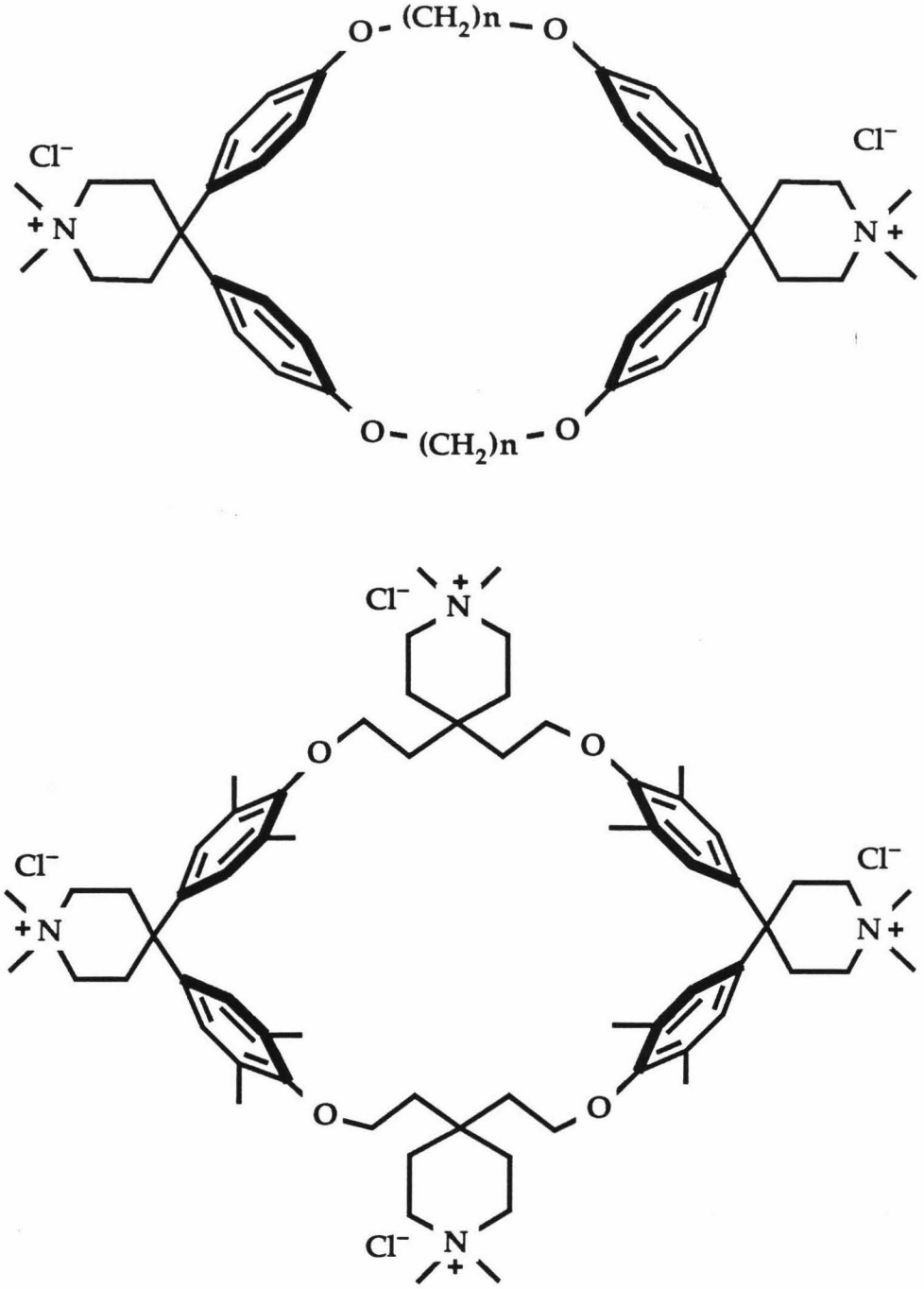

Figure 1.3: Two of Diederich's spiropiperidinium based macrocycles.

CMC's.[29] An important conclusion reached from a collection of his results is that flat aromatic guests, when sterically possible, prefer one type of orientation within the various hosts. Aromatic guests line up so that they lie between the diphenylmethane units at each end of the host. They lie in a plane defined by points equidistant from the two phenyl rings of each diphenylmethane unit. This orientation maximizes any π-stacking interactions between host and guest aromatic rings, and also allows extra stabilization when positive charges of the host, originally placed exterior to the binding site, can swivel to make close contacts with negatively charged aryl sulfonate guests. Importantly, guests always choose this plane as a binding location even when steric interactions do not force them to do so. Many different guest orientations in individual guest-host pairs occur, but the guest always lies in this plane. This type of guest orientation occurs repeatedly as Koga[21] and Diederich[29] have both shown by NMR, and Koga has shown with his crystal structure.[13] We also demonstrate the special importance of π-stacking interactions to the binding event. (See Chapter 4.)[35]

In some of his NMR studies,[29] Diederich expressed concern about interpreting NMR shifts in host-guest systems since many interactions

influence guest NMR spectra. The issue here is: how do we know when we are observing the results of a simple 1:1 host-guest binding event? If we observe a guest NMR spectrum, then add host, the spectrum will change as some portion of the guest will exist as the host-guest complex having different chemical shifts. If the on-off process of the guest is slow on the NMR time scale, then both free and bound guest can be observed. If the process is rapid on the NMR time scale, then a time-averaged spectrum is observed where chemical shifts are weighted averages of contributions from all species present in their respective amounts. Many things can be happening in time-averaged spectra. As well as 1:1, other binding stoichiometries can be present. Also, the aggregation properties of the host-guest complex can be different from those of pure host. Host-guest aggregates could influence NMR spectra, thereby making detailed interpretations inaccurate. This is a particular concern of Diederich. Most of Diederich's quantitative NMR studies are done in organic solvents where aggregation is less of an issue, or in water under slow exchange or saturation conditions where the chemical shifts of the guest protons in the host-guest complex are known.

Diederich's concerns are valid, but we feel that there is a great deal of

qualitative and quantitative data available from studying binding events by NMR. As Koga[21], and Diederich[28] and Vögtle[3] have argued, and as we believe[36], specific shift patterns upon binding indicate specific interactions. The numerous specific shift patterns seen by different researchers with many host-guest pairings remain difficult to rationalize with a random micellar-type binding model. Indeed, we have evidence for the existence of two binding modes within one host-guest system; a specific guest orientation at low concentrations, and a random non-selective orientation, more consistent with aggregate binding at higher concentrations above the host CMC. (See Chapter 3.)

Diederich used liquid-liquid extraction (LLE) and solid-liquid extraction (SLE)[28] as methods for determining K_a's for aqueous host-guest systems. These two methods are well suited for water insoluble guests (solubilities $\leq 10^{-4}$M). Diederich's hosts bind many aromatic water-insoluble guests with K_a's of $10^3 - 10^7\ M^{-1}$. The magnitude of these binding constants correlates directly with the water-insolubility of the guests. As the aqueous environment becomes more energetically unfavorable for a given guest, the non-polar environment of the host cavity becomes more energetically favorable. This is a consistent result for flat aromatic water-insoluble guests

with Diederich's hosts.

Diederich also performed other experiments that demonstrate th potential of these types of hosts in other uses. His hosts greatly accelerate the transport of neutral insoluble arenes through water relative to diffusion.[28] These properties could find a use in separation science.

Diederich has also progressed towards artificial enzymes by functionalizing his hosts.[11,37] He showed greatly increased rates for the benzoin condensation with his thiazolium-functionalized hosts. The greatest rate enhancements require the presence of a full cavity receptor site as well as the catalytic functionality.[11]

Diederich also studied host-guest donor-acceptor interactions in organic solvents and methanol/water mixtures.[35] He found stronger binding between his electron-rich donor hosts and electron-deficient acceptor guests than with donor guests. The donor-acceptor differences are worth about a factor of 1.5 in K_a, with all guests binding in the same general conformation at room temperature. The electron-deficient portions of his various naphthalene guests were bound on the average slightly deeper within the cavity of his donor hosts. In methanol-*d4*, the attractive forces are enthalpic

in nature. Upon moving to a methanol/water mixture, the K_a's increased for all guests, and at the concentration ranges studied, no differences in K_a's were observed. Diederich concludes that hydrophobic forces drive aqueous binding, though he makes no attempt to observe selectivities in K_a's possibly produced by donor-acceptor interactions. We have performed a detailed study that demonstrates selectivities caused only by differences in donor-acceptor interactions in water. (See Chapter 3.)[36]

Diederich has also attempted to observe chiral recognition by his hosts in water. Early attempts failed when his chiral molecules failed to act as hosts.[38] He later made a chiral host that did form diastereomeric complexes with both enantiomers of a guest.[39]

Vögtle has made a number of host compounds that complex hydrophobic guests in water. His hosts are based on diphenyl and triphenyl methane,[40] as well as other,[41] basic units, linked together with a variety of functionalities. They follow trends seen for similar hosts in the field. His hydrophobic cavities complex hydrophobic moieties, and his crown ether-type structures complex polar ions. Vögtle has built a host that encapsulates non-functionalized adamantane, by drawing the water-insoluble guest into

the aqueous phase.[41]

Vögtle made the first synthetic carbocyclic host.[42] (See Figure 1.4.) This host, solubilized with two, flexible tetra-carboxylate substituted chains, associates with cationic guests, but has a K_a of only 200 M^{-1} with ANS. Though no K_a values or control experiments are reported, Vögtle believes (from single concentration, host + guest NMR experiments) that his floppy tetra-anion hosts include various benzylic trimethylammonium salts.[41] No conclusive evidence for the exact mode of binding is presented, but cationic guests undoubtedly complex directly with the carboxylates of the host, thus benifitting from strong electrostatic attractions.

Lehn also synthesized anionic,[43] as well as other hosts.[44] He built two separate enantiomers of tetra-anion host using the familiar diphenylmethane unit, linked with tartrates. (See Figure 1.5.) These hosts bind monocations with modest affinities ($K_a = 10^2 - 10^3$), and dications with strong affinities ($K_a > 10^4$). Lehn presumes that the ammonium groups of his guests associate with the carboxylates of his flexible hosts, and that the aliphatic and aromatic groups associate with the hydrophobic portions. His data shows that strong electrostatic attractions are the most important

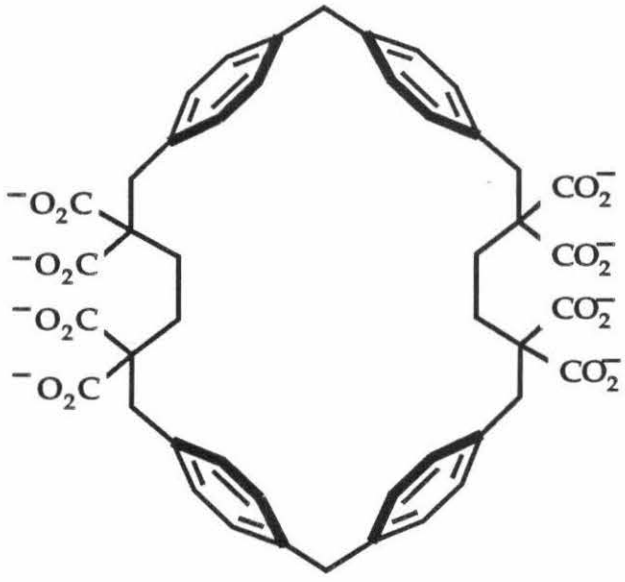

Figure 1.4: Vögtle's octa-anion carbocyclic host.

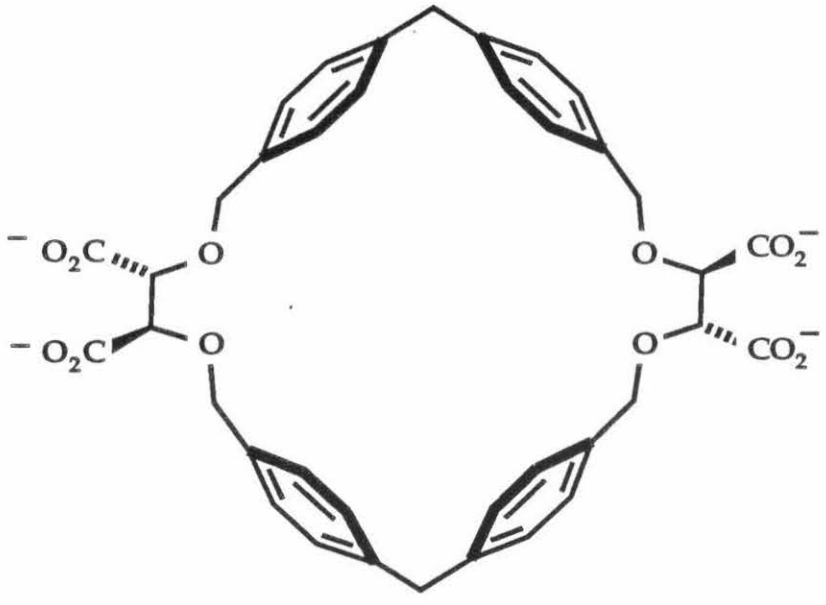

Figure 1.5: Lehn's chiral tetra-anion macrocyclic host.

driving force for binding in his host-guest systems, because increasing the hydrophobic surface among similar guests lowered binding affinities, and increasing the number of complementary charges on the guests greatly increased the binding affinities. Lehn recognizes the difficulty of measuring such very strong binding affinities using NMR, and reports his largest binding constants as lower limits.[43]

In work with a slightly different emphasis, Rebek has built hosts that effectively bind and orient guests in simple[45] and allosteric systems.[46] He also has built shape-selective reagents which perform specific transformations because of the steric constraints that they impose upon substrates.[47] Rebek's work in organic solvents is especially interesting. He has shown that a groove or cleft as a receptor, rather than a full macrocyclic cavity, can be sufficient for a strong and specific binding interaction.[48-53] Rather than exclude functionality from the interiors of his hosts, Rebek specifically includes complementary functionalities, which bind and orient guests within the receptor site. Some of Rebek's studies[52,53] in organic solvents, as well as another study by Hamilton[54], demonstrate the ability of π-stacking interactions to further orient a guest that is primarily attracted to a host with hydrogen bonds.

Combined, the studies of Rebek and Hamilton demonstrate that strong electrostatic interactions, hydrogen bonding and sometimes π-stacking combine to attract guests without encapsulation. These studies in organic solvents do not involve hydrophobic binding, but yield information about fundamental attractive forces between molecules, which we can use in our own studies.

We observe two clear trends in the various host-guest studies. Both Koga's[18-21] and Tabushi's[23,24] early studies first revealed results that occur repeatedly for all researchers in the field. First, opposite charges on the host and guest enhance, but by no means guarantee, binding. Similar charges on the host and guest weaken or destroy the observable binding attraction Sometimes complimentary charges directly interact with each other. This is a strong electrostatic attraction and has a large influence on the binding event. Indirect opposite charge interactions between host and guest, though less well understood, are clearly an important attractive binding force.

Second, equimolar amounts of open-chain, partial host fragments that contain host functionality but no preorganized cavity show greatly decreased binding compared to the intact host structure. This second result is an important control experiment that is discussed in detail later. An extension

of this result, demonstrated by Diederich[55] and Vögtle[40] is that building a more completely enclosed cavity, basket shaped instead of toroidal, increases the strength of binding by creating a more hydrophobic cavity. Indeed, incrementally increasing the hydrophobicity within a series of hosts can incrementally increase the strength of hydrophobic binding to a given guest.

Other important contributors to the field of molecular recognition include: Whitlock,[56-58] Stoddart,[59-66] Collet,[67,68] Murakami.[69-71] All of these researchers' efforts have contributed to a basic understanding of some aspect of molecular recognition usually centered around the hydrophobic binding event. We feel our own work has added to this understanding, and helps answer some of the unexplored questions in the field.

CHAPTER 2

Synthetic Design and Synthesis

Our effort in the field of molecular recognition commenced in 1982. We observed the work of the early researchers and embarked on an improved design of hosts. Our hosts have design features that we feel best allow us to study molecular recognition in water. These design features are discussed below.

Our hosts must be water soluble over a range of several pH units, and this range should include values at or near neutrality. This allows us to work around physiological pH ranges and under conditions where many chemical linkages are stable to the surrounding environment. The polar hydrophilic groups, which introduce host water-solubility, should be rigorously excluded from the binding region. The receptor site maintains its hydrophobic nature if the hydrophilic portions of the host are rigidly held remote from the binding cavity.

A rational synthesis, where we maintain control of the size, shape, flexibility, and functionality of the host, is vital to our overall design. If we can easily vary the properties of our hosts, we allow a range of studies using different hosts binding a single guest. This lets us study how steric interactions between host and guest affect binding affinities.

The flexibility of the host is also important. Substantial reorganization

of the host upon binding costs entropy, lessening the thermodynamic driving force. Cram and others originally demonstrated the value of preorganized, well-defined receptor sites for strong binding.[72] A preconstructed receptor reduces any entropic cost of reorganizing the host. A perfectly rigid host, however, might show strong binding only with those few guests that fit the exact steric demands of such an inflexible receptor. Overly tight binding is probably not the optimal situation for future enzyme models and catalysts. For our present systems though, we can learn a great deal from hosts that bind a large number of guests tightly. We feel that the most informative binding studies should use a preorganized, yet somewhat flexible, host, which offers a well-defined receptor site to an assortment of guests.

We also desire the ability to functionalize our hosts at will. A simple binding association for a given series of guests could become stronger and more selective with the addition of certain complementary functionalities. Functional groups placed on a host skeleton can interact or even react with guest molecules.[73] To explore these possibilities, we must have a readily functionalized basic host structure that can be easily modified for future generations of more complex receptors.

The last major design feature of our system is that we need simple efficient syntheses of our hosts. Furthermore, if we can construct chiral hosts without significantly lengthening our synthesis, we can explore possible enantioselectivities in binding and eventually construct asymmetric catalysts. We believe that an intrinsically chiral receptor site has a distinct advantage over an achiral receptor site that is perturbed by one or more stereogenic centers, though this has yet to be proven.[74,75] Simple, efficient, flexible syntheses of intrinsically chiral hosts would be ideal for this research.

The design criteria discussed above are important, because our research is an iterative process. The lessons learned from preliminary experiments must be easily incorporated into future generations of hosts. This can only occur if the final host structure is readily accessible in good yield. A short efficient synthesis, with all the features mentioned above, leads quickly to generations of rationally improved hosts.

All of these design considerations are demonstrated by our synthetic scheme. We base our macrocyclic structure on dibenzobicyclo[2.2.2]octane. This system forms in a Diels-Alder reaction between anthracenes and suitable dienophiles. C_2 symmetric adducts of 1,5- and 2,6-substituted

anthracenes are ideal building blocks for dissymmetric macrocycles containing a helical twist.

This project focuses on 2,6-disubstituted etheno-anthracene adducts, as they provide several beneficial features to our host structures. Several 2,6-disubstituted anthraquinones are commercially available, or easily synthesized, as starting materials.[76] These dibenzobicyclo[2.2.2]octane-based adducts have a concave hydrophobic surface, away from the etheno-bridge, that becomes a hydrophobic roof, or floor, in the final host structure. The dienophile functionality, introduced at the etheno-bridge by the Diels-Alder reaction, is held rigidly away from this hydrophobic surface. (See Figure 2.1.) Thus direct interactions between these water-solubilizing groups and the receptor site are minimized. This satisfies one of our initial design requirements.

A variety of dienophiles can be used to introduce different substituents at the bridge. This lets us manipulate the type of water solubilizing group which we use. Though we have focused primarily on carboxylates as solubilizing groups, other anionic, cationic or nonionic groups can easily be placed on the etheno-bridge.[77] The Diels-Alder reaction is also convenient because an asymmetric version of this reaction yields a rational synthesis to

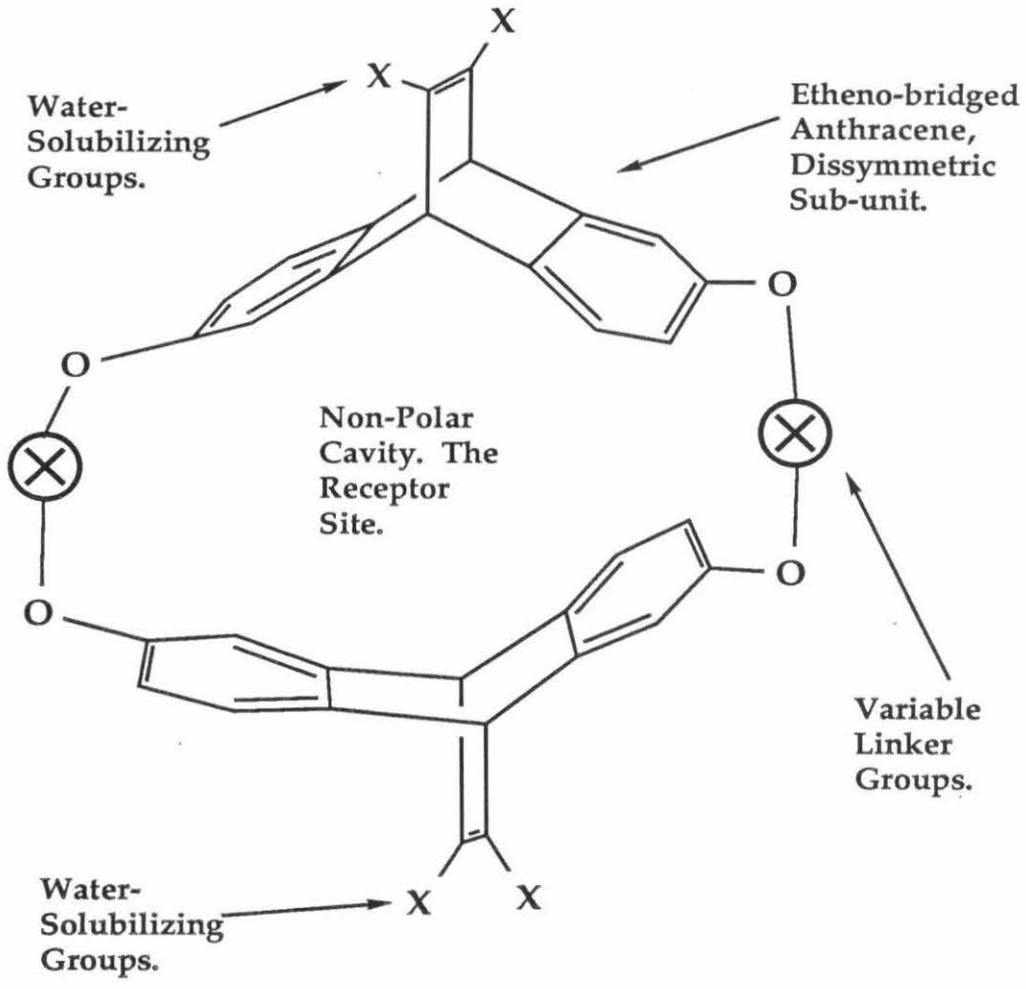

Figure 2.1: Our general host-macrocycle structure showing the various features of our design.

the single optically pure, D_n symmetric, host enantiomer of choice.

The two dibenzobicyclo[2.2.2]octane units are then connected together by two linker units to form macrocycles. (See Figure 2.1.) Two equivalents of a Diels-Alder adduct and two equivalents of an easily varied linker (typically an α,ω-dibromide) are coupled at high dilution to afford the macrocycles. In this one step, we build our final three-dimensional receptor site. Minor modifications yield the water-soluble host. Importantly, this host structure contains an easily constructed, well-defined, preorganized binding cavity.

With this synthetic scheme, we feel that we successfully elaborate easily obtained simple molecules into macrocyclic host structures well suited for the study of molecular recognition in water. The details of our synthetic procedure follow.

Synthesis

Our synthesis begins with commercially available 2,6-dihydroxyanthraquinone (**1**), which is reduced in a modified literature procedure[78,79] using aluminum amalgam to 2,6-dihydroxyanthracene (**2**) in >90% yield. (See Scheme 2.1.) Compound **2** is reacted directly with dimethyl

Scheme 2.1:

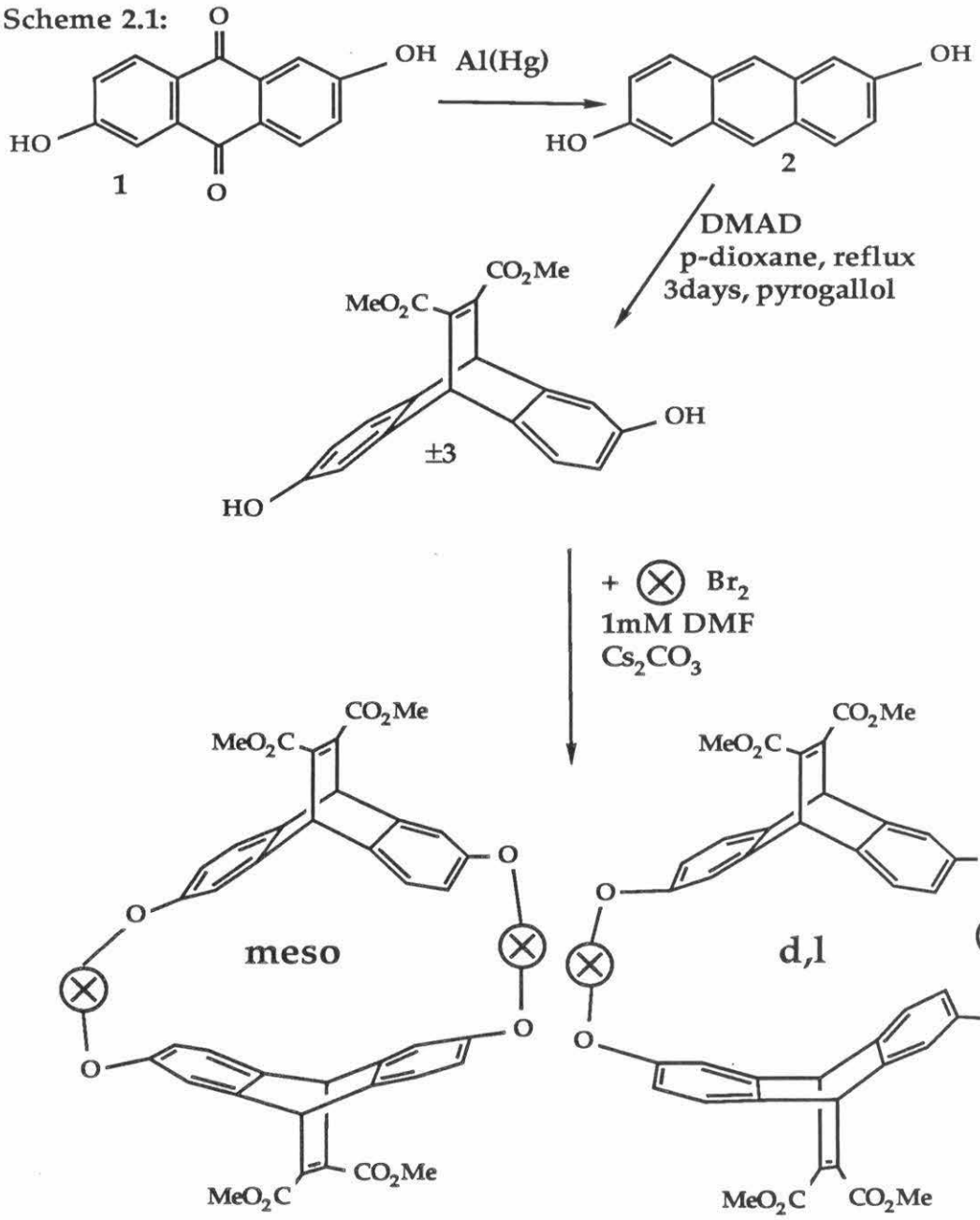

⊗ = o-xylyl =4a

= m-xylyl =5a

= p-xylyl =6a

⊗ = o-xylyl =4b

= m-xylyl =5b

= p-xylyl =6b

acetylenedicarboxylate (DMAD) in refluxing dioxane for three days yielding 60-70% Diels-Alder adduct (**3**).[80] This reaction requires a great excess of DMAD, and a large amount of polymeric material forms during the reaction, yet the reaction does produce multi-gram quantities of the desired adduct **3**. The numbering scheme for the different protons of our Diels-Alder adducts and macrocycles is shown in Figure 2.2.

An undesirable reaction of the ethenoanthracene moiety is a di-π-methane rearrangement.[81] This is an unfortunate photochemical side reaction which can destroy our Diels-Alder adducts or any other of our molecules which contain the ethenoanthracene unit. We can protect our molecules from the di-π-methane rearrangement if we avoid exposing them to short wavelength light (< 300 nm). Also, when we avoid solvents which sensitize the photochemical rearrangement, such as benzene or acetone, the undesired reaction is minimized. Our different ethenoanthracene-adduct intermediates undergo this reaction at very different rates; in all cases they react much faster in solution than as solids. Routine protection from long-term exposure to light is adequate to protect these molecules. Fortunately, the reaction seems to be slow in water, and decomposition of our host solutions over extended periods of time is not observed.

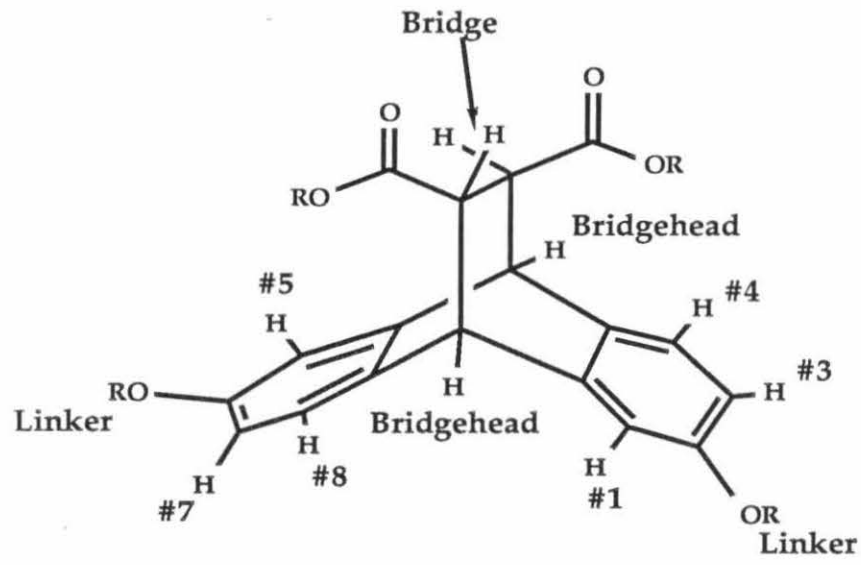

Figure 2.2: The numbering scheme for our Diels-Alder adducts and macrocycles. The label for each proton is placed next to its position. This is an example of an *anti*-ethano-adduct. The numbering scheme is gereral for all adducts and macrocycles. Etheno-bridged molecules have no bridge protons.

We tried many different macrocyclization procedures with **3**, and almost all work to some degree. The reported procedures are the results of trying a large number of reactants and co-reactants, concentrations, temperatures, addition rates and reaction times. The best procedures use equivalent amounts of **3** and xylylene dibromides added to excess Cs_2CO_3 (5 equivalents) in dry DMF.

Extremely dry DMF, free of dimethylamine, is necessary for a successful reaction. Because the desired reactants are at sub-millimolar concentrations, hydroxide and dimethylamine can compete with the phenolate displacement of the bromide. The DMF is dried by vacuum distillation from calcined CaO (500 °C, 8h) then stored over at least two separate batches of freshly dried 4Å molecular sieves for one week each. DMF is extremely hygroscopic and should be handled accordingly.

Cesium carbonate is also essential for a successful reaction. Different reasons have been given for the success of Cs_2CO_3 as a base for alkylations.[82,83] The diffuse, solvated cesium cation may allow better access of the anion nucleophile to the reactive center. Alternatively, Cs_2CO_3, a stronger base than traditional K_2CO_3, may speed up the reaction.[84] Also,

Cs_2CO_3 is very hygroscopic, and the excess reagent may scavenge trace water. The mechanistic details are not understood,[82] but Cs_2CO_3 works well in all phenolate alkylations and macrocyclizations that we tried.

The macrocyclization procedure is run two ways. When making *meso* and *d,l* macrocycles, an equivalent each of bisphenol **3** and dibromide is dissolved to 1mM in DMF, and Cs_2CO_3 added to start the reaction. When we make the enantiomerically pure macrocycles the contents of a syringe containing a 15mM solution of both bisphenol (**3***R* or **3***S*, Scheme 2.5) and dibromide is slowly pumped (<0.5 mL/h) into an equal volume of rapidly stirred DMF containing excess Cs_2CO_3. The syringe pump procedure will sometimes give slightly lower yields. Both reactions finish in two days at room temperature when the linker precursors are benzylic bromides. Less active alkylating agents as linker precursors require heating and longer reaction times.[84]

The yields of these reactions are quite high (18-36%) (See Table 2.1) These yields may not seem high until we consider the chemistry involved; typical yields for similar processes are much lower.[84] In our system, four pieces must come together, in exactly the correct fashion, to yield dimer

macrocycles. There are inumerable possibilities for oligomerization. We have equipped the subunits for large ring closures with features that promote closure vs oligomerization. Both characterized and uncharacterized higher oligomers do form, but we attribute the high portion of dimer to the preorganized shape of **3**. Large rings (32-membered in the case of the p-xylyl linker) often close slowly because of the entropy cost of bringing the two reactive ends together. The rigid ethenoanthracene subunit freezes out many degrees of freedom, and enforces a concave shape to the forming macrocycle. This helps bring the ends together so they will react.

Table 2.1: Macrocyclization yields

Linker =x - xylyl	Total isolated macrocycle yield (%)
ortho **4a +4b**	24
meta **5a +5b**	36
para **6a +6b**	18

Racemic **3** makes two dimer macrocycle diastereomers when linked with *ortho, meta* or *para* xylyl linkers (**4–6a , 4–6b**). Heterochiral coupling

with two opposite enantiomers of **3** yields C_{2h} symmetric *meso* compounds **4–6a** having a plane of symmetry which cuts through the linkers and a C_2 axis which splits both etheno bridges. Cyclization with racemic **3** is the method of choice for making the *meso* compounds **4–6a**. Homochiral coupling with racemic **3** yields sets of D_2 symmetric racemic *d,l* pairs **4–6b** having three mutually perpendicular C_2 axes: one which splits the etheno bridges, as in the meso compound, one which splits the linkers and a third which passes through the middle of the binding region (not touching any bonds or atoms). The symmetry elements of the dimer macrocycles are shown in Figure 2.3.

The *meso* and *d,l* diastereomers are separated by HPLC on silica gel. They were originally identified by a comparison of physical properties to other known *meso* and *d,l* macrocycles with different linkers.[85] Later, when we synthesized a single enantiomer of the macrocycle, this assignment was confirmed.[36]

With the macrocycles in hand, only the last step, the unmasking of the water-solubilizing functionality, remains. The hydrolysis of the four methyl esters to the tetra-cesium carboxylates proceeds easily and in good yield, as

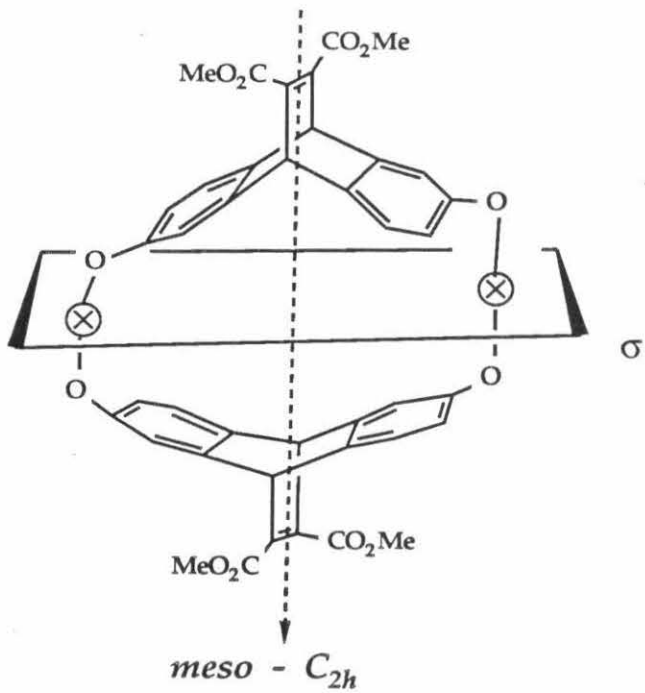

meso - C_{2h}

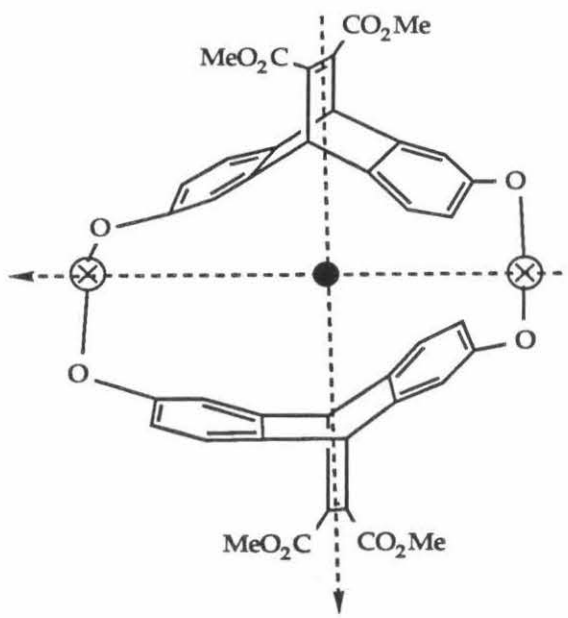

d,l - D_2

Figure 2.3: The 2 dimer macrocycle diastereomers, shown here with their symmetry elements.
---------- = a C_2 axis.

long as the free acids are not isolated. The free acids of our hosts are formally substituted maleic acids (maleic acid pK_a =6.1 and 1.8[86]). As free acids, our macrocycles self-destruct; the strong acid cleaves the acid labile benzyl-phenyl ether linkages which occur four places in each host. Fortunately, these molecules are easily handled as their carboxylate salts.

Our saponification procedure is shown in Scheme 2.2. In our standard hydrolysis procedure, excess cesium hydroxide in DMSO/water cleaves the methyl esters of **4–6** in 18h at 35-40 °C. The DMSO is then removed with ether washes or lyophilization. The residue is dissolved in water, passed over a cation-exchange resin (ammonium form), lyophilized, neutralized with CsOH and dissolved in the buffer used for binding studies. The overall yield for this last step ranges from 80-95%. Ester hydrolysis with lithium hydroxide yields water insoluble, DMSO soluble, tetra-lithium salts.

The overall yields for the transformations of **1** to water soluble macrocycles range from 5–15% for **O**,**M** and **P**.

The *meso* and racemic *d,l* xylyl-linked hosts (±**O**,±**M**,±**P**; *meso* and *d,l*) were useful for a number of binding studies (Chapters 3 and 5).[85,87] In the next generation of studies, we chose to look at our resolved chiral

Scheme 2.2:

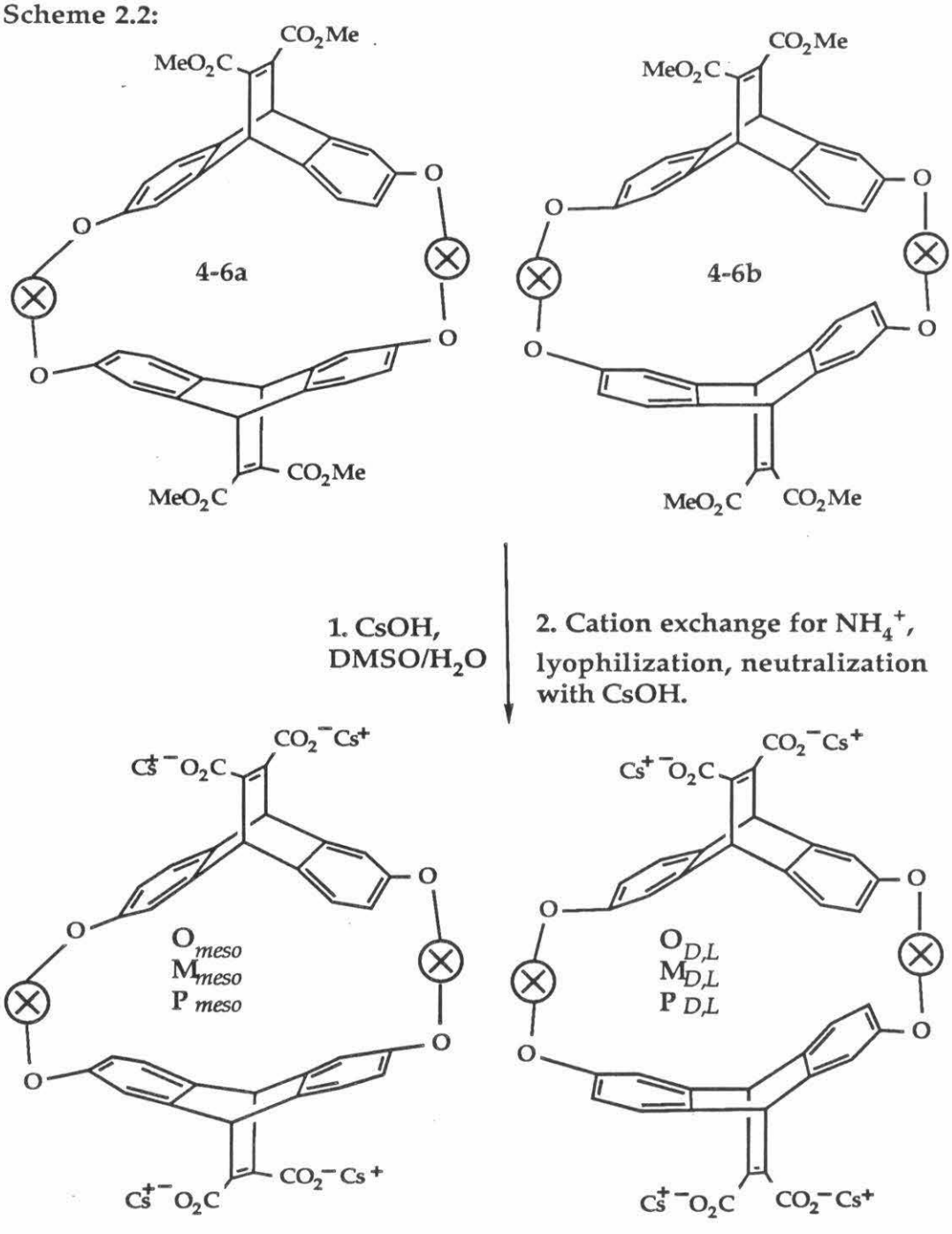
CO2Me
MeO2C
4-6a
4-6b
1. CsOH,
DMSO/H2O
2. Cation exchange for NH4+,
lyophilization, neutralization
with CsOH.
CO2−Cs+
Cs+−O2C
O meso
M meso
P meso
O D,L
M D,L
P D,L

macrocycles as hosts. Differences in binding affinities and conformations between the different guest enantiomers binding a single host enantiomer reveal details about the specific interactions involved with the binding event. We wished to obtain enantiomerically pure **3**. Macrocyclizations with resolved **3** yield one enantiomer of D_n symmetric oligomeric macrocycles. Originally, we tried many classical resolutions of the bisacid of **3** and its derivatives, but obtained only partially optically enriched material.[88]

The Diels-Alder reaction creates the stereogenic centers in compound **3**, the two bridgehead carbons. We decided to use an asymmetric Diels-Alder reaction to attempt our resolution. These reactions have been thoroughly studied,[83,89-92] and a number of cases of excellent selectivity have been demonstrated.[93,94]

Consider the reaction between a chiral fumarate and a 2,6-di-substituted anthracene. (See Scheme 2.3.) Either face of the olefin can react with either face of the anthracene yielding four diastereomers. Dimenthyl fumarate (**7**) is a convenient chiral dienophile, which has shown excellent diastereoselectivity in Lewis acid-catalyzed Diels-Alder reactions with

Scheme 2.3:

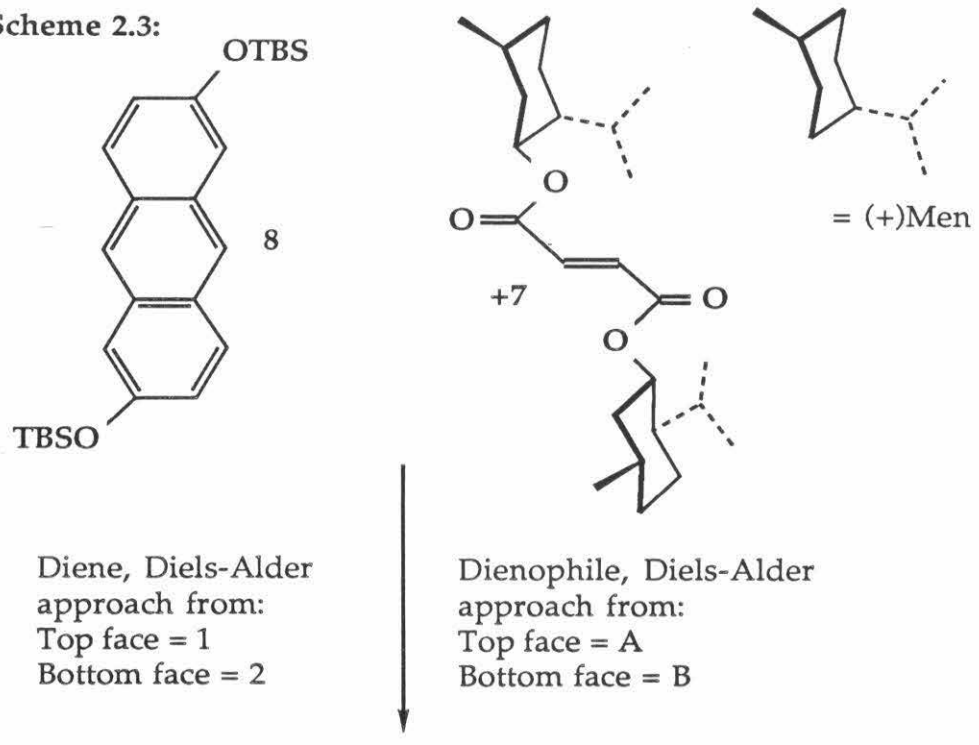

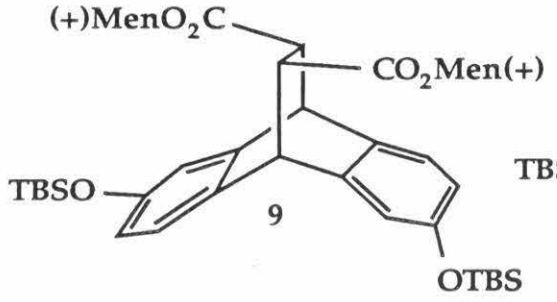

syn Adduct from faces 1 + A (**9**)

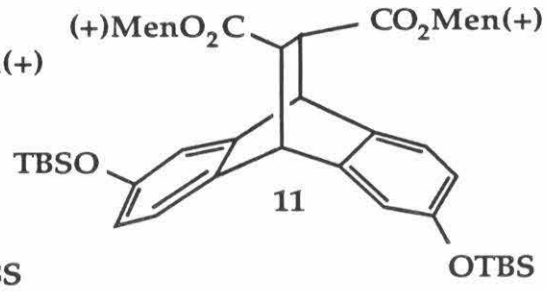

anti Adduct from faces 1 + B (**11**)

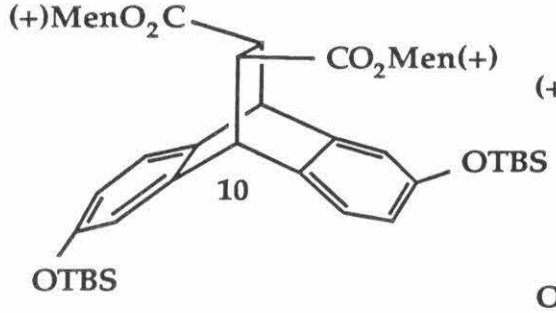

anti Adduct from faces 2 + A (**10**)

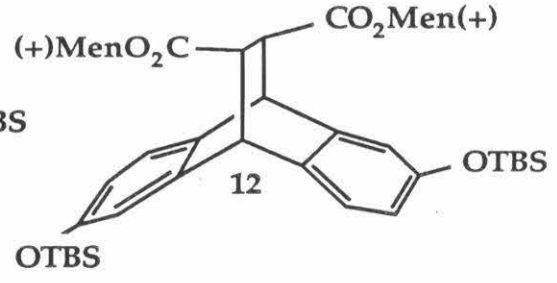

syn Adduct from faces 2 + B (**12**)

anthracenes.[93] The faces of **7** are diastereotopic, and in the reaction with the two faces of a diene, they react at different rates. When **7** complexes with a Lewis acid, such as Et_2AlCl, the difference between the two sides of the olefin is magnified, because a more rigid conformation is enforced.[83] (See Figure 2.4) This yields the excellent selectivities which we see. Also, complexation of an electron-deficient dienophile with a Lewis acid activates the dienophile. Lewis acid catalyzed Diels-Alder reactions proceed at much greater rates (Table 2.2), than their uncatalyzed counterparts.

Either enantiomer of dimenthylfumarate (**(+)-7** or **(–)-7**) and 2,6-di-*t*-butyldimethylsiloxyanthracene (**8**) react in the presence of 5 equivalents of Et_2AlCl below 0 °C, yielding Diels-Alder adducts. The reaction shows complete facial selectivity at the olefin, yielding only one *syn* and one *anti* adduct. The four possible Diels-Alder products from the reaction of **(+)-7** and **8** are shown in Scheme 2.3. The *syn* adducts have ester groups pointing over the 2 and 6 positions of the dihydroanthracene portion of adducts **9** and **12**. The *anti* adducts have ester groups pointing over the unsubstituted 3 and 7 positions of the dihydroanthracene portion of the adducts **10** and **11.** (See Scheme 2.3.) Because of consistent published selectivities in Diels-Alder

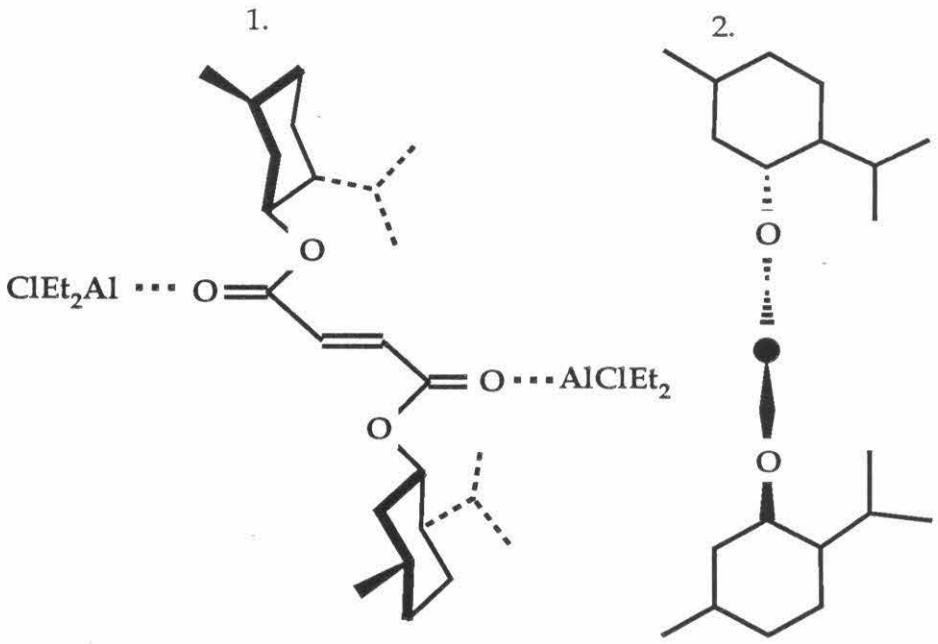

Figure 2.4: Two idealized views of **(+)7**·$2Et_2AlCl$ as a Lewis acid complexed dieneophile.

1. (+)-Dimenthylfumarate, view down onto the less hindered Diels-Alder approach face.

2. Looking down the C=C bond, a side view of 1. The less hindered approach is from the left; the more hindered, from the right.

reactions involving **7**,[83,90,91,93,94] we believe that the two major adduct diastereomers formed from **(+)-7** and **8** are **9** and **10**; those from the less hindered side of the **(+)-7** ·2Et_2AlCl complex. The uncatalyzed thermal reaction, in refluxing toluene, yields all 4 diastereomers **9–12.** NMR experiments, where we quantitatively contaminate samples of **9** with **12** and **10** with **11**, show that we can easily detect <2% contamination resulting from reaction of the more hindered face of the dienophile.

Table 2.2: The reactions of **(+)-7** and **8**.

Reaction temperature, duration, and the ratio of diastereomers formed.

		Thermal Rxn.	Catalyzed with excess Et_2AlCl		
Adduct	(from faces)	(110°C)	0 °C (5h)	-45 °C (15h)	-78 °C (24h)
9	1 + A	1.0	1.1	1.7	8.0
11	1 + B	1.5	N.D.	N.D.	N.D.
10	2 + A	1.0	1.0	1.0	1.0
12	2 + B	1.0	N.D.	N.D.	N.D.
Chemical Yield		*	80%	62%	26%

N.D. = Not detected. We could easily detect any diastereomer which was 2% of the total adducts.

* This reaction was not complete after 50h at 110 °C, and was stopped at ≈ 60% conversion.

We also see some selection between the faces of **8**. This diene selectivity changes from a slight *syn* adduct preference at 0 °C to an 8/1 *syn* adduct preference at -78 °C. Unfortunately, the chemical yield of the reaction drops with the temperature. (See Table 2.2.) The *syn* adduct might be expected to show more steric congestion as it forms, because of contact between the bulky menthyl groups of **7** and *t*-butyldimethylsiloxy groups of **8**. When the *anti* adduct forms these contacts are avoided. The selectivity is the reverse from what we expected. The *syn*-adduct preference may arise because the aryl oxygens coordinate favorably with the Et_2AlCl as **7** and **8** approach.

The adduct mixture, **9** and **10**, is separated from any unchanged starting materials by flash chromatography. Compound **9** crystallizes from the adduct mixture when a 0.15 M solution of the adducts in pentane at room temperature is chilled slowly to -100 °C. Compound **10**, and any remaining **9**, are isolated by flash chromatography of the mother liquors.

We assign the identities of the diastereomers on the basis of two results. The 2-dimensional ^1H-^1H nuclear Overhauser enhancement correlated NMR (NOESY) spectra help identify the two diastereomers. (See Figure 2.5.) The essential data are the crosspeaks between the bridge protons

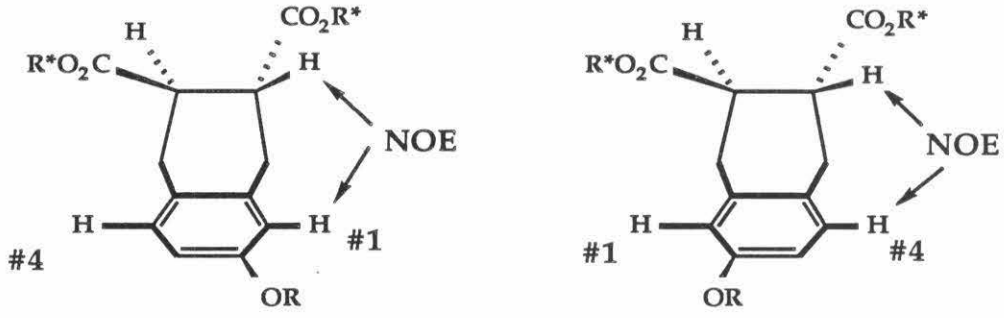

anti·10 syn·9

Figure 2.5: The NOE cross peaks for the syn and anti adducts from the two NOESY experiments.

and those on the aromatic ring. These protons are part of the rigid core of the molecule and are held at fixed distances from each other. The bridge protons are close (2-3 Å) to the 4,8-protons in adducts **9** and **12**, and close to the 1,5-protons in adducts **10** and **11**. The bridge protons are far (5-6Å) from the 1,5- and 3,7-protons in **9** and **12**, and far from the 4,8- and 3,7-protons in **10** and **11**. Indeed, one diastereomer shows a bridge-aromatic crosspeak only between the bridge and the 4,8-protons (**9**) and the other only between the bridge and the 1,5-protons (**10**). Homonuclear correlated 2-dimensional (COSY's) spectra of the same two samples under similar conditions reveal no crosspeaks between the bridge and aryl protons. The COSY spectra show that *J*-coupling, which might cause the crosspeaks of interest in the NOESY experiments, does not exist.

Also, the aromatic region chemical shift patterns in the ^{1}HNMR spectra of **9** and **10** match qualitatively with the patterns of a *syn* and *anti* adduct pair reported in the literature.[95] The *syn* and *anti* assignment from the NOESY experiment supports the assignment made from the NMR shift pattern comparison. Additionally, patterns of optical rotations for other 2,6-disubstituted ethenoadducts with known absolute configurations are completely consistent with our assignment.[95] A correct *syn*/*anti* assignment

is essential, because this assignment, along with the assignment of olefin facial selectivity in the Diels-Alder reaction,[93] determines the absolute configuration of the final host macrocycles.

The *syn* and *anti* adducts are synthetically modified to the two enantiomers of **3**. (See Scheme 2.4.) By separating the two diastereomeric adducts, we have formally solved the problem of separating the enantiomers of our macrocycle building block **3**.

The conversion of the ethanoadducts **9** to **3** $_R$ or **10** to **3** $_S$ is straightforward. Compound **9** or **10** is quantitatively oxidized within minutes at room temperature to an etheno-adduct with diphenyl diselenide and potassium *t*-butoxide in toluene/THF. Without intermediate work up, the silyl ethers are cleaved by the addition of isopropanol and HCl (37% aq). This deprotection takes 18h at room temperature, and after work up yields 98% ethenoadduct-bisphenol-bismenthylesters **13** from **9**, or **14** from **10**. (See Scheme 2.4.) These phenols, **13** and **14**, can be crystallized from ether. We made menthyl ester macrocycles from **13** and **14** by our standard macrocyclization procedures, but the α,β-unsaturated menthyl ester macrocycles did not saponify cleanly.[96,97]

The menthyl esters of **13** or **14** are exchanged for methyl esters by

Scheme 2.4:

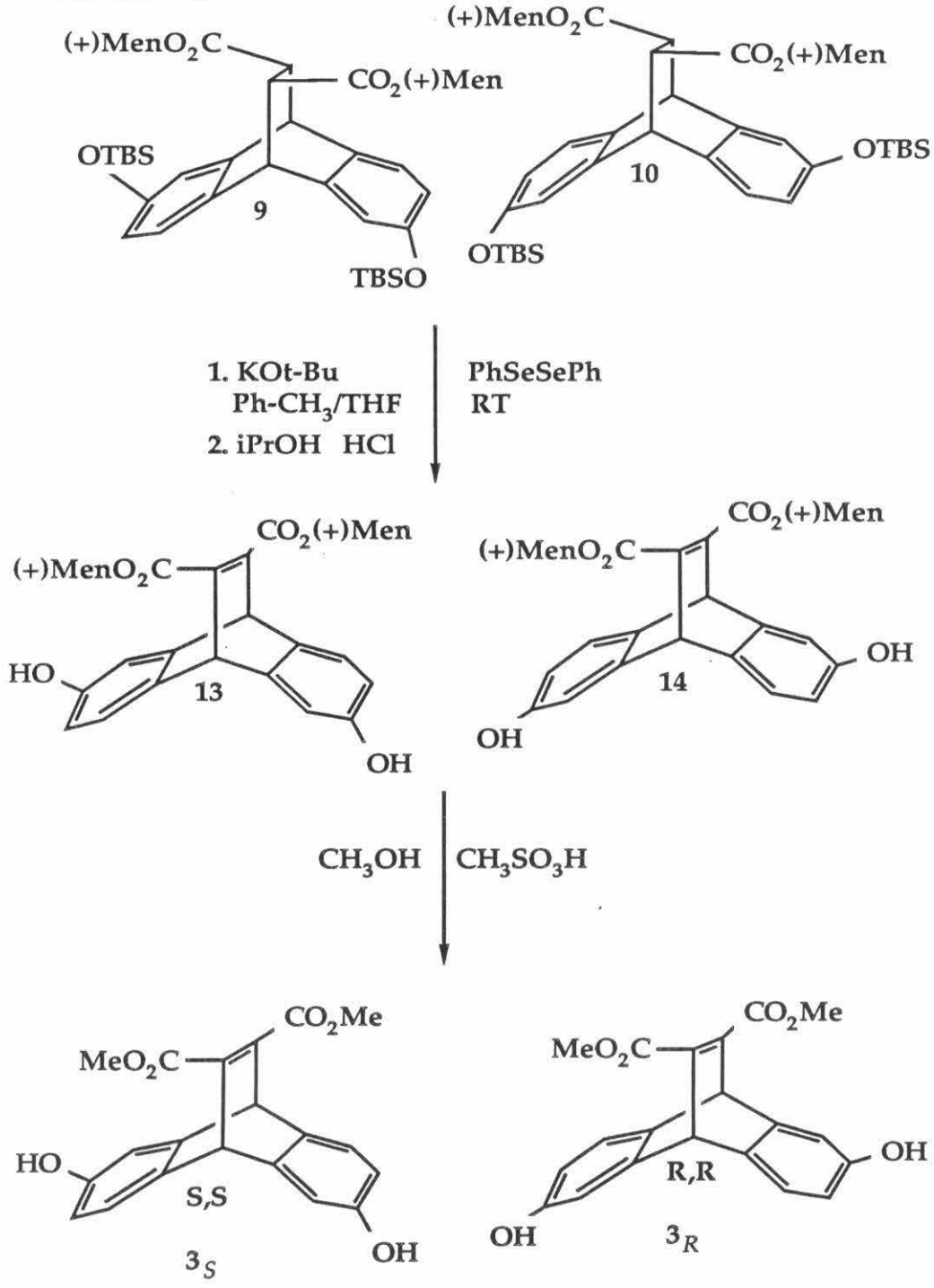
(+)MenO2C
CO2(+)Men
OTBS
9
TBSO
(+)MenO2C
CO2(+)Men
10
OTBS
OTBS
1. KOt-Bu
Ph-CH3/THF
2. iPrOH HCl
PhSeSePh
RT
CO2(+)Men
(+)MenO2C
HO
13
OH
CO2(+)Men
(+)MenO2C
14
OH
OH
CH3OH
CH3SO3H
CO2Me
MeO2C
HO
S,S
OH
3S
CO2Me
MeO2C
R,R
OH
OH
3R

refluxing them in methanol with methane sulfonic acid catalyst. The yield is 90-95% after flash chromatography. Compound **3** can be crystallized from chloroform. The product of each reaction is a single enantiomer of **3** (**3***S* from **13**, or **3***R* from **14**).

The reactions above start with **(+)-7** . (See Scheme 2.4.) The entire reaction sequence was also performed starting with **(–)-7** . When **(–)-7** was used, *syn* adduct was elaborated to **3***R* and the *anti* adduct elaborated to **3***S*. Both routes generated the products with equal efficiency, but if very large scale preparations were to be run, the route from (–)-1*R*,2*S*,5*R*-menthol would be cheaper.

From **3***S* or **3***R*, we use our proven macrocyclization procedure to make single enantiomers of macrocycles. (See Scheme 2.5.) We consider the macrocycles made from **3***R* and **3***S* to be enantiomerically pure. Other enantiomer contamination of **3** would come from impure samples of **9**, **10**, **13** or **14**. In each case, the offending diastereomer, which would eventually cause partially racemic **3**, is easily identified and removed. Furthermore, the macrocyclization procedure enriches the optical purity of the macrocycles as compared to that of **3**. As the optical purity of **3** increases, a larger portion of

Scheme 2.5:

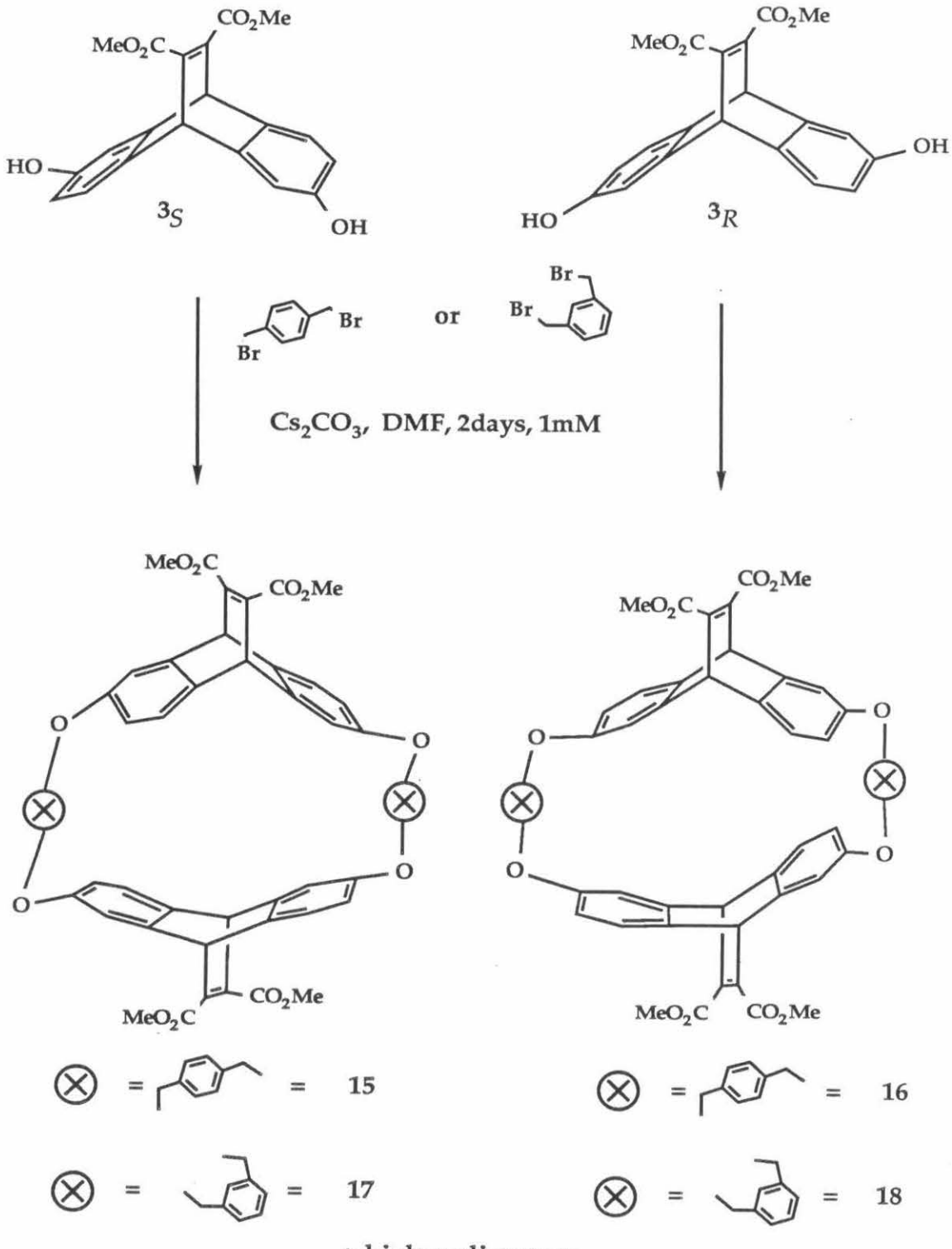
CO2Me
MeO2C
HO
OH
3S
3R
Br
or
Cs2CO3, DMF, 2days, 1mM
O
15
16
17
18
+ higher oligomers.

Scheme 2.6:

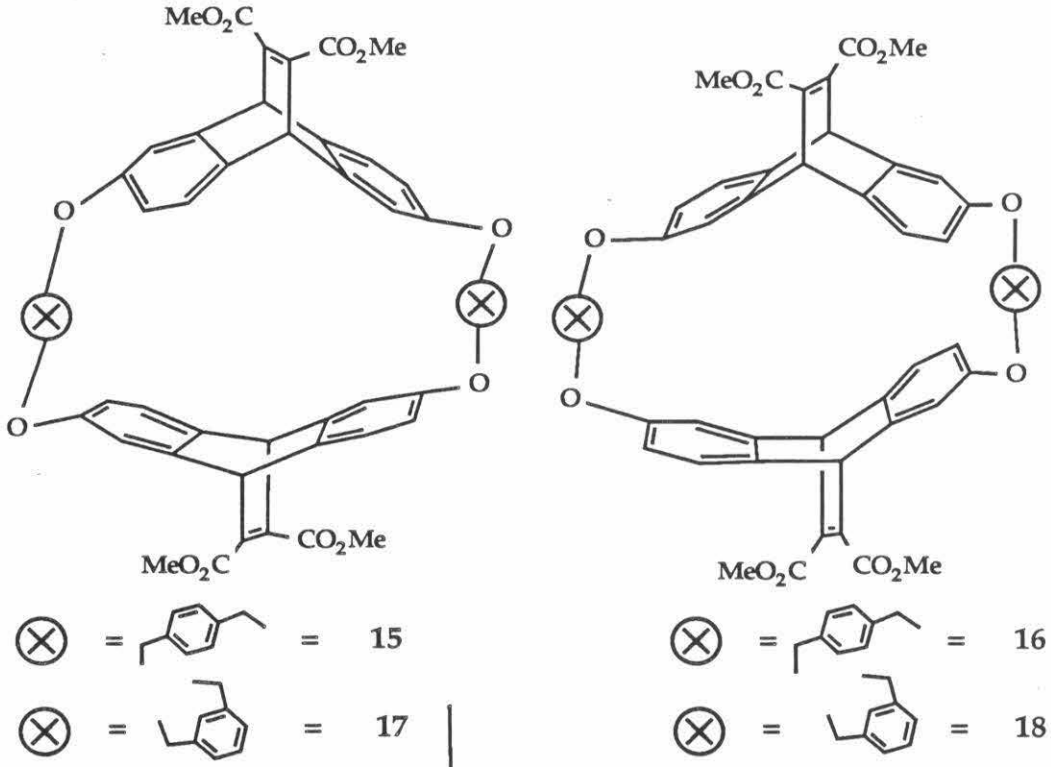
MeO2C
CO2Me
MeO2C
CO2Me
CO2Me
MeO2C
MeO2C
CO2Me
= 15
= 16
= 17
= 18
1. CsOH, DMSO/H2O
2. Cation exchange for NH4+, lyophilization, neutralization with CsOH.
Cs+ −O2C
CO2− Cs+
Cs+ −O2C
CO2− Cs+
15 → PS
17 → M S
16 → PR
18 → MR
Cs+ −O2C
CO2− Cs+
Cs+ −O2C
CO2− Cs+

the minor enantiomer is funneled off to form *meso*-macrocycles. For example, assuming equivalent formation rates[98], a 10/1 **3**$_R$ to **3**$_S$ ratio yields 100:1 *R*:*S* dimer macrocycle, with about 15% *meso*-diastereomer formed; a 100:1 **3**$_R$ to **3**$_S$ ratio yields 10000:1 **15**:**16**, with about 2% *meso*-diastereomer formed. We have never detected any *meso* compounds arising from coupling of **3**$_R$ to **3**$_S$ when we use **3**$_R$ or **3**$_S$ obtained via Scheme 2.4. We expect that our macrocycles **15**–**21** have >99.9% ee.

Saponification of **15**–**18** is performed as mentioned earlier yielding hosts **P**$_S$, **P**$_R$, **M**$_S$ and **M**$_R$. (See Scheme 2.6.)

One interesting feature of our hosts is their optical rotations. The $[\alpha]_D$ of **3**$_S$ is –60°, whereas the rotation of **15** is +144°. The more floppy *p*-xylyl linked *S,S,S,S,S,S*-trimer macrocycle (**19**) (Figure 2.6) has a rotation of only +17°. The meta-linked macrocycles show the same trend. **17** has a rotation of +58°, the *m*-xylyl linked *S,S,S,S,S,S*- trimer (**20**) a rotation of –19°, and the *m*-xylyl linked *S,S,S,S,S,S,S,S*-tetramer (**21**) (Figure 2.7) a rotation of –65°. The helical D_2 symmetric dimer macrocycles have an intrinsically dissymmetric chromophore which counteracts the intrinsic rotation of the bicyclic subunit. As the macrocycles grow larger, they become more flexible,

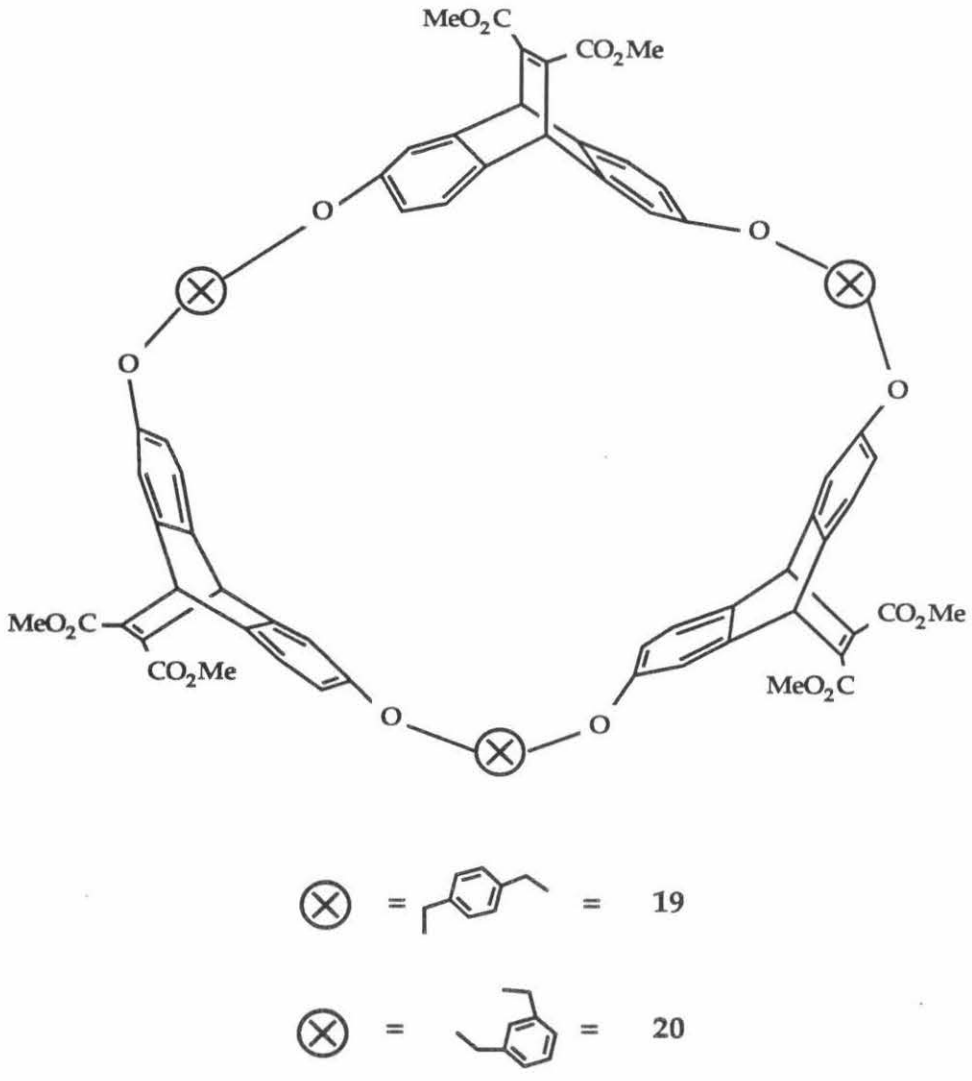

Figure 2.6: The trimer macrocycle structures.

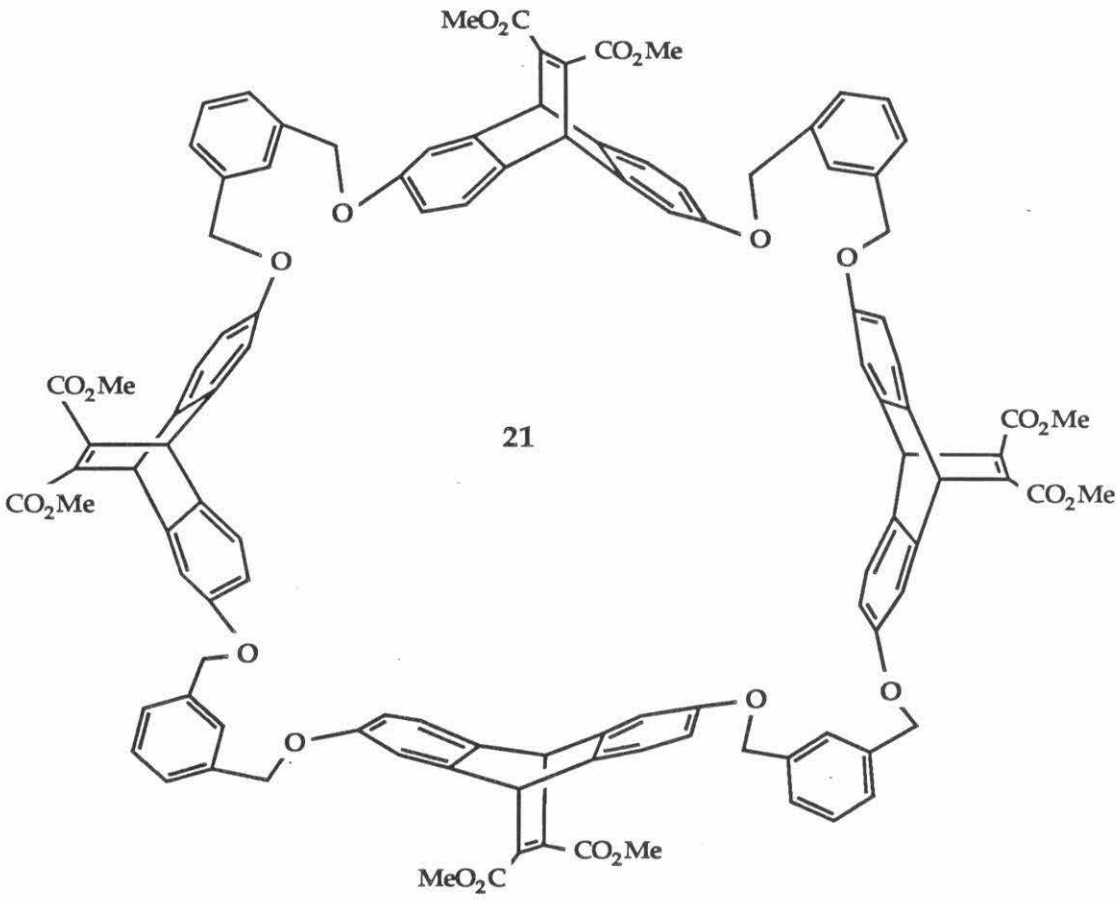

Figure 2.7: *S,S,S,S,S,S,S,S*-tetramer m-xylyl macrocycle **21**.

and lose this conformationally enforced sense of twist, thus reverting to an optical rotation similar to the bicyclic subunit.

Good evidence exists for a strong conformational preference in **15**. Intramolecular nuclear Overhauser enhancements reveal that a single time-averaged conformation at the aryl-O-CH_2 group predominates. (See Figure 2.8.) Irradiation at the 3,7-protons of **15** shows an enhancement of the upfield proton of the O-CH_2 group, and at the 4,8-proton. Irradiation of the 1,5-protons, under identical conditions, shows an enhancement of only the bridgehead protons. This shows that both the O-CH_2 protons are not proximate to the 1,5-protons, and that one of the O-CH_2 protons is near the 3,7-position. The geometry shown in Figure 2.8 is the prevailing geometry at the O-CH_2 group of the ester in dichloromethane solution. The oxygen to sp^3 carbon bonds are aligned such that the methylene groups lie in the vicinity of the 3- and 7-protons. We cannot say which of the two methylene hydrogens is actually near the 3 and 7 protons. (See Figure 2.2 for the proton numbering scheme.) Upon lowering the temperature to -90 °C, no evidence for other conformations is seen; **15** maintains real or time-averaged D_2 symmetry.

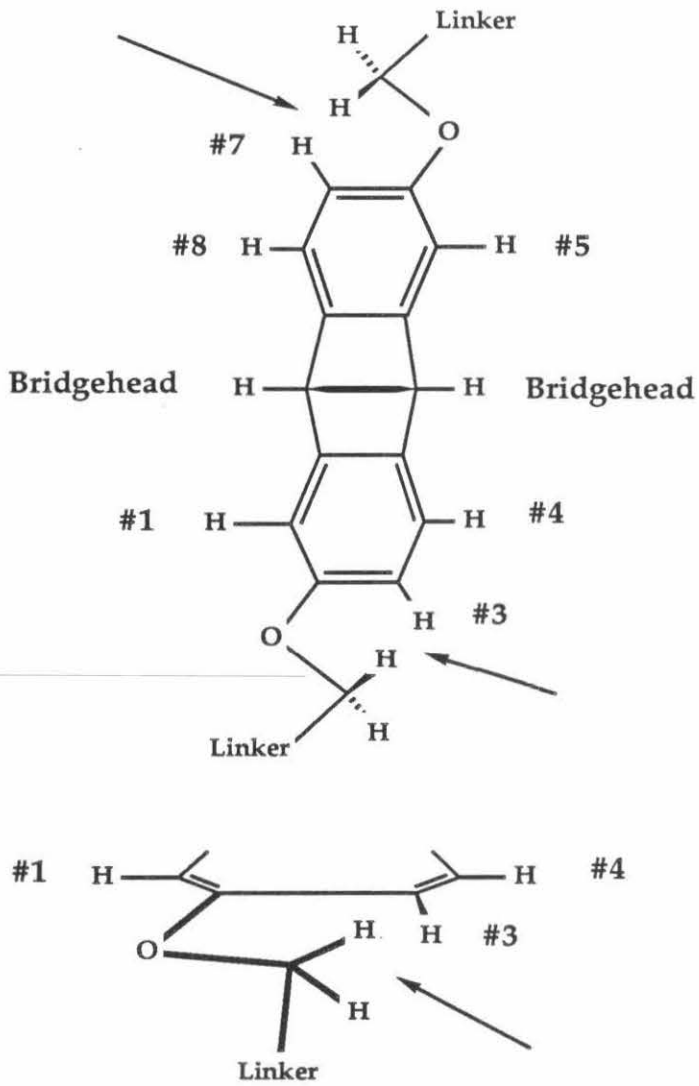

Figure 2.8: Two views of the preferred aryl-O-CH_2 conformation in **15**. One of the O-CH_2 protons is proximate to the 3 or 7 proton on the aromatic ring of the bicyclic system. The close contacts are indicated by arrows in the two views.

The eight step synthesis from **1** yields ≈ 3-5 % each of two enantiomeric hosts. This is a good yield, considering the chemistry involved and the flexibility of the synthesis. Optically pure **3** is the key intermediate, available from **1** in 53% yield (total for both $\mathbf{3}_R$ and $\mathbf{3}_S$). These molecules allow the synthesis of future generations of hosts.

CHAPTER 3

Control Experiments and Binding by NMR

With our host molecules in hand, we started studying the binding properties of different host-guest systems. First we performed vital control experiments. Then, once we were confident that we understood the basic nature of the host-guest association, we could proceed to binding experiments using NMR. We, as do many other researchers, find NMR yields a wealth of both qualitative and quantitative data, allowing us to explore the details of the binding event.

Control Experiments.

Important control experiments are absolutely necessary whenever we measure binding affinities. We must rule out binding due to host aggregates. Unless we do, we cannot be certain that changes we observe upon mixing host and guest are caused only by monomeric binding within the cavities of our macrocyclic hosts.

In a crude sense, our host structure resembles that of a classic surfactant. Standard surfactant molecules possess two regions, a polar, water-soluble region and a non-polar hydrophobic or greasy region. These molecules are used to solubilize hydrophobic, water-insoluble species in a detergent fashion. In water, aggregates of surfactants dissolve hydrophobic molecules with their non-polar portions and move them into solution using the solubilizing power of their polar sections. This is one type of intermolecular association or binding interaction. This detergent type

interaction has been extensively studied, as it has enormous commercial value, but this is exactly the type of interaction we must avoid.

Surfactants aggregate to reduce the amount of hydrophobic surface area presented to the surrounding water. This reduces the amount of highly organized water around such surfaces.[99] Aggregates take many forms such as micelles, vesicles or bilayers. These organized structures form at the critical micellar concentration (CMC). Below the CMC the solutions are dilute enough so that the free energy gained from a lack of association is greater than that from aggregation. Each compound has its own characteristic CMC depending on the solvent.

We prefer to perform the binding experiments below the CMC; at concentrations where only monomeric host is present, thus we can observe binding events involving single host molecules.

Critical micelle concentrations can be measured in many ways.[28,30,100] We choose to use NMR, as it is most convenient, and NMR determined CMC's have been shown to agree with CMC's determined by other methods.[28,101] The theory behind an NMR CMC determination is simple.[101] As an aggregated sample becomes more dilute, the complex nature of the aggregate changes. Individual aggregates contain fewer and fewer molecules,

until the concentration is low enough that only momomeric sample is present. As the nature of the aggregates changes the individual environment around each nucleus changes. This change appears in the NMR spectrum (especially ^1H NMR). When below the CMC, the surroundings of each nucleus no longer change on the time-averaged NMR time scale, and the position of a given signal remains constant. A plot of chemical shift vs. concentration shows the CMC at the point where the chemical shifts start to change as the concentration increases. (See Graphs 1–3.) Also, ^1HNMR signals broaden considerably at concentrations much above the CMC, as the mixture becomes heterogeneous.

Host-guest-complex aggregation is another issue that might confuse our interpretation of binding experiments.[29] Most of our guest molecules have surfactant-type structures. Substituted trimethylammonium derivatives, and other ammonium salts, are used commercially as phase-transfer catalysts and surfactants. These molecules have aggregation behavior of their own, and certainly could aggregate in the presence of our hosts as mixed aggregates, or as a host-guest-complex aggregates.

Several situations might arise upon binding different guests. If our hosts bind neutral, water-insoluble guests, then we have increased the net

hydrophobic surface which we must solubilize using the same host carboxylates. This could lower the CMC of the host-guest complex relative to free host. Binding charged, water-soluble guests might lower or raise the CMC of the complex. If oppositely charged host and guest functionalities complexed directly with each other, the complex would be more hydrophobic than the free host and guest, and the CMC would drop. If the charged guest went to the receptor site it might disrupt aggregation by placing charged units in the middle of a hydrophobic aggregate structure. This could raise the CMC.

We did not determine CMC's for our host-guest complexes. To determine these numbers, we would first need to know the binding constant between a given host and guest, and then determine the CMC by an independent method. Light scattering would be appropriate for these measurements. As discussed below, even if some aggregation might be occurring, detailed information can come from NMR experiments. Also, we see specific evidence for aggregate-type binding when operating above the host CMC for the host-guest pair **P** + ATMA. (See the results sections later in this chapter.)

We determined the CMC's of three representative hosts: $\mathbf{P}_{meso}$, in

cesium phosphate buffer; $\mathbf{P}_R$, in borate-d buffer; and $\mathbf{M}_R$, in borate-d buffer. The two *p*-xylyl-linked hosts showed obvious breaks in their chemical shift changes with increasing concentration. These are shown in Graphs 1 and 2.

$\mathbf{P}_{meso}$ shows variable chemical shifts above $\ln[\mathbf{P}_{meso}] = -7.0$ (900 μM). This is taken as the CMC, and all binding experiments were performed below this concentration. $\mathbf{P}_R$ has a lower CMC. Graph 2 shows variable chemical shifts above $\ln[\mathbf{P}_R] = -8.3$ (250 μM). Binding experiments with a single enantiomer of **P** were performed below 250 μM of host. The chiral host has a CMC 3-4 times lower than the achiral host. This could be a consequence of the change in operating buffer (cesium phosphate to cesium borate), or more likely a consequence of the ability of the enantiomerically pure molecules to stack together differently. All the D_2-symmetric $\mathbf{P}_R$ molecules have complimentary senses of twist, and might more easily fit together in a fashion that would minimize the the hydrophobic surface exposed to the surrounding solvent.

$\mathbf{M}_R$ shows different behavior in the CMC plot, Graph 3. We observe no clear end to the chemical shift changes as the concentration drops. Only the signals of two protons change significantly over a large concentration range.

The linker O-CH_2 signal and the very broad, unassigned linker signal both move downfield as host concentration drops, until they cannot be observed above the noise. These downfield shifts are consistent with each host molecule experiencing less of the shielding influence of its neighbors as the concentration drops. We cannot be certain that we are operating below the CMC of $\mathbf{M}_R$ when we do our binding experiments ($[\mathbf{M}_R] \leq 250\ \mu M$). Probably some aggregation of host is occurring, so we rely on chemical shift evidence to provide information about the binding event. Even though aggregation may influence our interpretation of the binding event, we feel that specific and consistent chemical shift-change patterns among the protons of the guest reveal detailed information about how our receptor sites interact directly with individual guest molecules. Similar chemical shifts upon binding for all the protons of a guest are consistent with aggregation events.

Half-molecule Controls

The second important control experiment is what we call the half-molecule control. We need to know what features of our host molecules cause the binding event. Is a given guest entering the preorganized cavity of

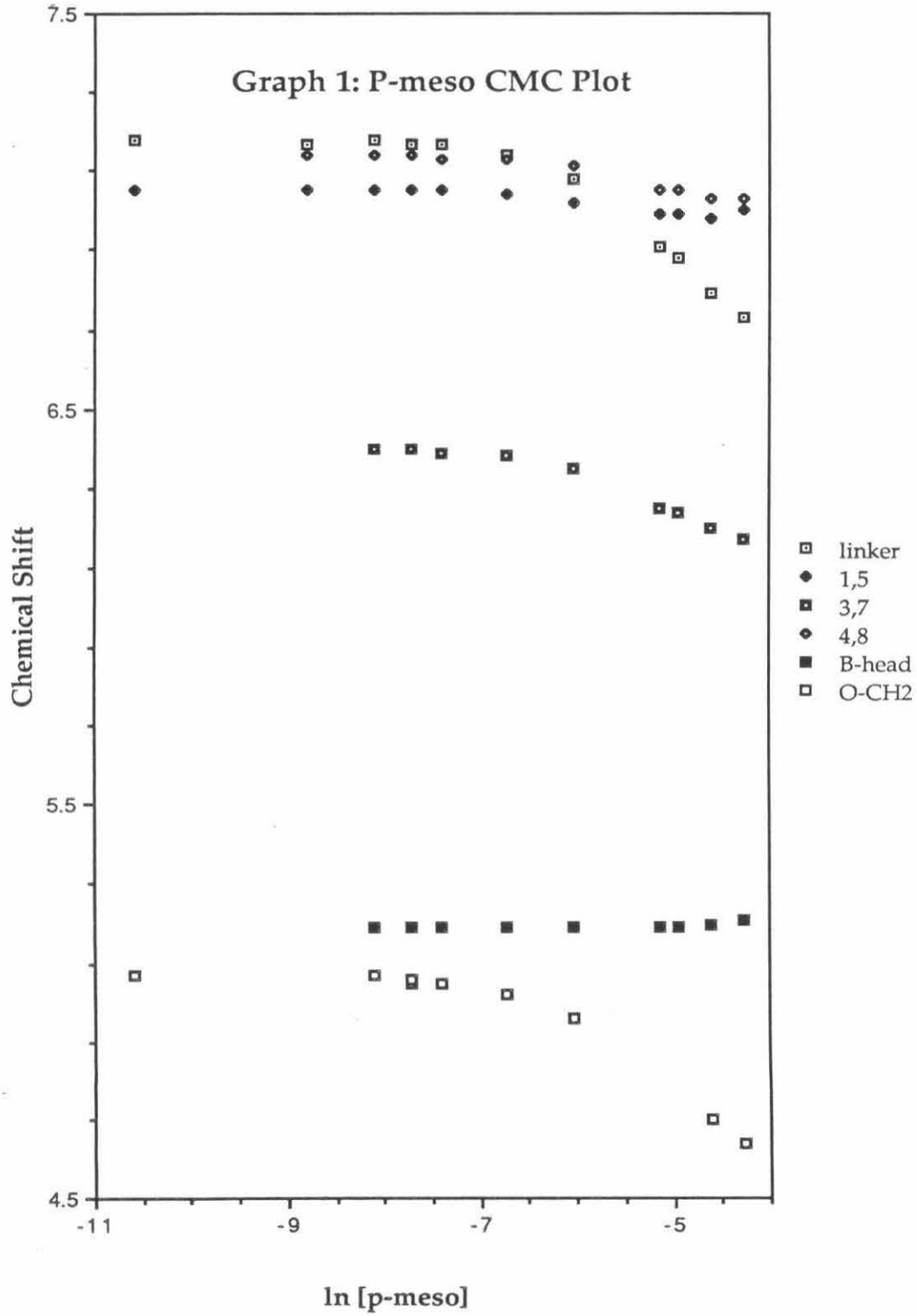
Graph 1: P-meso CMC Plot
7.5
6.5
5.5
4.5
Chemical Shift
-11
-9
-7
-5
ln [p-meso]
linker
1,5
3,7
4,8
B-head
O-CH2

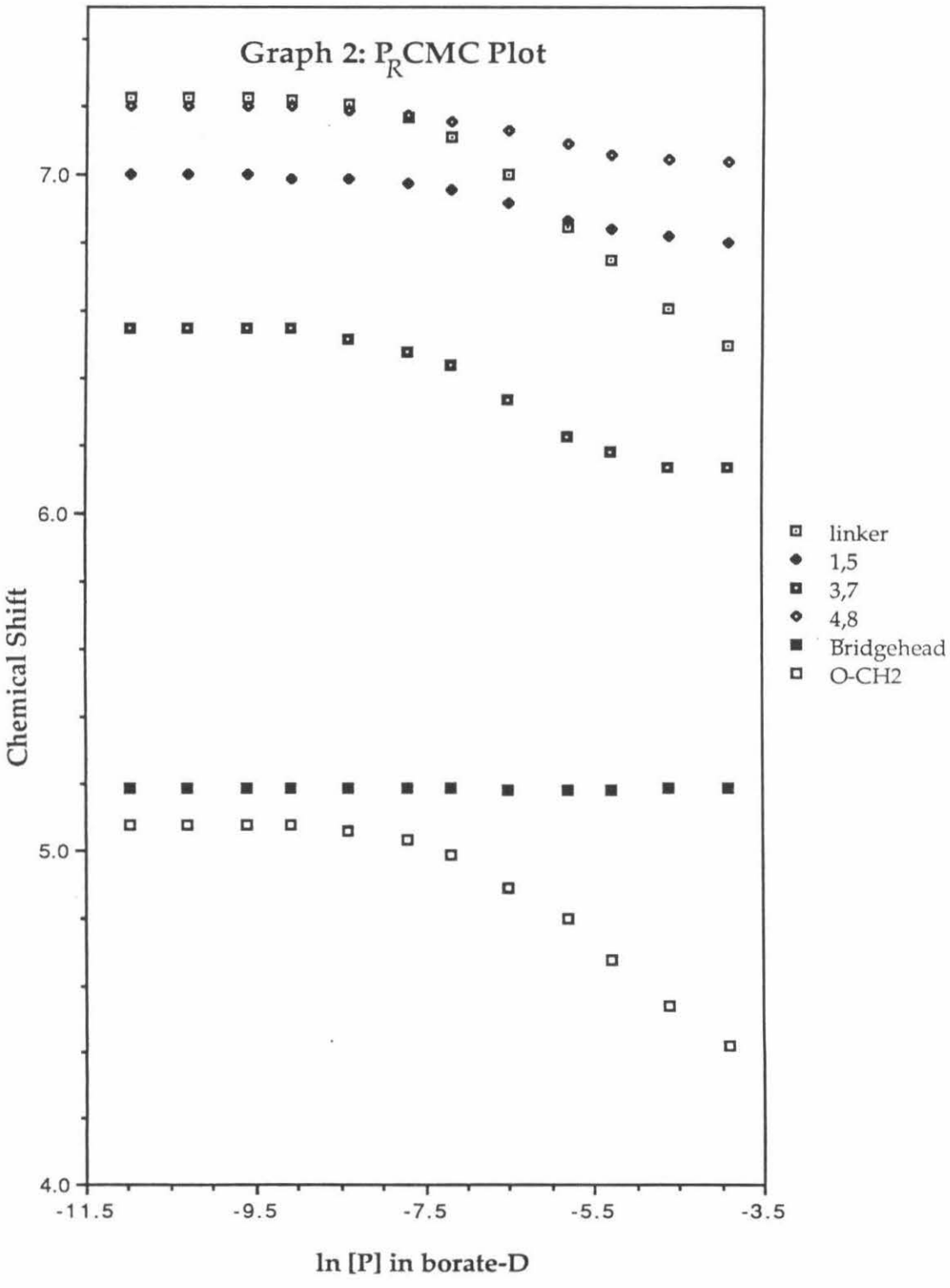
Graph 2: P_RCMC Plot
7.0
6.0
5.0
4.0
Chemical Shift
-11.5
-9.5
-7.5
-5.5
-3.5
ln [P] in borate-D
linker
1,5
3,7
4,8
Bridgehead
O-CH2

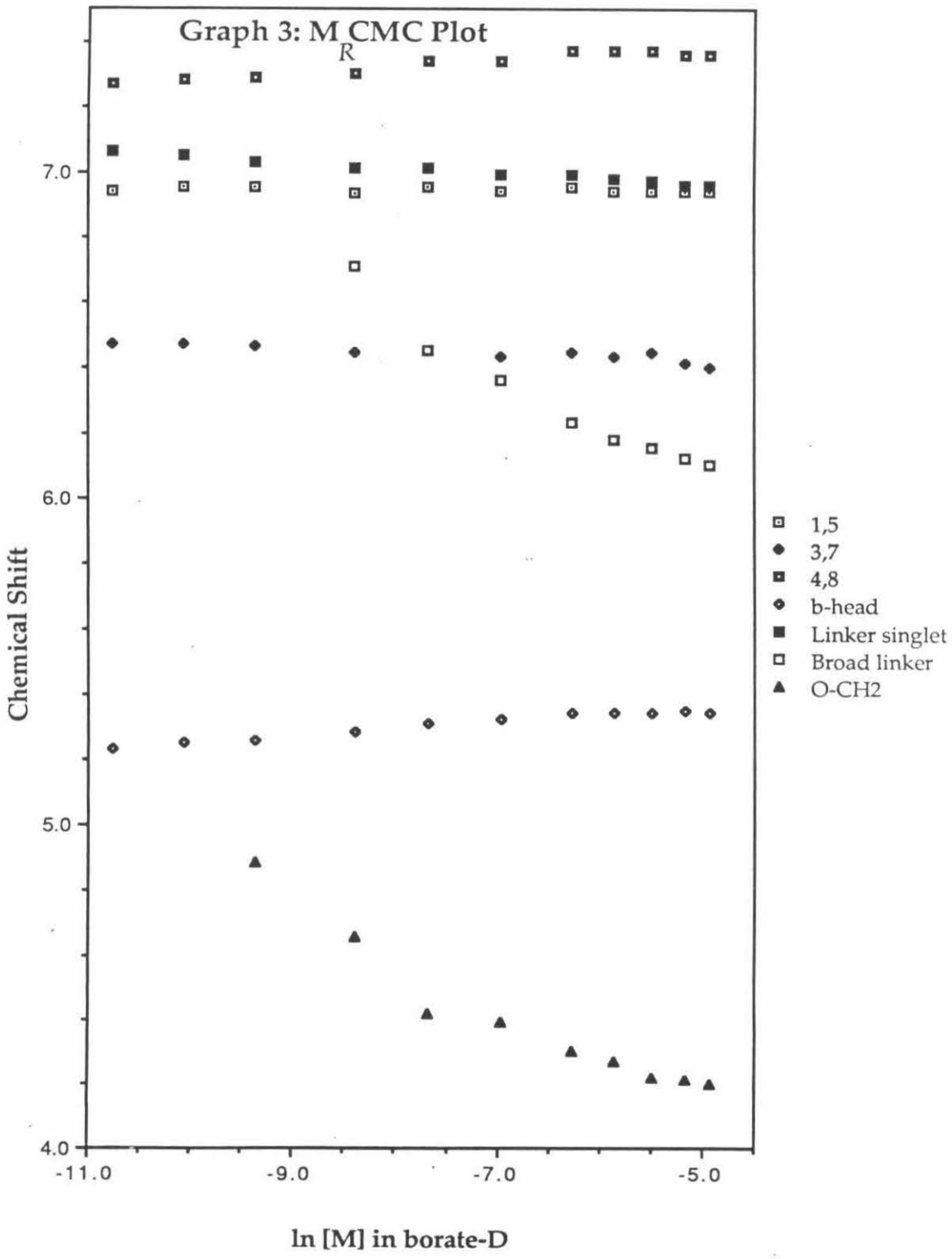
Graph 3: M CMC Plot
R
7.0
6.0
5.0
4.0
Chemical Shift
-11.0
-9.0
-7.0
-5.0
ln [M] in borate-D
1,5
3,7
4,8
b-head
Linker singlet
Broad linker
O-CH2

our hosts, or are there other interactions, such as exterior aromatic stacking or ion pairing, which cause hosts and guests to come together? We precede all of our binding experiments with an experiment in which we use double the concentration of half-molecule 2,6-diethoxy-9,10-dihydro-9,10-ethenoanthracene-11,12-dicarboxylate dicesium salt (**23**) instead of host. This host mimics all aspects of host molecular size, shape and charge distribution, but importantly there is no pre-organized cavity.[102]

For all of our studies, experiments with **23** consistently show very minor evidence of complexation. In the NMR binding experiments, we observe small, non-specific chemical shift changes, with a variety of guests, in both phosphate and borate buffers. Such small shifts are not appropriate input for our MULTIFIT program, (See Chapter 4) and often give unrealistic or nonsensical results. In many cases the digital resolution of our NMR experiments can be >10% of the calculated maximum upfield shifts. Though we cannot calculate accurate binding affinities for the studies with **23**, we feel that no significant evidence for complexation exists. The observed chemical shift changes are typically 100 times greater for a given host-guest complex as compared to the half-molecule control.

Similar results are observed in the extraction studies. (See Chapter 5.)

Compound **23** can extract very minor amounts of guests, as compared to the full macrocycle hosts. The calculated binding affinities for the controls were no more accurate than for the other extraction studies, but generally the affinities of **23** are 10^3-10^4 times smaller than host affinities when measurable. The different affinities calculated in the binding experiments with **23** and dimeric hosts demonstrate the necessity of a pre-organized macrocyclic cavity for the strongest binding interactions. As discussed in the introduction, these results are consistent with others in the field.[27]

NMR binding studies

After we study the aggregation behavior of our hosts, we are ready to observe their binding behavior. Our hosts are extremely well suited for ^{1}H NMR studies, because their spectra are so simple. The D_2-symmetric hosts have molecular weights of >1300 g/mol, yet their proton spectra consist of only 6-8 sets of signals. The signals from the electron-rich aromatic rings of the bicyclic subunit (the 1, 5-; 3, 7-; and 4, 8-protons), and those of the linkers (1 signal for **P**, 2 for **O**, and 3 for **M**) appear at 6.4-7.2 ppm. The signals of the bridgehead and methylene protons appear near the signal of the solvent at

4.6-5.2 ppm. Importantly, the entire upfield region of the spectrum is empty. This allows us to observe aliphatic guest signals without obstruction. The downfield (>7.4 ppm) region of the spectrum, where the signals of many electron-deficient aromatic guests appear, is also free of host signals. We record the guest signals (and sometimes the host signals) as their time-averaged chemical shift positions move (usually upfield) with increasing percentage guest bound. The uncluttered spectra facilitate accurate data collection.

If we use enantiomerically pure host and racemic guest, we observe the signals of two diastereomeric host-guest complexes. This phenomenon has received much attention in the literature,[22,39] but in no way implies any selectivity in the binding event. Diastereomers are different. They must have different NMR spectra. We *always* see diastereomer differentiation when racemic host or guest is used in a binding experiment. When one signal shows for a methylene group of a free guest, usually two signals appear upon binding. Spectra of host-guest complexes reveal details about binding orientations and nothing about the magnitude of the binding affinities. As we will see in the results discussed in this chapter, diastereomeric host-guest complexes may or may not have different binding

Figure 3.1: The flat aromatic guests.

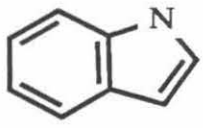

G1
Indole

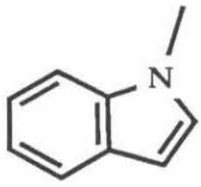

G2
N-Methylindole

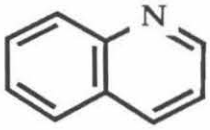

G3
Quinoline

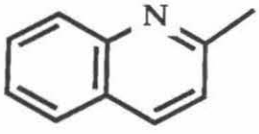

G4
Quinaldine

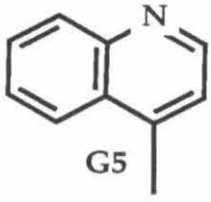

G5
Lepidine

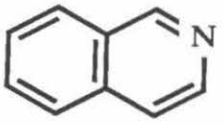

G6
Isoquinoline

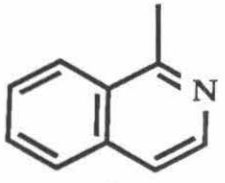

G7
1-Methylisoquinoline

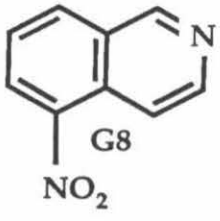

G8
5-Nitroisoquinoline

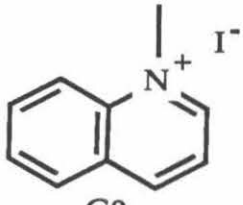

G9
N-Methylquinolinium iodide

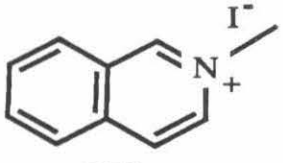

G10
N-Methylisoquinolinium iodide

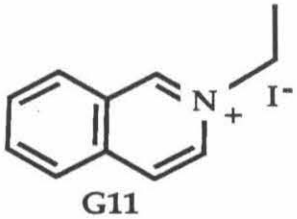

G11
N-ethylisoquinolinium iodide

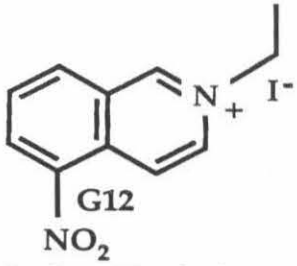

G12
5-nitro-N-ethyl-isoquinolinium iodide

affinities; we can tell only if both affinities are measured independently.

We study a number of guests that have a variety of steric and electronic features, so that we learn as much as possible about our hosts and their ability to interact with different guest features. Figure 3.1 shows the flat aromatic guests that are bound with different binding affinities according to their electronic properties.[35,103] The detailed results of the binding experiments are discussed later in this chapter. The methodology of the NMR binding experiments is discussed in Chapter 4. The calculated maximum upfield shifts for the guest protons are tabulated in Chapter 8.

We also observed a number of non-flat guests, mostly substituted trimethylammonium (TMA) derivatives, and explored the strong attraction between the TMA group and our hosts. More guests are shown in Figure 3.2. Enantiomerically pure TMA derivatives were studied as well, in an investigation of the possible enantiospecific binding abilities of our chiral hosts. The enantiomerically pure guests are shown in Figure 3.3.

Throughout the course of the discussion, we will refer to compounds **IV**, **V** and **C**; hosts with tetramethylene, pentamethylene and *trans*-1,4-dimethylenecyclohexyl linker groups respectively. These three hosts were studied by Michael Petti in our group. Many references are made to these

Figure 3.2: More of the water soluble guests.

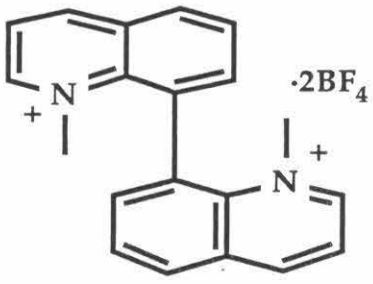

G13
N,N'-Dimethylbiquinolinium bis(tetrafluoroborate)

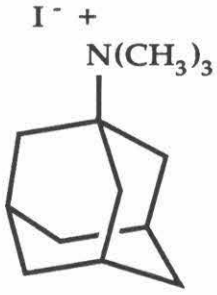

G14
Adamantyltrimethyl-ammonium iodide (ATMA)

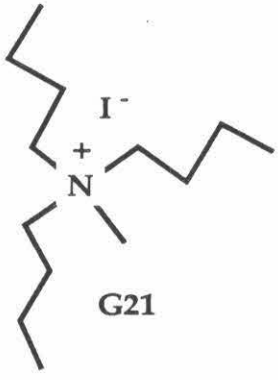

G21
Tributylmethylammonium iodide

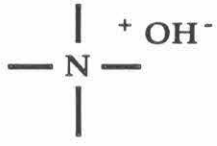

G17
Tetramethylammonium hydroxide

Figure 3.3: Enantiomerically pure guests.

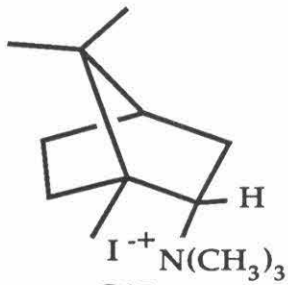

G15
(–)-Bornyl-TMA

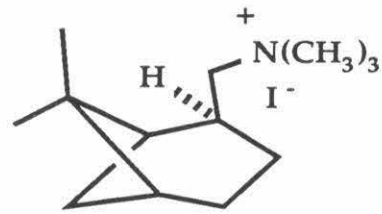

G16
(–)-Myrtanyl-TMA

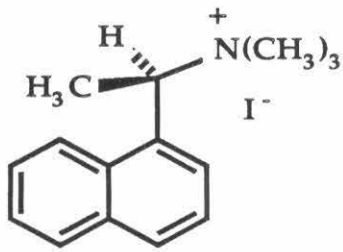

(+)-G18
R-Naphthethyl-TMA

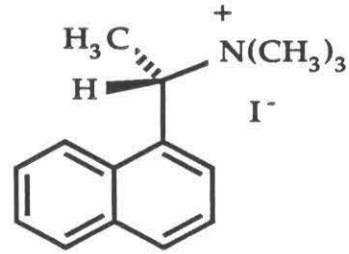

(–)-G18
S-Naphthethyl-TMA

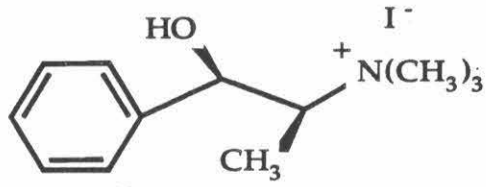

G19
Dimethyl-(–)-ephedrine

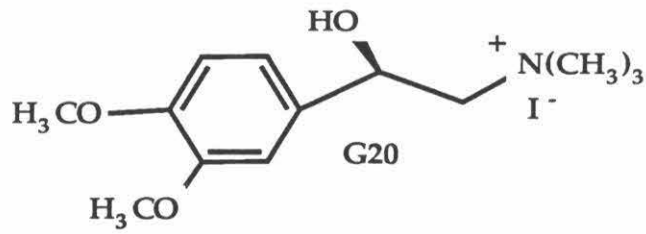

G20
Tetramethyl-(–)-epinephrine

compounds, as studies with them support the results of this work. The details of their syntheses and binding studies are discussed elsewhere.[36,85,104]

P + flat guests

Flat aromatic guests bind within **P** with moderate to exceptionally strong affinities. (See Table 3.1.) **P** binds all of these guests in a conformation decidedly different from the toroidal binding conformation that we envisioned from modeling studies.

Consistent and specific chemical shift changes occur upon the formation of host-guest complexes between **P** and **G1-G12** (flat aromatic guests having C_s symmetry, Figure 3.1). All the proton signals of the guests move upfield. The individual proton signals of **P** also show specific changes. Several host protons move upfield; the 1,5-; 3,7-; O-CH_2; and linker protons all experience shielding upon binding flat aromatic guests. The 4,8-protons shift downfield, as they are deshielded in the presence of the guest. The bridgehead protons are not influenced by the binding event, and do not shift. All of these shifts indicate that **P** binds these guests in a C_2-symmetric rhomboid conformation. (See Figure 3.4.) The two approaches to the cavity

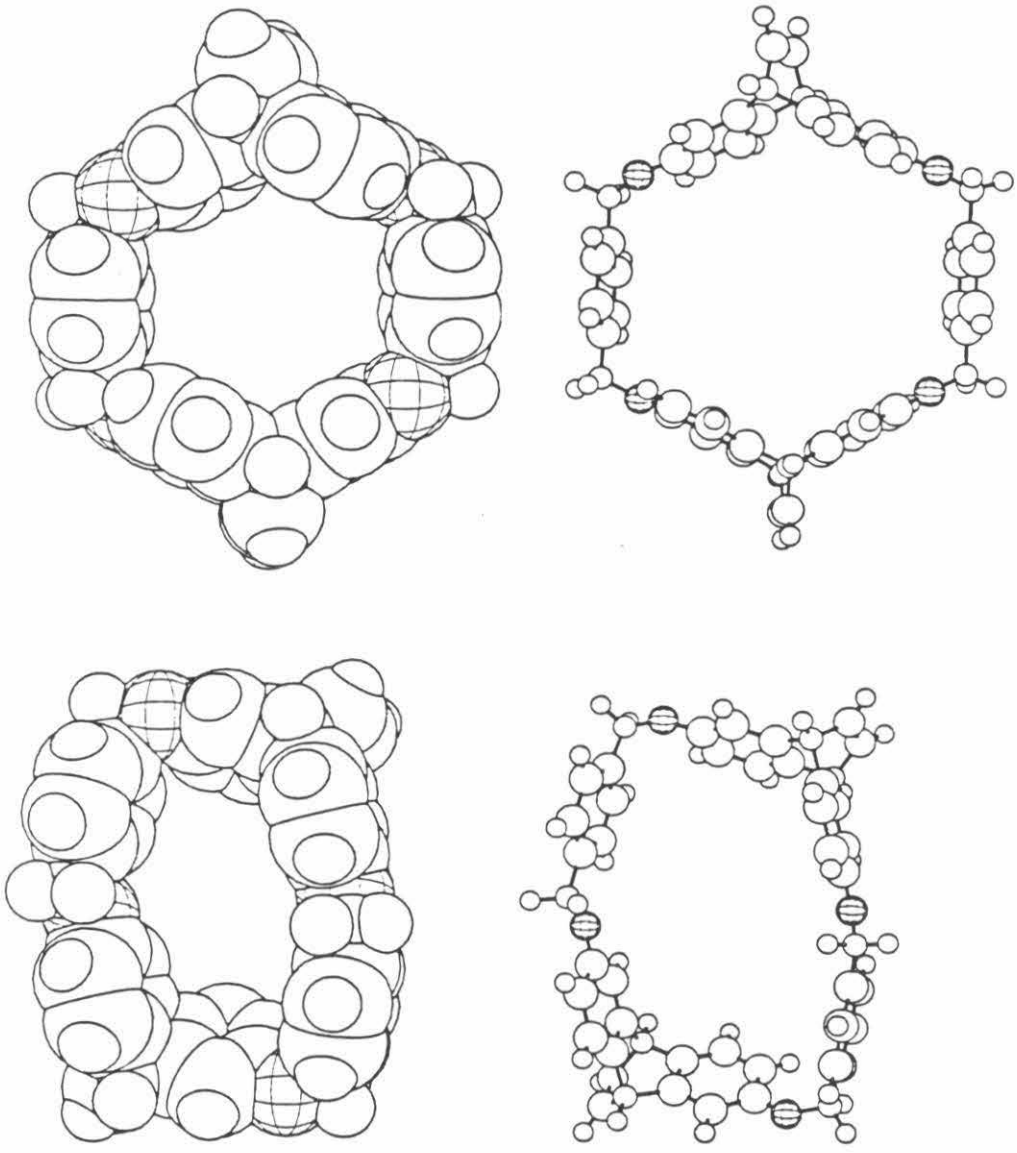

Figure 3.4: The toroid (top), and rhomboid (bottom) comformations for host P_R. The oxygen atoms are hatched, and the cesium carboxylates are truncated for clarity.

are inequivalent in the rhomboid conformation, and the guest binds at the slightly more open side of the host receptor site. This allows the 4,8-protons which lie along the edge of the guest to be deshielded, and the remainder of the host protons to be shielded by the anisotropy above and below the σ plane of the flat guest.[103,105] The bridgehead protons are too far from the guest, and do not experience a significant environment change upon binding.

Table 3.1: Binding parameters for **P** and **M** with guests **G1–G13**.

Guest	Host = **P**		Host = **M**	
	$-\Delta G°$[a]	$K_a(M^{-1})$	$-\Delta G°$[a]	$K_a(M^{-1})$
G1	4.2	1400	[c]	
G2	4.5	2100	4.4	1700
G3	5.4	10000	4.6	2600
G4	5.5	11000	4.5	2000
G5	6.2	38000	4.5	2100
G6	6.3	47000	4.6	2500
G7	6.4	55000	4.5	2100
G8	[b]			
G9	7.6	400000	6.7	100000
G10	7.2	200000	6.6	77000
G11	7.3	260000	6.5	66000
G12	6.7	90000		
G13	[b,d]		[d]	

[a] In kcal/mol at 295K; the values listed are accurate to ±200 cal/mol.

[b] In the presence of host, the guest peaks are extremely broad. Their positions cannot be determined accurately.

[c] No significant complexation observed.

[d] Binding affinities cannot be determined between racemic guests and enantiomerically pure hosts, using our current methods.

The rhomboid cavity is well suited for a naphthalene-sized guest. These guests fit snugly within the cavity without any excess space that would require water molecules to be placed in the hydrophobic receptor site. This situation maximizes hydrophobic binding. We see this with the electron-rich indole (**G1**) and 1-methylindole (**G2**) guests. Here, no strong donor-acceptor (D/A) interactions should exist between the host and guest, which are both electron-rich. The driving force for binding should result from van der Waals attractions between the sparingly soluble indoles and the encapsulating host, as well as from the energy gain associated with expelling the highly organized water surrounding the free host and guest. These interactions result in moderate binding affinities of $-\Delta G°_{295} \approx 4.2$ kcal/mol.

Table 3.2: Solubilities of several guests as determined in borate-d buffer at pD ≈ 9.

Guest	Solubility (M)
G1	0.016
G2	0.0032
G3	0.078
G4	0.023
G5	0.014
G6	0.037
G7	0.030
G9	0.52
G10	0.45
G14	0.14

The rhomboid conformation binds many of the flat aromatic guests with much higher binding affinities. Additional favorable D/A interactions strengthen the binding. The rhomboid conformation is ideally suited for π-stacking interactions with flat aromatic guests. Four of the six aromatic rings of **P** can lie directly above and below the plane of the bound guest. Strong π-stacking D/A interactions are indeed observed between the electron-rich hosts and the electron-deficient quinoline and isoquinoline guests. Similar results with **C** (which has no aromatic linkers*) indicate that the anisole rings of the ethenoanthracene units dominate the π-stacking. These additional attractions are worth at least 1 kcal/mol in binding affinity. (See Table 3.1.) The actual stabilization is probably greater, because the quinolines and isoquinolines are more water soluble than the indoles, (see Table 3.2) and thus should experience a reduced hydrophobic-type attraction.

Quaternized guests quinolinium (**G9**) and isoquinoliniums (**G10**–**G12**) have greatly increased binding affinities with **P**. Very large stabilizations are observed ($\Delta G°_{295} > 7$ kcal/mol) for the N-methyl derivatives **G9** and **G10**, and the N-ethyl derivative **G11**. These are especially notable because these guests are half-molar soluble in the aqueous operating buffer (Table 3.2), and

hence are quite stable when free in solution. This special attraction is an added ion-dipole interaction with the polarizable aromatic linkers. Importantly, **P** binds the charged and uncharged flat aromatic guests in the same conformation. Only slight variations of guest orientation exist among the series **G1–G12**, as determined by the chemical shift-change patterns for the signals of the host and guest. These variations are simply to accommodate any methyl groups protruding from the guests. The flat guests which are substituted in the 2-position (**G4**, **G10–G12**) bind slightly turned from the binding position of the other guests (**G1–G3**, **G5–G9**) because the rhomboid conformation cannot accommodate the entire guest along their longest dimension. The ethyl groups of **G11** and **G12** clearly protrude farther from the receptor site than any other part of the guests. These are only minor readjustments among the guests, and do not affect favorable π-stacking with **P**.

An alternate explanation for the increased binding affinities of the charged guests **G9–G12** is an attractive ion-dipole interaction set up by the electron-deficient nitrogen of the quaternized guest lying between two electron-rich ether oxygens of the host (symbolized, O–N–O). Stoddart demonstrated in several crystal structures[60-66] that a favorable O–N–O

alignment exists in host-guest complexes between electron-rich benzo- and naphtho-crown ether hosts and electron-deficient bipyridinium guests.[59-66] The rhomboid conformation of our hosts can bind guests **G1**–**G12** so as to include this O–N–O alignment. This local arrangement of our hosts and guests would be practically identical to those of Stoddart's crystal structures: two macrocycle oxygens separated by 7-8Å with a quaternized nitrogen of the guest in between. Our NMR-shift evidence cannot define the exact guest orientation upon binding. An O–N–O alignment might exist. Our interpretation of the data remains the same either way.

While the attractive forces associated with an O–N–O alignment may contribute to the stabilities of our host-guest complexes, we feel that the major cause of the increased binding affinities between our hosts and the charged guests is the ion-dipole attraction between the polarizable aromatic rings of the host and the positive charge of the guests. In the rhomboid conformation, host **C** has oxygens in practically the exact same positions as **P**. If the O–N–O alignment caused a large stabilization, then **C** should show the increases in binding affinities shown by **P**. **C** shows the similar affinities for the charged and uncharged flat guests **G3**–**G7**, **G9**, **G10**. The differences in linker structure must cause the differences in binding affinities.

Furthermore, when compared to neutral guests **G1**–**G8**, **M** also shows a large increase in binding affinities for charged guests **G9** and **G10**. We do not see any way that the chemical shift changes upon binding can be consistent with an O–N–O orientation in the host-guest complexes of **M**.

Additional evidence rules out steric considerations as the source of the increased stabilization. As examples, compare guests **G10** with **G4**, and **G9** with **G5** or **G7**. These guests have the same basic shapes (those of a 1- or 2-substituted naphthalene), but the charged guests have the largest binding affinities, and the uncharged guests have smaller similar affinities. This shows that guests with the same size, shape and binding orientation have binding affinities that differ only according to the nature of the guest electronic structure.

The ion-dipole attraction we observe between positively charged nitrogens and aromatic rings is not a novel phenomenon. Burley and Petsko's studies of a number of protein crystal structures indicate a attraction between the electron-deficient nitrogens of lysine, arginine, asparagine and glutamine and the π-faces of phenylalanine, tyrosine and tryptophan.[106] The amino groups of the mentioned residues also avoid the positive dipole at the edges of the aromatic side chains. The electron-rich tyrosine residues have

the highest percentage of amino-aromatic contacts. The most probable amino-aromatic distance is 4.75Å; this is approximately the distance from the center of the aromatic ring of **P** to the center of an isoquinolinium nitrogen bound in the rhomboid conformation. The ion-dipole attraction that we observe is thus similar to the amino-aromatic interaction both observed in proteins and predicted by theory.[107]

When **P** binds the quaternized flat guests, one other phenomenon occurs. The kinetics of the binding event start to become slow on the NMR time scale. This results in broader signals which become difficult to observe at our operating concentration range. The broad signals sharpen upon warming the solution. This effect is also observed with the nitro-aromatics **G8** and **G12** and dissymmetric **G13** .

If we could cool our solvent (the D_2O unfortunately freezes ≈ 5 °C), we would see the signals for both free and bound guest. We could then determine the K_a by an integration of the two signals instead of the iterative fitting procedure discussed in Chapter 4. Slow binding on the NMR time scale allows both a straightforward calculation of K_a, and an unambiguous determination of the guest proton D-values. With future generations of

guests, which have extremely large binding affinities or have slow on/off rates, we hope to observe both free and bound guest.

We experimented with one non-flat quinolinium guest, N,N'-dimethyl-8,8'-biquinolinium bis(tetrafluoroborate) **G13**, synthesized as a racemate. Though binding affinities for this guest were not determined, the binding behavior of **G13** was qualitatively similar to **G9**. Extreme broadening of the guest peaks makes exact chemical shift positions ambiguous. This guest probably does not bind in the rhomboid conformation, but clearly shows a strong affinity for the host.

M + flat guests.

All flat aromatic guests which we studied bind to **M** in a single orientation. The time-averaged bound guests lie in a plane approximately equidistant from the bridgehead carbons of the two ethenoanthracene units. The edges of the guests point at the *m*-xylyl linkers. Figure 3.5 shows a schematic of this binding conformation. As with host **P**, only slight changes in guest binding orientations occur, and these are to accommodate the steric demands of the individual guest within the series **G1–G7, G9–G11**.

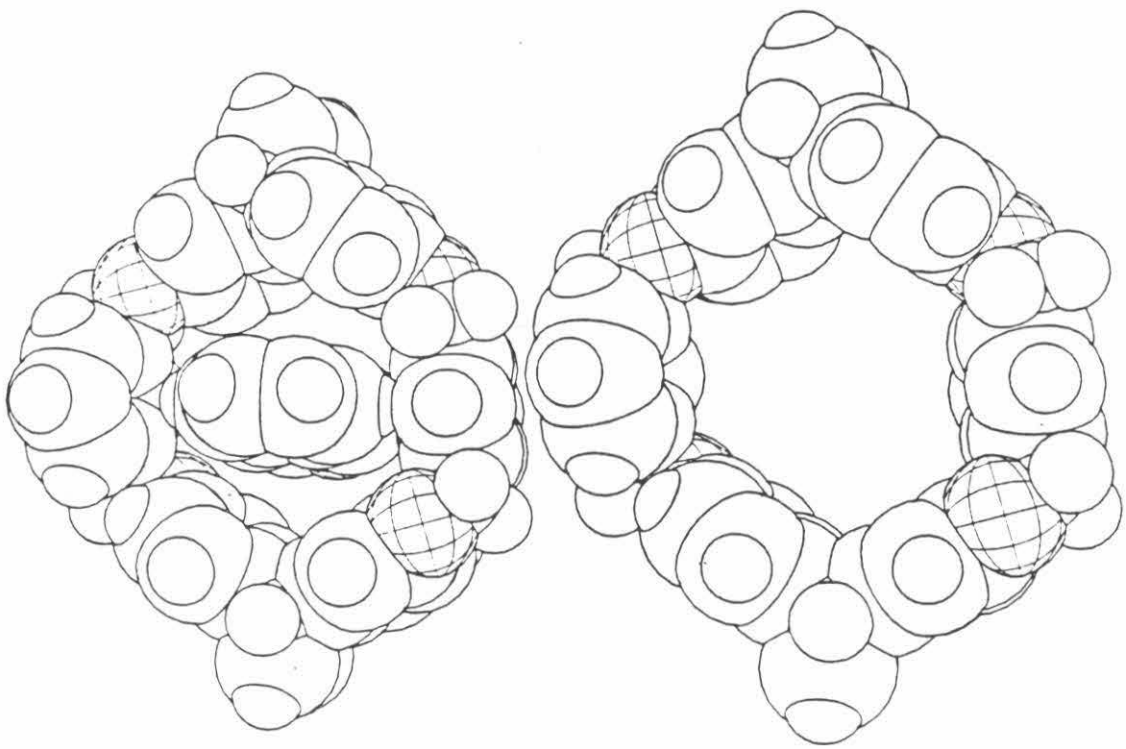

Figure 3.5: Space filling schematic of host $\mathbf{M}_R$ in a toroid conformation (left), and the same host with isoquinoline (**G6**) in the receptor site. No exact binding conformation is implied; the picture is simply consistent with the chemical shift changes observed upon mixing solutions of $\mathbf{M}_R$ and **G6**. The linker proton signals of the host move downfield, and all other host signals move upfield. All guest proton signals move upfield. In the figure, the heteroatoms are hatched, and the cesium carboxylates are truncated for clarity.

Only two values for binding affinities are observed within our error bars. (See Table 3.1.) The neutral flat aromatic guests show a moderate attraction towards **M** ($\Delta G°_{295}$= 4.5±0.2 kcal/mol), and the charged quinolinium and isoquinolinium guests show an exceptional attraction towards **M** ($\Delta G°_{295}$= 6.5±0.2 kcal/mol). The only exception is indole where no significant complexation is observed, and a binding affinity is not calculated.

Importantly, the chemical shift changes upon binding indicate that every flat guest binds in an identical orientation. The chemical shift changes of the host demonstrate the binding orientation. The protons associated with the ethenoanthracene (1,5; 3,7; 4,8; Bridgehead; and O-CH_2) *all* move upfield substantially. The protons of the linker *all* move downfield: the proton *meta* to the alkyl substituents on the linker ring shifts the farthest, the adjacent equivalent protons shift the next farthest, and the proton between the alkyl substituents shifts the least. All the flat guests show this exact same pattern with **M** regardless of their binding affinities.

We feel that the source of these host shifts is the presence of the aromatic guests, not a change in host conformation, because the magnitudes of the shifts are much larger than those observed when **P** binds ATMA (a

host chemical shift change that we ascribe to a host conformational change). Also, if **M** existed in a collapsed conformation, upon opening up to a binding conformation, we would expect the protons of the ethenoanthracene unit to move downfield instead of moving upfield as they do in the presence of guest. These observations strongly indicate that the observed chemical shifts represent one specific type of host orientation.

Modeling studies do not demonstrate an obvious single preferred host conformation. **M** seems to be able to adopt a number of similar conformations which would accommodate our guests and be consistent with the NMR shift data. None of this family of host conformations stands out as being especially well suited for extensive π-stacking interactions. This may account for the moderate binding affinities between **M** and the flat guests. These binding affinities are probably made up mostly of hydrophobic interactions enhanced slightly by some favorable π-stacking.

The extra strong binding affinities for the charged flat guests is a direct measurement of the strength of the ion-dipole effect. The neutral guests and charged guests have the same binding orientations. They possess greatly increased water solubilities (Table 3.2), yet *increase* their binding affinities by 2.0 kcal/mol. The charged guest, in close proximity to the surrounding

polarizable aromatic rings of the host, strongly benefits from the new ion-dipole interaction, even though strong π-stacking interactions are not available (as they are in the rhomboid conformation of **P** with these guests).

One could conceivably argue that the charged guests associate primarily with the oppositely charged carboxylates of hosts **P**, **M**, and **C**. Again we argue that this is highly unlikely. Only if the guests lie within the highly anisotropic receptor site, will their chemical shift positions be so greatly influenced by the surroundings. Besides, any counterion-type association would have a limited effect upon the chemical shifts of the host and guest, and would not greatly influence our binding analysis.

We have achieved one of our original goals: our host receptors are the preferred environment for a number of highly water-soluble guests, as compared to the surrounding solvent. A number of design features of our receptors contribute to their efficiency: the rigid, pre-organized, complementary cavity allows maximum van der Waals contacts while occluding structured water; the aromatic "floor and ceiling" of the rhomboid conformation maximizes π-stacking interactions; and the polarizable aromatic rings have an added ion-dipole attraction to positively charged guests.

P + M bind ATMA.

Early studies with CPK molecular models suggested that an adamantyl derivative would complement the size and shape of our receptor sites. The cylindrical shape fits well within an idealized toroid binding conformation of our hosts. (See Figure 3.4.) We chose adamantyltrimethylammonium iodide (ATMA, **G14**) as an ideal adamantyl derivative for three reasons. First, ATMA is very water soluble, so we can vary its concentration during binding experiments. Second, ATMA has C_{3v} symmetry, requiring a three-fold degeneracy of all protons. This allows us to easily interpret its NMR spectra at the low concentrations necessary for binding experiments. Third, ATMA is readily available from 1-adamantylamine.

Adamantyl derivatives have been studied as guests with different types of hosts, namely cyclodextrins. Detailed thermodynamic parameters have been determined for cyclodextrin hosts binding various adamantyl derivatives.[108,109] These detailed studies deconvolute the parameters of 1:1 and 2:1 host-guest complexes using microcalorimetric and pH titrations. The

results are similar for many host-guest pairs.[108] Small negative ΔH and ΔS values combine to yield moderately exothermic binding affinities. The more water-soluble guest of a charged-uncharged pair binds with a smaller affinity (carboxylate smaller than carboxylic acid, ammonium smaller than amine). The largest binding affinities belong to the host-guest pairs that fit snugly together. This suggests that a combination of van der Waals attractions and favorable solvent reorganization drives the binding event. One notable exception to the above trend is the binding of 1-adamantyl carboxylate to γ-cyclodextrin. This pair shows a moderate binding affinity ($\Delta G°_{295} = -5$ kcal/mol), but the binding event is endothermic $\Delta H = 1.2$ kcal/mol and $\Delta S = 21$ eu. Other cyclodextrin-adamantyl complexes show positive entropies of binding, but none nearly as large. This result is explained[108] as strict hydrophobic binding (solvent reorganization) where the host is too large to benefit from strong van der Waals attractions, though other non-negatively charged adamantyl derivatives bind with much smaller entropies. Some variable temperature studies were performed in our own work with ATMA (**G14**) as the guest.[104] They show results similar to the majority of the cyclodextrin studies; small negative enthalpies and near-zero entropies for

ATMA binding to hosts **5C** and **4C**.

Host **P** binds ATMA very strongly (K_a = 92000M^{-1}). Not only is the association strong, but the cylindrical guest has a specific orientation within the toroid receptor site of **P** as demonstrated by specific chemical shift patterns.[36,87] (See Table 3.3.) **P** binds ATMA such that the C_3 axis of the guest lies roughly along the particular C_2 axis of the host that is parallel to the etheno bridges and that passes through the receptor cavity without touching host atoms or bonds.

There are four rings of protons in ATMA: the ring of methyl protons "A", the ring of methylene protons "B", the ring consisting of both methine protons "C" and of 1/2 the diastereotopic methylene protons "D_1", and finally the other 1/2 of the diastereotopic methylene protons "D_2". (See Figure 3.6 for the ATMA proton identification scheme.) For each proton we calculate D-values, defined as the difference in chemical shift between free and bound states.

With host **P**, the B protons have the largest D-values, all six are directly under the rings of the host. The A protons have somewhat smaller D-values as the time-averaged position of the spinning methyl group always places

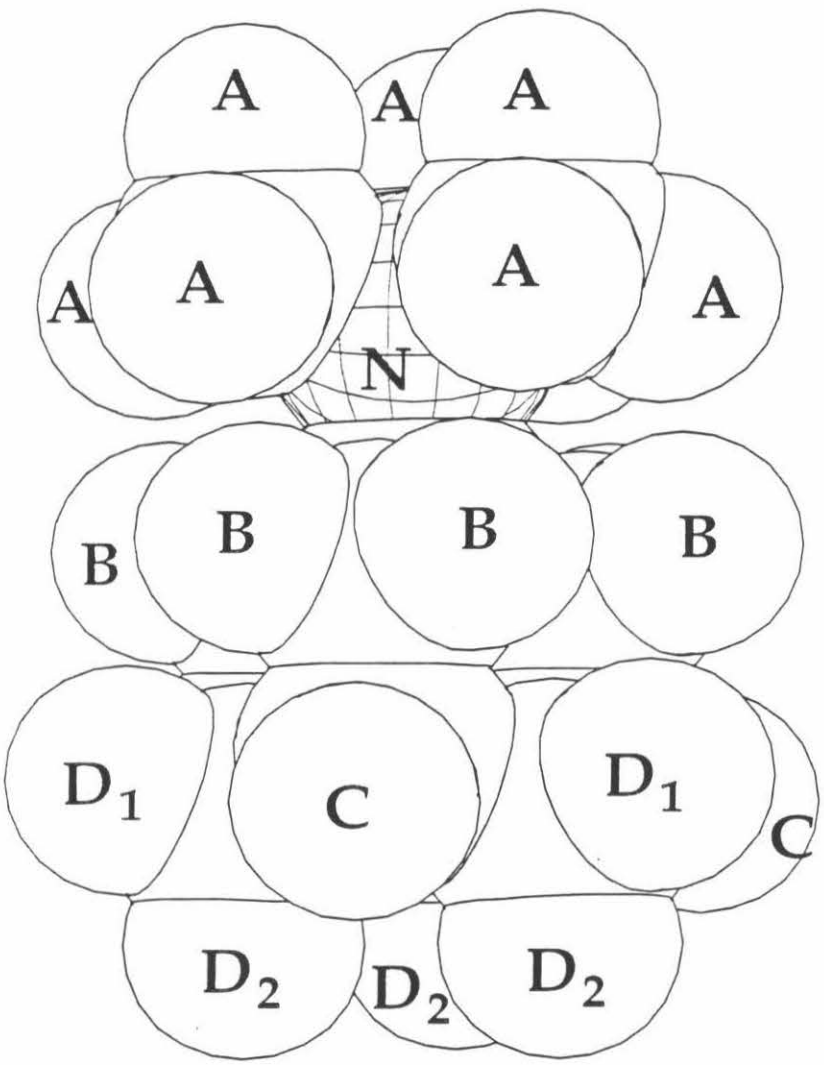

Figure 3.6: The different protons of ATMA: A, B, C, D_1, D_2.

one proton pointing away from the ring anisotropy of the host (in a parallel direction to the D_2 protons). The C and D_1 protons have still smaller but similar D-values as their position when bound is just within the edge of the host cavity. The D_2 protons point away from the surrounding host, out into the solvent, and have the smallest D-values among the ATMA protons bound within **P**.

All of the *p*-xylyl-linked hosts bind ATMA similarly including ±**P** in the phosphate buffer and $\mathbf{P}_R$ *or* $\mathbf{P}_S$ in borate-d. The numbers we originally reported[87] in the phosphate buffer change when our new MULTIFIT procedure is applied to the same data. In phosphate, the binding affinity for P*meso* apparently is much stronger than that for ±**P**. We now think that the numbers determined in the original studies (phosphate buffer) are suspect. The major limitation of these early studies was that over the course of each run, the NMR experiments covered a very limited range of percentage host and guest bound. The fitting procedure is extremely sensitive when solving for large binding constants. We must use data from as large a range of percentage bound as possible, so the multifit procedure can accurately solve for the binding parameters. Our early experiments were not wrong, but we

operated in a range where any small systematic error could yield large variations in the determined binding affinities and D-values. The inconsistencies in our data caused us to report our binding constants as lower limits. We now can determine binding affinities with better accuracy ($-\Delta G°_{295}$ ±0.2 kcal/mol). Not only are our concentration determinations more accurate[110], but we conduct the NMR binding experiments over as large a range as the magnitude of the binding constant allows.

Table 3.3: K_a [a], $-\Delta G°$ [b] and D-values[a,c] for the **P** hosts binding ATMA.

host	D_A	D_B	D_C	D_{D1}	D_{D2}	K_a, M^{-1} [a]	$-\Delta G°$	range[f]
P*meso* [d]	1.70	2.60	1.01	1.18	0.56	990000	8.1	15%
±**P** [d]	1.81	2.89	1.18	1.34	0.65	130000	6.9	15%
P_S [e]	1.76	2.77	1.15	1.24	0.75	80000	6.6	80%
P_R [e]	1.99	3.19	1.24	1.35	0.77	74000	6.6	80%

[a] As determined by the multifit procedure. (See Chapter 4.)
[b] In kcal/mol at 295K; the values listed are accurate to ± 200 cal/mol.
[c] The values for each proton are reported in ppm.
[d] Values determined in phosphate buffer, pD ≈ 7.5.
[e] Values determined in borate-d buffer, pD ≈ 9.0.
[f] The range of percentage guest bound covered in the NMR binding experiment as determined from the calculated K_a.

Differences of binding affinities for a given guest certainly exist between **P***meso* and ±**P**. These differences might not be observable within our reported error bars. We must consider the free energy cost of reorganization from the

ground state. In water, any different affinity of ATMA for $\mathbf{P}_{meso}$ could result because the twisted cavity of $\pm\mathbf{P}$ must reorganize differently than the less twisted cavity of achiral $\mathbf{P}_{meso}$. There seems to be a trend that the *meso* diastereomers bind with higher affinities than the chiral diastereomers. We do not see any obvious reason for such a large discrimination.

The specific chemical shifts upon binding for each ATMA proton unambiguously demonstrate the ability of **P** to bind ATMA in an extremely specific orientation, but this is not the only type of binding that occurs. Specific evidence for another binding mode exists. At higher concentrations, near or above the CMC of **P** the changes in chemical shifts upon adding host become the same for all the ATMA protons. The specific pattern, observed at lower concentrations, no longer occurs above the CMC of the host. Instead, non-specific chemical shift changes occur, in which all the protons A, B, C, D_1 and D_2 show similar changes in environment with increased percentage guest bound. This is completely consistent with non-specific binding in which the guests associate randomly among aggregates of host and host-guest complex. Even as the guest remains bound in the original orientation, aggregates of more host molecules bring additional anisotropy around the

portion of the bound guest which remains exposed to solvent. This yields overall non-specific upfield shifts of the guest.

This is a demonstration of why we operate below the CMC's of our hosts. Above the aggregation threshold, one-to-one binding no longer necessarily occurs. We cannot rule out aggregate-type binding anytime that random, non-selective upfield shifts of the guest occur upon adding host.

The host protons also shift slightly when **P** binds ATMA. All of the host protons move slightly downfield when the host-guest complex forms. This could arise from the host binding the positively charged TMA group. The linker proton signal moves the farthest downfield (≈ 0.2ppm). This is consistent with the chemical shift changes found when **P** binds non-aromatic TMA guests. We feel that this extra shift of the linker-proton signal arises from a change in host conformation upon binding. If the linkers spin in the free host, then their protons are partially exposed to the shielding anisotropy of the ethenoanthracene units and should show a time-averaged upfield shift. When **P** binds a guest in the toroid conformation, then the linkers no longer spin, and they should move slightly downfield. If **P** encapsulates a guest in the toroid conformation, and its linker signal does not shift, we believe a slight shielding influence exists at the linker that compensates the

downfield shift resulting when **P** freezes its linkers.

Interestingly, the adamantyl group alone is not sufficient functionality for strong binding with **P**. Binding experiments with 1-adamantanol showed little evidence of complexation. Changes in guest chemical shifts were barely measurable over a wide range of host-guest concentrations and concentration ratios. Adamantanol is smaller than ATMA, but also freely water-soluble over the ranges of the binding experiments. We expected adamantanol to show at least weak hydrophobic-type binding. Evidently, the driving force for binding adamantanol is insufficient for significant complexation to occur. We conclude that the TMA group is responsible for the majority of the binding affinity between ATMA and **P**. We see this result throughout this work: our hosts have a special affinity for the TMA group.

ATMA, as a guest, shows different binding modes with our different hosts. (See Figure 3.7 for examples of host + ATMA spectra.) Both host **P** and **C** can orient ATMA in their binding sites, yet **P** has a stronger binding affinity by >1.2 kcal/mol. Hosts **P** and **C** are practically identical in size, shape and degrees of flexibility; the only difference between them is their linker structure. The 1,4-dimethylenecyclohexyl linkers of **C** are generally considered to be more hydrophobic than the *p*-xylyl linkers of **P**,[3,13,111] so

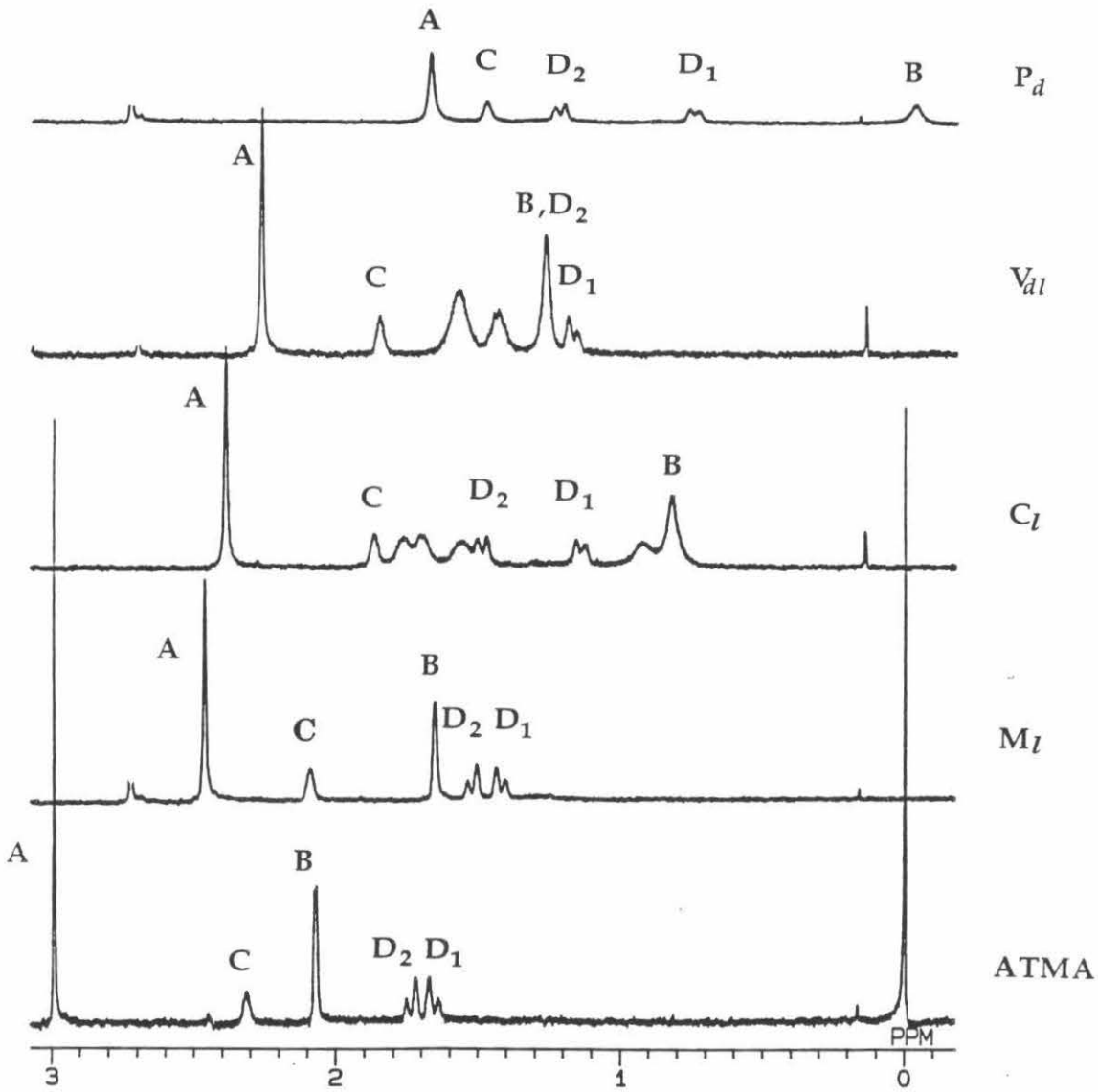

Figure 3.7: ^{1}H NMR spectra of ATMA with various hosts. $[H]_0 = [G]_0 =$ 150μM in borate-D. The peaks at 2.75ppm (DMSO) are truncated for clarity. External reference at 0.00ppm.

hydrophobic binding should make the **C**·ATMA complex more stable, if hydrophobicity is the largest stabilizing force. The aromatic linkers of **P** are more polarizable than the aliphatic linkers of **C**, and should cause the **P**·ATMA complex to be more stable if the ion-dipole effect is the largest stabilizing force. We consider the increased binding affinity of **P**·ATMA to be a direct consequence of the ion-dipole effect. The aromatic linkers of **P** must be the source of the added attraction to ATMA. If increased hydrophobic binding is stabilizing the **C**·ATMA complex as compared to the **P**·ATMA complex, we cannot tell.

Table 3.4: K_a [a], $-\Delta G^{\circ}$ [b] and D-values[a,c] for the **M** hosts binding ATMA.

host	DA	DB	DC	DD_1	DD_2	K_a, M^{-1} [a]	$-\Delta G^{\circ}$	range[e]
M_S [d]	1.28	1.02	0.54	0.58	0.52	8800	5.3	60%
M_R [d]	1.02	0.82	0.43	0.46	0.42	16000	5.7	60%

[a] As determined by the multifit procedure.
[b] In kcal/mol at 295K; the values listed are accurate to ± 200 cal/mol.
[c] The values for each proton are reported in ppm.
[d] Values determined in borate-d buffer, pD ≈ 9.0.
[e] The range of percentage guest bound covered in the NMR binding experiment.

M binds ATMA in a different fashion. The guest has a strong

association with **M** (K_a =10000M^{-1}), but the guest is not specifically oriented as it is with **P**. **M** does not encapsulate ATMA, even though CPK modeling studies indicate that ATMA can fit tightly within the cavity provided. Evidently, the steric demands for complete encapsulation are too strict, thus **M** adopts a slightly less favorable binding conformation (as compared to **P**).

When bound within **M**, the D-values for the A and B protons are much larger than the the smaller values for the C, D_1 and D_2 protons. The host must exist in a partially folded conformation with the guest bound in a hydrophobic cleft. The charged end of the guest is deepest within the cleft and the remainder of the guest points out towards the surrounding water. Almost certainly, we observe the time-averaged result of several similar host and guest binding orientations. One specific orientation, even within a cleft, should differentiate between the C and D_1 set and the D_2 protons. We do not observe this differentiation. Also, **M** has many conceivable conformations with similar binding sites. The linkers can swing into a number of conformations without changing the conformation around aryl-O-CH_2- bonds. This could lead to the semi-specific binding which we observe. The observed results of **M** binding ATMA show the aliphatic portions of the

guest experience moderate hydrophobic binding, and the TMA group maximizes favorable ion-dipole interactions by nesting as close to as many host aromatic rings as possible.

The binding affinities of **M** and **V** are the same for ATMA, as are the guest orientations in the binding sites. We might expect a larger binding affinity for **M** as compared to **V** because of an added attraction between the TMA and the aromatic linkers of **M** (as is observed in the comparison between **P** and **C**). This is not observed. Evidently, the hydrophobic polymethylene linkers of **V** stabilize the **V**· ATMA complex from increased hydrophobic binding to the same extent that the aromatic linkers of **M** stabilize the **M**· ATMA complex from the ion-dipole effect.

Studies of enantioselective binding with various trimethylammonium (TMA) substituted guests.

A series of NMR binding experiments were performed with the chiral aromatic-linked hosts (**M** and **P**), and a series of chiral TMA-substituted guests (TMA guests). We wished to see if our somewhat rigid hosts could discriminate between enantiomers of guests by binding them with

substantially different free energies. The interactions between a single host enantiomer and opposite guest enantiomers are necessarily diastereomeric, but unless the differences between diasteriomeric complexes are substantial, the eventual usefulness of such systems is limited. We would like to design systems that can separate guest enantiomers. This requires both a strong and a selective binding event.

We synthesized a series of enantiomerically pure TMA guests by alkylating various amines. These are shown in Figure 3.3, along with their binding parameters in Tables 3.5–3.7. The bornyl-TMA (**G15**) and myrtanyl-TMA (**G16**) guests were chosen because of their similarity in size and shape to ATMA. As ATMA has a strong binding affinity for **M** and **P**, we felt these two globular aliphatic TMA guests would similarly fill the receptor site for hydrophobic binding while bringing the TMA moiety into a favorable position for an ion-dipole interaction with the host. The only strong binding affinity is between **P** and **G15** . **P** + **G16** and **M** + **G15** and **G16** show only moderate K_a's which are not much larger than the values of simple tetramethylammonium cation (**G13**) as a guest.

As **M** cannot bind ATMA fully enclosed within its receptor site, it also

cannot include similarly sized bornyl-TMA or myrtanyl-TMA. The D-values calculated for bornyl-TMA and myrtanyl-TMA with **M** show that the TMA end of the guest experiences by far the largest upfield shifts as it complexes with the host. The remainder of the guest simply hangs out into the water. The result is only moderate stabilization upon binding these two guests.

$\mathbf{P}_R$ and $\mathbf{P}_S$ both bind bornyl-TMA strongly. Here, the D-values indicate that some of the aliphatic portion of the guest is also pulled into the cavity of the host. The D-value for the TMA is the largest for all the guest protons, but the remainder of the molecule is also strongly associated with the host cavity. This is not as evident when **P** binds myrtanyl-TMA. Here the TMA group is complexed in clear preference over the remainder of the guest. Note that in the myrtanyl-TMA structure the TMA group extends out farther from the main aliphatic skeleton than in bornyl-TMA. The stronger binding for bornyl-TMA might arise from the proximity of the aliphatic skeleton to the TMA. This difference is small, but could cause the bornyl-TMA to experience greater hydrophobic binding as the TMA is brought into an optimal position for ion-dipole interactions.

Though **P** binds bornyl-TMA strongly, it shows no enantiodiscrimination. Interestingly, **P** binds myrtanyl-TMA less strongly, but with much greater enantioselectivity. The factor of 2.7 in K_a for myrtanyl-TMA binding to the opposite enantiomers of **P** is substantial. The K_a of 2300M^{-1} for **P** *S* binding myrtanyl-TMA shows that this association is equivalent to that of **P** *S* binding tetramethylammonium (**G13**), which is purely an attraction to the TMA group. **P** *R* binding myrtanyl-TMA has a K_a of 6300 M^{-1}. This diastereomer has an extra = 0.5 kcal/mol in stabilization as compared to **P** *S* binding myrtanyl-TMA. The nature of this extra stabilization is not clear as the guests bind the enantiomers of **P** in similar conformations.

Table 3.5: Binding parameters for **P** *S* and **P** *R* with guests **G15** –**G17** , **G21** .

Guest	Host = **P** *S*		Host = **P** *R*	
	$-\Delta G°^a$	$K_a(M^{-1})$	$-\Delta G°^a$	$K_a(M^{-1})$
G15	6.5	66000	6.4	56000
G16	4.5	2300	5.1	6300
G17			4.5	2300
G21	5.2	7000		

[a] In kcal/mol at 295K; the values listed are accurate to ± 200 cal/mol.

We also studied chiral guest TMA's containing aromatic rings. (See Table 3.6 and Figure 3.3.) Guests **G18 –G20** provide a series of different molecular environments to place within the host receptor sites. For **G18** binding to **P**, both enantiomers of host and guest provide an excellent cross check of our own results. The two enantiomeric host-guest pairs **(+)-G18** + P_R and **(–)-G18** + P_S as well as the pair **(+)-G18** + P_S and **(–)-G18** + P_R should show identical binding behavior in an achiral solvent. This crosscheck gives us a good estimate of the reproducibility of our experiments. Binding constants determined on enantiomeric host-guest pairs are the same number determined independently. The spread in the numbers obtained helps determine our reported error bars on the binding affinities (± 0.2 kcal/mol).

Table 3.6: Binding parameters for P_S and P_R with guests **(–)-G18** , **(+)-G18 –G20** .

Guest	Host = P_S		Host = P_R	
	$-\Delta G°$[a]	$K_a(M^{-1})$	$-\Delta G°$[a]	$K_a(M^{-1})$
(+)-G18	5.9	25000	6.7	90000
(–)-G18	6.3	45000	5.8	20000
G19	4.7	3300	4.6	2400
G20	5.8	20000	5.7	18000

[a] In kcal/mol at 295K; the values listed are accurate to ± 200 cal/mol.

When binding **G18**, P_R and P_S show enantiodiscrimination in the magnitude of the association constants. Also, distinct and consistent chemical shift changes in both hosts and guests demonstrate different binding orientations for the two diastereomeric complexes. The host-guest enantiomeric pair P_R + **(+)-G18** and P_S + **(–)-G18** has a larger binding affinity than the pair P_R + **(–)-G18** and P_S + **(+)-G18** .

For both pairs, the TMA portion of the guest is bound deepest within the receptor site; the naphthalene is at the edge of the cavity, only partially enveloped by the host. **P** binds **G18** in the toroid conformation, not in the rhomboid conformation. Evidently, when the host binds the TMA portion of **G18**, and part of the naphthalene ring, the complex is more stable than if the host were to bind the naphthalene ring in the rhomboid conformation with the TMA group sticking out into the water. This is true for both diastereomeric **P** + **G18** combinations though they represent different binding orientations. The P_R + **(+)-G18** and P_S + **(–)-G18** pair binds with the C-CH_3 group placed into the cleft of the ethenoanthracene and the smaller methine hydrogen pointing into the xylyl linker. The P_R + **(–)-G18** and P_S + **(+)-G18** pair binds with the C-CH_3 group pointing into the linker

and the methine hydrogen pointing into the ethenoanthracene cleft. (See Figure 3.8) The weaker binding with the P_R + (–)-G18 and P_S + (+)-G18 pair could be a consequence of an an adverse steric interaction between the C-CH_3 group and the host linker when the TMA is at its most favorable position.

Host P binds G19 more weakly than G18, but in the same orientation. Again, the TMA is placed within the center of the toroid conformation host and the aromatic ring sticks out into the water, but the net attraction is weaker and no enantiodiscrimination is observed. The presence of the hydroxyl group of G19 could be the reason for the weaker association experienced with P. The solvated polar alcohol should desire to remain in the water, and would be destabilized by the hydrophobic receptor environment. The nature of the binding event between P and G20 reinforces these conclusions.

P binds G20 with no enantiodiscrimination and a strong binding affinity of 5.8 kcal/mol. Interestingly, P binds G20 in a different orientation than G19. G20 binds with its aromatic ring in the host receptor, as do the flat aromatic guests G1–G12. G20 binds with its TMA group outside the

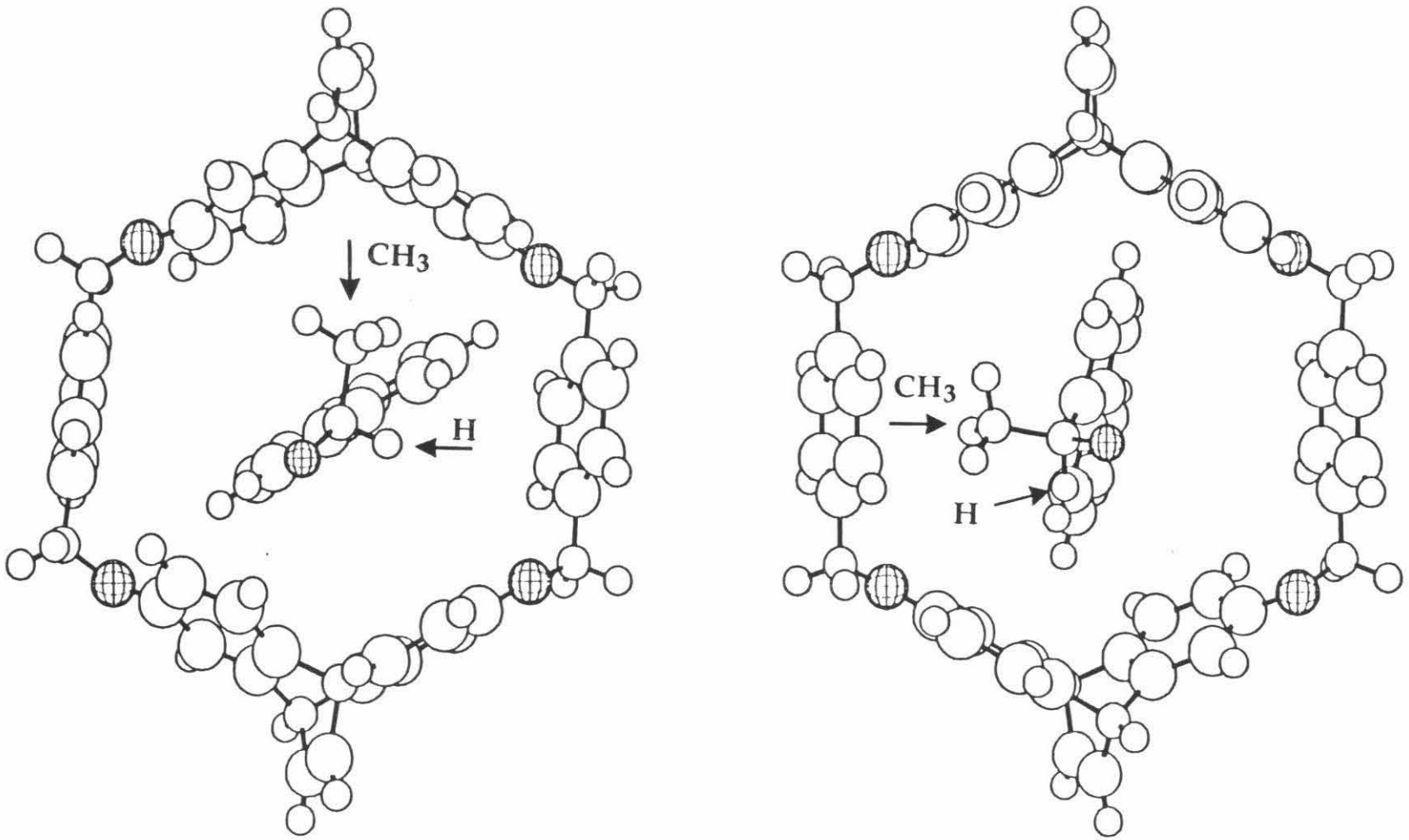

Figure 3.8: Ball and stick schematics of two possible binding conformations for host P_R with guests **(+)-G18** (left), and **(–)-G18** (right). The benzylic methyls and hydrogens are indicated by arrows. The heteroatoms are hatched, and the cesium carboxylates and TMA groups are truncated for clarity.

cavity of the receptor unlike the other TMA guests. Chemical shift data are consistent with the host adapting the rhomboid binding conformation. (See Figure 3.4.) The tri-substituted benzene in **G20** is roughly the size and shape of a naphthalene moiety, and fits well within the cavity of rhomboid **P**. The dimethoxy substituted ring of **G20** is very electron-rich, so we might not expect a strong stabilization when this ring sits within the six electron-rich rings of **P**, but its presence in the cavity is clearly preferred. The D-value of the TMA is much smaller than those of the other methyl groups which clearly sit deeper within the host.

The binding orientation between **P** and **G20** has also been observed with hosts **C** and **V**, which have more hydrophobic, aliphatic linkers. **C** and **V** bind *p*-nitrobenzyltrimethylammonium iodide with the aromatic ring of the guest more closely associated to their receptor sites than the TMA group. Hosts **C** and **V** can bind by including attractions from hydrophobic binding to the nitro-aromatic guest as well as strong π-stacking between this electron-deficient guest and the electron-rich anisole-type rings of the host. When binding **G20**, host **P** should not benefit from these π-stacking interactions

Considering that even electron-rich indoles bind **P** with about 4.0

kcal/mol of binding energy, the affinity of **G20** towards **P** is reasonable. The hydrophobic aromatic ring binds within the hydrophobic host cavity; the water soluble alcohol and TMA functionalities bind at the edge of the cavity, exposed to the water. The overall attraction is still strong, 5.8 kcal/mol. Many of the other host-guest pairs have the opportunity to bind in this fashion but do not. This alternate mode of binding for **G20** probably exists for two reasons. First, **G20** can fill the rhomboid receptor. Second, this conformation keeps the alcohol hydroxyl group outside the hydrophobic cavity, avoiding the energetic cost of desolvating this polar group. Binding a polar hydroxy group is consistently an unfavorable event for our hosts.

When **P** binds **G20**, a balance of binding energies is involved. Other data suggest multiple binding modes may exist in similar situations. $\mathbf{P}_{meso}$ binds benzyltrimethylammonium bromide and *p*-nitrobenzyltrimethylammonium iodide such that both ends of the guest molecules (TMA and aromatic ring) have similar large D-values, and the middle of the guest (CH_2) has an even larger D-value.[104] This might indicate two modes of binding that have similar energetics. One where the TMA of the guest binds with an ion-dipole attraction, and another where the aromatic ring binds with π-stacking and hydrophobic attractions. For most guests the

TMA group prefers the receptor site of **P**. **G20** is the only guest that binds more stably with **P** having the TMA group placed outside the receptor cavity.

Table 3.7: Binding parameters for M_S and M_R with guests **G15 –G21** .

Guest	Host = M_S		Host = M_R	
	$-\Delta G°^a$	$K_a(M^{-1})$	$-\Delta G°^a$	$K_a(M^{-1})$
G15	4.7	2900	4.9	4300
G16	4.7	3100	5.1	5900
G17			4.7	3000
G18	4.2	1400	4.7	3300
G19	4.7	3000	4.9	4000
G20	4.7	3100	5.1	5800
G21			5.0	4900

[a] In kcal/mol at 295K; the values listed are accurate to ± 200 cal/mol.

In contrast to **P**, **M** binds the chiral TMA guests uniformly. All of the *non-flat* TMA guests (**G15 –G21**) bind within experimental error of the same K_a (4300 M^{-1}) The two exceptions are ATMA (discussed earlier, K_a = 10000 M^{-1}) and the pair M_S + **(–)-G18** (K_a = 1400M^{-1}). These uniform moderate associations are attractions between the TMA of the guest and the polarizable aromatic rings of the host, combined with slight hydrophobic attractions. In all cases, the TMA group is most closely associated with the

anisotropy around the host framework, and shows the largest change in environment among the different protons of the guests. Little enantiodiscrimination is demonstrated by **M**. The different binding affinities for opposite enantiomers of **M** binding **(–)-G18** are just outside our stated error bars.

Summarizing the results of the studies of binding chiral guests, we see that the opposite enantiomers of **M** and **P** do not demonstrate strong enantiospecificity with the asymmetric guests **G15**, **G16**, **G18**–**G20**. Either enantiomer of our hosts, which we consider fairly rigid, can adopt different conformations that bind most of these guests equally well. Minor changes in host conformation allow optimal positioning of the TMA groups of the various guests. The enantioselectivity that we do observe outside our large error bars represents a selectivity of about 3 to 1. Our hosts possess too many degrees of freedom to bind all the asymmetric guests with high enantiospecificity.

Our guests also probe the effects of guest rigidity and pre-organization[73] upon the binding event. We look at the binding affinities of the series of TMA guests that are nearly isomers, but differ in three-dimensional structure and rigidity. ATMA (**G14**), bornyl-TMA (**G15**), myrtanyl-TMA

(**G16**) and tributylmethylammonium iodide (**G21**) are aliphatic ammonium salts with similar molecular formulas. **G14** and **G15** are rigid, **G16** has very slightly more conformational flexibility, and **G21** is an extremely floppy molecule. The control guest for this series is tetramethylammonium (**G13**).

Both **P** and **M** have the highest affinity for ATMA among the series of aliphatic guests. (See Tables 3.3 and 3.5.) **P** binds **G15** strongly and both **G16** and **G21** to about the same moderate extent. After ATMA, **M** binds the other aliphatic guests with the same affinity ($-\Delta G°_{295} = 4.9 \pm 0.2$kcal/mol. See Tables 3.4 and 3.7.)

ATMA has a special affinity for our hosts as compared to all the other TMA guests studied. The adamantyl skeleton ties back the aliphatic skeleton slightly and may allow the charged TMA group better access to favorable ion-dipole interactions with the hosts. Also, the smooth, cylindrical shape of ATMA fills complementary host cavities or clefts snugly, maximizing hydrophobic-type binding.

Rigidity seems to have little effect on the binding affinities of the other aliphatic guests. **G15** has a high affinity for **P** as compared to **G16**. This affinity difference seems difficult to rationalize with the observation that **G15** is slightly more rigid or preorganized than **G16**. **G16** is much more

rigid than **G21**, yet binds with a similar or lower affinity. The TMA group striving for the most favorable strong ion-dipole interaction seems to be the major driving force for all of these binding events. If favorable hydrophobic binding can accompany this event, then the binding affinity is increased. If no additional stabilizing or some destabilizing interactions occur when the guest is in position for ideal ion-dipole interactions, then the overall binding affinity is decreased. The fact that **M** binds guests **G15** –**G17**, **G21** with the same affinity supports this conclusion. With **M**, the guest TMA groups associate most closely with the host. The remainder of the guest molecule has various binding interactions that have minor influences on the overall binding affinity.

Conclusion

After observing all the results, we conclude that out hosts are able to successfully bind a large variety of different guests with strong affinities. Strong binding of very water-soluble guests demonstrates true molecular recognition. The driving force of hydrophobic binding alone seems insufficient to bind water-soluble guests. Other stronger forces, such as π-

stacking interactions and the ion-dipole effect, are the major binding forces in our systems, and the largest binding affinities (such as **P** + **G10**) result when a host-guest pair can bind using all of these attractive forces.

Our hosts show some enantiospecificity in binding chiral guests. Though the magnitude of the observed enantiospecificities might not be useful for racemate separations, we do have some insight into how differential binding affinities arise. With the naphthethyl-TMA guests **(+)-** and **(–)-G18** , the placement of the larger group (methyl vs. hydrogen) into the more complementary portion of the receptor leads to stronger binding. (See Table 3.6 and Figure 3.7.) Future generations of hosts could exploit these initial observations and create much improved receptor sites.

CHAPTER 4

Computational Procedures, and Examples of Binding Data

We primarily use ^1H NMR to probe binding affinities between various hosts and guests.[116] Detailed interpretations of our binding experiments are reported in the previous chapter, but some examples of how we calculate the results of a typical binding experiment are shown below. The NMR binding experiment is extremely informative. Specific chemical shift changes reveal the change in environment for an individual proton. The calculated binding affinities and D-values taken together provide us with the information necessary for the detailed interpretation of an entire host-guest association event. Trends in chemical shift changes are solved for binding affinities and maximum upfield shift values (D-values). Positive D-values are reported as upfield shifts upon complexation.

At the fast exchange limit on the NMR time scale, the observed signal (δ_{obs}) for a given host or guest proton is a time-averaged signal weighted by the relative fraction of bound (X) and free (1-X) species multiplied by their respective chemical shifts, δ_{bound} and δ_{free}.

$$\delta_{obs} = X(\delta_{bound}) + (1 - X)(\delta_{free})$$

We perform an NMR binding experiment by incrementally adding

host solutions to a solution of guest and recording the chemical shift changes after each step. The chemical shifts change because the percentage of host and guest bound changes over the course of the experiment. These changes are a unique response to the binding behavior of the particular host-guest pair, and indirectly represent the K_a for the host-guest complex. The MULTIFIT[36,113] procedure simultaneously fits the data from all recorded chemical shift and concentration changes to a single best K_a and a set of best D-values. Over some number of experiments (N), our fitting procedures minimize the function X^2 defined below as

$$X^2 = \sum_{i=1}^{N} (\delta_{calc\,i} - \delta_{obs\,i})^2$$

In the simple fitting procedure, the "goodness of fit" is measured by the root-mean-square (RMS) deviation defined in the equation below. We consider the data to be good if the RMS for a given proton is less than 1% of the calculated D-value.

$$RMS = [\,1/N \sum_{i=1}^{N} (\delta_{calc\,i} - \delta_{obs\,i})^2]^{1/2}$$

In fact, all of the errors considered do not represent the irreproducibility among our different experiments. We report a confidence limit for the binding affinities of ±0.2 kcal/mol in $-\Delta G°_{295}$. This error is a factor of 2 in K_a. For a given experiment, we can operate reproducibly within rather tight error bars. When we attempt to reproduce a number of independently determined values (for example opposite enantiomer hosts with achiral guests), the resulting K_a values have a much larger spread. Because of this error, we report the larger confidence limits for our binding affinities.

The fitting procedure for the binding affinity also yields the chemical shift differences between the bound and free species (D-values). The relative magnitudes of the D-values within a given host or guest show which parts of the molecule are under the strongest shielding or deshielding influences.

Three examples of binding data, as carried through the MULTIFIT analysis, are shown in Tables 4.1, 4.2, and 4.3. The calculated D-values, along with pictures of each of the guests, are shown in Figures 4.1, 4.2, 4.3. The host-guest pairs are **P**$_R$ + **G20**, **P**$_R$ + **G14**, and **M**$_S$ + **G10**. The results of these experiments (performed on a 400MHz NMR spectrometer) are to be

published in Reference 36.

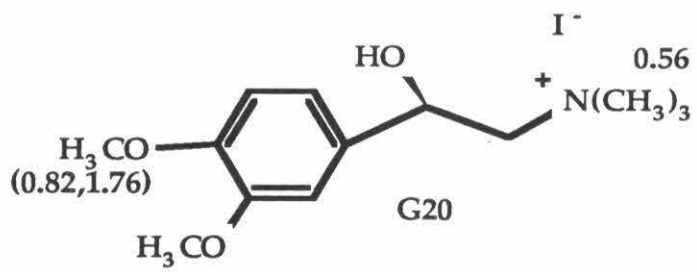

Figure 4.1: Calculated D values (ppm) for P_R + **G20** .

Table 4.1: Output of the MULTIFIT program for the experiment P_R + **G20** .

Best Binding constant = **18137** (M^{-1})

Overall RMS deviation = 0.6966 Hz

PROTON 1: N-Methyl

Chemical Shift of free guest = 1315.92 Hz

Chemical shift of bound guest = 1092.59 Hz

Maximum Upfield Shift = **223.33** Hz

RMS deviation = 0.393 Hz

$[H]_{total}$	$[G]_{total}$	Chem Shift Observed	Chem Shift Calc'd	Calc'd -Obs'd	% G Bound
24.6 µM	408 µM	1303.47	1304.14	0.67	5.277
59.3 µM	393 µM	1286.87	1286.90	0.03	12.994
112 µM	370 µM	1260.01	1259.55	-0.46	25.239

176 μM	343 μM	1225.34	1225.67	0.33	40.411
245 μM	312 μM	1190.92	1190.82	-0.10	56.018

PROTON 2: O-Methyl

Chemical Shift of free guest = 1552.49 Hz

Chemical shift of bound guest = 1223.31 Hz

Maximum Upfield Shift = **329.19** Hz

RMS deviation = 0.341 Hz

$[H]_{total}$	$[G]_{total}$	Chem Shift Observed	Chem Shift Calc'd	Calc'd -Obs'd	% G Bound
24.6 μM	408 μM	1534.67	1535.12	0.45	5.277
59.3 μM	393 μM	1510.01	1509.72	-0.29	12.994
112 μM	370 μM	1469.07	1469.41	0.34	25.239
176 μM	343 μM	1419.19	1419.46	0.27	40.411
245 μM	312 μM	1368.41	1368.09	-0.32	56.018

PROTON 3: O-Methyl

Chemical Shift of free guest = 1557.37 Hz

Chemical shift of bound guest = 855.29 Hz

Maximum Upfield Shift = **702.10** Hz

RMS deviation = 1.089 Hz

$[H]_{total}$	$[G]_{total}$	Chem Shift Observed	Chem Shift Calc'd	Calc'd -Obs'd	% G Bound
24.6 μM	408 μM	1520.51	1520.32	-0.19	5.277

59.3 μM	393 μM	1467.04	1466.14	-0.90	12.994
112 μM	370 μM	1381.10	1380.16	-0.94	25.239
176 μM	343 μM	1271.73	1273.64	1.91	40.411
245 μM	312 μM	1164.80	1164.07	-0.73	56.018

The data shown are: the best overall binding constant (K_a =18137 M^{-1}, $\Delta G°295$=-5.7 kcal/mol); the D values for each of the protons; the differences between the calculated and observed chemical shifts; and the percentage guest bound calculated for each experiment. The D-value for the TMA group (223Hz, 0.56ppm) as compared to those of the methoxy groups (329Hz, 0.82ppm and 702Hz, 1.76ppm) shows that the TMA group is less influenced by the anisotropy of the host receptor site than the methoxy groups. The range of percentage guest bound (5-56%) is adequate for the program to solve for an accurate K_a. This is well behaved data, as the RMS for each proton is much less than 1% of the calculated D value.

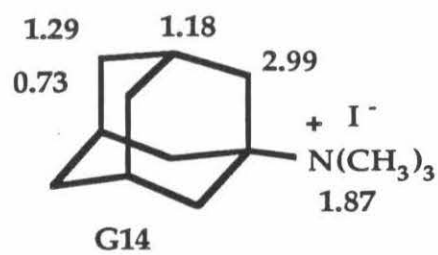

Figure 4.2: Calculated D values (ppm) for P_R + **G14**.

Table 4.2: Output of the MULTIFIT program for the experiment P_R + **G14** .

Best Binding constant = **92101** (M^{-1})

Overall RMS deviation = 5.78 Hz

PROTON 1: N-Methyl (A)

Chemical Shift of free guest = 1196.78 Hz

Chemical shift of bound guest = 451.03 Hz

Maximum Upfield Shift = **747.75** Hz

RMS deviation = 4.77 Hz

$[H]_{total}$	$[G]_{total}$	Chem Shift Observed	Chem Shift Calc'd	Calc'd -Obs'd	% G Bound
1.04 μM	54.5 μM	1183.84	1184.91	1.07	1.587
5.00 μM	52.4 μM	1135.50	1138.52	3.02	7.791
12.9 μM	48.3 μM	1033.69	1041.22	7.53	20.803
26.6 μM	41.1 μM	863.77	867.92	4.15	43.980
49.0 μM	40.2 μM	701.11	695.67	-5.44	67.016

PROTON 2: Methylene (B)

Chemical Shift of free guest = 829.59 Hz

Chemical shift of bound guest = -367.50 Hz

Maximum Upfield Shift = **1197.09** Hz

RMS deviation = 10.37 Hz

$[H]_{total}$	$[G]_{total}$	Chem Shift Observed	Chem Shift Calc'd	Calc'd -Obs'd	% G Bound
1.04 μM	54.5 μM	809.08	810.59	1.51	1.587
5.00 μM	52.4 μM	733.64	736.32	2.68	7.791
12.9 μM	48.3 μM	562.50	580.56	18.06	20.803
26.6 μM	41.1 μM	294.70	303.11	8.41	43.980
49.0 μM	40.2 μM	38.82	27.35	-11.47	67.016

PROTON 3: Methine (C)

Chemical Shift of free guest = 924.81 Hz

Chemical shift of bound guest = 455.26 Hz

Maximum Upfield Shift = **469.55** Hz

RMS deviation = 3.34 Hz

$[H]_{total}$	$[G]_{total}$	Chem Shift Observed	Chem Shift Calc'd	Calc'd -Obs'd	% G Bound
1.04 μM	54.5 μM	919.19	917.36	-1.83	1.587
5.00 μM	52.4 μM	886.96	888.82	1.27	7.791
12.9 μM	48.3 μM	822.51	827.13	4.62	20.803
26.6 μM	41.1 μM	714.60	718.30	3.70	43.980
49.0 μM	40.2 μM	614.10	610.14	-3.96	67.016

PROTON 4: 1/2 Methylene (D_1)

Chemical Shift of free guest = 633.33 Hz

Chemical shift of bound guest = 148.43 Hz

Maximum Upfield Shift = 514.90 Hz

RMS deviation = 4.89 Hz

$[H]_{total}$	$[G]_{total}$	Chem Shift Observed	Chem Shift Calc'd	Calc'd -Obs'd	% G Bound
1.04 μM	54.5 μM	655.03	655.16	0.13	1.587
5.00 μM	52.4 μM	622.32	623.21	0.89	7.791
12.9 μM	48.3 μM	562.50	556.21	-6.29	20.803
26.6 μM	41.1 μM	428.71	436.88	8.17	43.980
49.0 μM	40.2 μM	321.78	318.27	-3.51	67.016

PROTON 5: 1/2 Methylene (D_2)

Chemical Shift of free guest = 695.19 Hz

Chemical shift of bound guest = 404.12 Hz

Maximum Upfield Shift = 291.07 Hz

RMS deviation = 1.29 Hz

$[H]_{total}$	$[G]_{total}$	Chem Shift Observed	Chem Shift Calc'd	Calc'd -Obs'd	% G Bound
1.04 μM	54.5 μM	690.92	690.57	-0.35	1.587
5.00 μM	52.4 μM	672.37	672.51	0.14	7.791

12.9 μM	48.3 μM	631.99	634.64	2.65	20.803
26.6 μM	41.1 μM	566.90	567.18	0.28	43.980
49.0 μM	40.2 μM	501.14	500.13	-1.01	67.016

The above data show the typical trend of D-values for the oriented binding of ATMA demonstrated by hosts **P** and **C** (D-values $A \approx B > C \approx D_1 > D_2$). The RMS deviations are larger for this host-guest pair than for $\mathbf{P}_R$ + **G20**, but still below 1% of the D-values for each proton. These larger D-values may indicate that there are small amounts of other processes occurring (multiple binding, aggregate binding, etc.). Only in one case do we see direct evidence of other events occurring with a large portion of host or guest (this host-guest pair at higher concentrations, discussed in detail in Chapter 3). We feel any significant secondary processes would manifest as very poor fits of the calculated to the observed data. High RMS values may reveal other binding events or experimental errors.

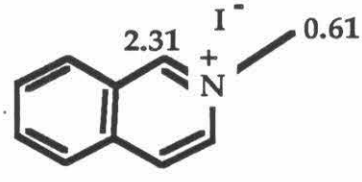

G10

Figure 4.3: Calculated D values (ppm) for $\mathbf{M}_S$ + **G10**.

Table 4.3: Output of the MULTIFIT program for the experiment **M$_S$ + G10** .

Best Binding constant = 63486 (M^{-1})

Overall RMS deviation = 2.54 Hz

PROTON 1: N-Methyl

Chemical Shift of free guest = 1806.40 Hz

Chemical shift of bound guest = 1542.07 Hz

Maximum Upfield Shift = 263.53 Hz

RMS deviation = 2.31 Hz

$[H]_{total}$	$[G]_{total}$	Chem Shift Observed	Chem Shift Calc'd	Calc'd -Obs'd	% G Bound
34.9 µM	322 µM	1774.90	1779.31	-4.41	10.28
73.9 µM	303	1744.14	1746.18	-2.04	22.85
121 µM	280 µM	1701.17	1702.21	-1.04	39.54
178 µM	252 µM	1646.97	1645.91	1.06	60.90
233 µM	226 µM	1601.31	1600.43	0.88	78.16

PROTON 2: #1 position on the isoquinolinium ring

Chemical Shift of free guest = 3858.15 Hz

Chemical shift of bound guest = 2912.55 Hz

Maximum Upfield Shift = 945.60 Hz

RMS deviation = 2.80 Hz

$[H]_{total}$	$[G]_{total}$	Chem Shift Observed	Chem Shift Calc'd	Calc'd -Obs'd	% G Bound
34.9 μM	322 μM	3756.59	3760.96	-4.37	10.28
73.9 μM	303 μM	3644.53	3641.98	2.45	22.85
178 μM	252 μM	3284.18	3282.28	1.90	60.90
233 μM	226 μM	3117.47	3119.09	-1.62	78.16

This last example shows the typical binding of a flat aromatic guest. The aromatic #1 proton shows a much larger D-value than the N-methyl protons (946Hz vs. 264Hz). This is typical for the binding of isoquinolines for both **M** and **P**. The 2-substituted quinolines and isoquinolines cannot fit their longest dimensions into the receptor sites, so the guest turns such that the methyl group sits slightly away from the region of highest anisotropy.

These are just three examples of how we obtain the data used to make conclusions about the binding events. A complete list of calculated D-values is tabulated in Chapter 8, and detailed interpretations of all the binding experiments are discussed in Chapter 3.

A more advanced version of the MULTIFIT procedure is being

developed by Richard Barrans in the Dougherty group that will include error bars derived from the inherent errors of the experimental procedure and weight the data accordingly. Four experimental errors will be considered: the standard deviation in the measurement of NMR peak positions, the standard deviation in the determination of host and guest stock-solution concentrations, the systematic standard deviation in the aliquots dispensed by the volumetric pipets, and the random standard deviation involved with the reproducibility of the pipetting procedures. This will yield standard deviations in δ_{obs} (σ_{dobs}) which will be used in the modified fitting function

$$X^2 = \sum_{i=1}^{N} \frac{(\delta_{calc\,i} - \delta_{obs\,i})^2}{\sigma_{dobs}^2}$$

This improved procedure will fit the data so that those with the least uncertain observed chemical shifts are weighted most heavily.

CHAPTER 5

Binding Studies Using Extraction Methods and Early Studies

Extraction studies are another technique we used to evaluate our hosts. Solid-liquid extraction (SLE) and liquid-liquid extraction (LLE)[28] techniques yield association constants for water-insoluble guests.

The solid-liquid extraction technique involves placing a sample of solid guest (ground to a powder to increase surface area) in a flask, and then adding a solution of the host of known concentration [H_0]. The solution is sonicated overnight, allowed to settle, and filtered through a 0.22 μm filter and/or centrifuged (13000 G, 10 min). A known portion of this solution is back-extracted with several (5-9) known volumes of a water immiscible solvent, such as isooctane or hexane. The back-extractions continue until all the guest is removed from the aqueous layer, as judged by ultraviolet spectroscopy. Surprisingly, as many as nine extractions may be necessary.

The liquid-liquid extraction experiment proceeds in the same way as SLE; however, instead of solid guest, an isooctane solution of the guest is used. The advantage of guest solutions is that such solutions have reproducible concentrations. In contrast, solid guest particles of variable size and surface area present a different amount of guest to the host solution, leading to inconsistent results if equilibrium is not reached. The LLE experiment also has its disadvantages. In the LLE experiment, complete

separation of the two phases after the initial extraction is essential. Any small amount of an organic guest solution in the aqueous phase drastically alters the apparent host-guest concentration. All of the host solution need not be removed for back-extraction, as long as a known fraction is.

The amount of the guest in the organic phase obtained from back-extraction is quantified by ultraviolet spectroscopy. We typically used flat aromatic guests such as naphthalene, anthracene, pyrene, etc., which have well known extinction coefficients[86]. Knowing the extinction coefficients of the guests and the relative volumes of the organic and aqueous phases, we can calculate the concentration of the guest in the original host solution. This total guest concentration ($[G_t]$) represents the free guest in solution plus the guest bound as host-guest complex. The amount of free guest in solution ($[G_f]$) is simply the concentration of a saturated guest solution in the operating buffer. This number ($[G_f]$) is determined by doing the same experiment (SLE or LLE),[114] except that buffer without host is used to extract the solid guest (SLE) or guest solution (LLE). The concentration of the host-guest complex ([HG]) is the total guest concentration present in the aqueous phase less the concentration of free guest ($[HG] = [G_t] - [G_f]$) The equation to

calculate the association constants is the same as before:

$$K_a = [HG] / [H] [G]$$

Expressed in the terms of this experiment where $[HG] = [G_t] - [G_f]$

$$K_a = \frac{[HG]}{([H_0] - [HG])[G_f]}$$

For a variety of host-guest combinations we obtained association constants in the 10^3 - 10^7 M^{-1} range.[85] Unfortunately, we could not obtain highly reproducible association constants with our hosts using these techniques. Though conceptually simple, the SLE and LLE experiments are extremely sensitive to trace contamination from the incorrect phase. We must accurately determine a number of values to derive precise association constants. Very small discrepancies in the calculated values of [HG] lead to large variations in the association constants.

We could not obtain precise quantitative data for the SLE/LLE experiments, yet we feel that the experiments were uniformly a qualitative success. Several controls show that our hosts are able to solubilize aromatic guests by inclusion within their hydrophobic cavities.

SLE/LLE studies using compound **23** (the "half-molecule" at $2[H_0]$)

always showed orders of magnitude less guest solubilization when compared to those studies done with full macrocycles whose cavities were large enough to encapsulate the guest. The molecular shape and charge distribution is not enough to bind these guests; the full macrocycle must be present.

Ultraviolet spectra of the host-guest complex in water show the presence of guest at orders of magnitude higher concentration than the guest's intrinsic water solubility. Several (5-9) extractions with a non-polar solvent are necessary to remove all of the guest from the aqueous layer. Importantly, without host present, these guests transfer quantitatively from the aqueous to the organic layer in a single extraction. The ±**P**· pyrene complex reveals that the long wavelength absorptions of the pyrene are shifted to lower energy (from 320nm to 328nm and from 334nm to 344nm) and the extinction-coefficient values are reduced. (See Figure 5.1.) Other guests demonstrate similar changes in their ultraviolet spectra upon binding. These changes are consistent with other host-guest complexes observed in the literature.[28] Also, we can rule out two types of detergent-type solubilization of guest. The fluorescence excitation of pyrene resulting from pyrene dimer is conspicuously absent from a host-pyrene solution. Only the fluorescence of pyrene monomer is present. This shows that only

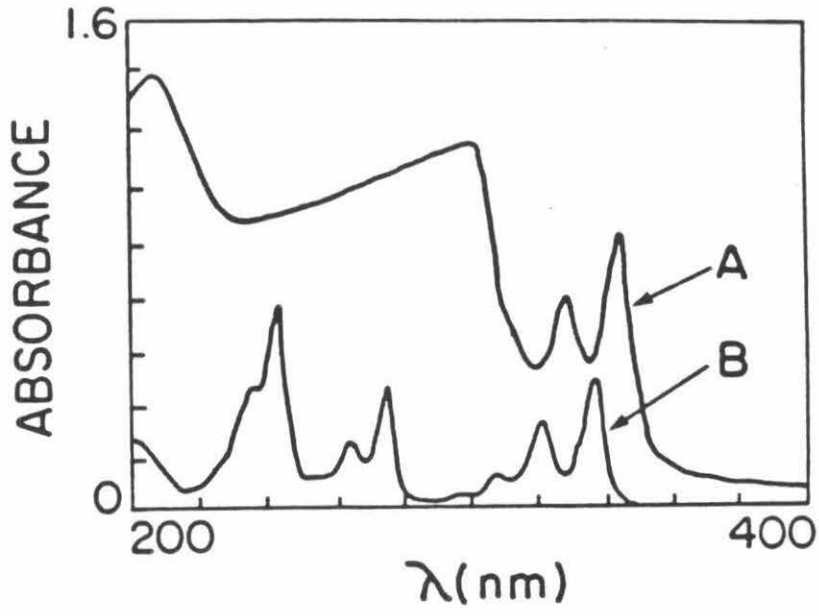

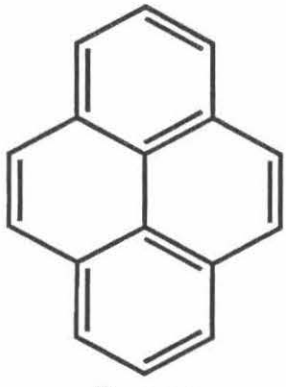

Pyrene

Figure 5.1:

A: UV spectrum of host-guest complex ±P + pyrene. Ka = 2000000 1/M as determined by back extraction.

B: UV spectrum of pyrene in isooctane.

monomeric pyrene, and not microcrystalline or stacked pyrene clusters are present in the host-pyrene solution. We also operate well below the critical micelle concentration (CMC) of our hosts as determined by NMR. This ensures that monomeric host, not aggregates of host molecules, are binding the guests. (See Chapter 3 for CMC graphs.)

There is one unresolved issue here which might be a source of error in these experiments as in the NMR experiments, and that is host-guest complex aggregation. CMC's for a series of different molecules drop as the charge-to-grease ratio decreases. Stated differently, a given polar or charged group can only solubilize a certain amount of hydrophobic surface. Increasing the hydrophobic surface for a constant amount of water-solubilizing ability leads to aggregates, which remove hydrophobic-water interactions at lower concentrations. When our hosts bind flat, water-insoluble aromatic guests, the charged-surface-to-hydrophobic-surface area ratio is substantially decreased. This might lead to irreproducible aggregates of varying host and guest concentrations even though we run these experiments well below the CMC of the free host. We might expect that if the host-guest complex were aggregating that pyrene dimer would show up in the fluorescence spectrum mentioned above, but not necessarily. This

issue could best be resolved by light-scattering experiments which would detect such aggregates.

The magnitude of K_a's determined for a water-insoluble guest by SLE/LLE must be interpreted cautiously, when compared to K_a's for the same host binding a water-soluble guest. Flat aromatic hydrocarbons typically have very small water solubilities.[114] For example, we determined the solubility of pyrene to be $1.2X10^{-6}$ M in 10 mM cesium phosphate buffer. Because of these low water solubilities the smallest measurable K_a for pyrene would be about 10^4 M^{-1} ($\Delta G°_{295}$ = 5.4kcal/mol). In the SLE/LLE experiments the guest is divided in a competition between host receptor site and solid guest or an organic solution of guest. Very little guest actually exists free in the water. In the SLE experiment the K_a is influenced by the stability of the solid within its crystal lattice. In the LLE experiment, the K_a is influenced by the thermodynamic stability of the guest in the organic solvent.

If the guest has a controllable (higher) water solubility, a binding experiment does not require excess guest, present in a second phase, to reach equilibrium. In this case the K_a is measured by other means (see the NMR binding section). More importantly the water-soluble guest is distributed in a

thermodynamic competition between host-guest complex and free guest, both dissolved in water. Here, the K_a can be interpreted strictly as the preference of the guest for the host receptor site as compared to the bulk water medium.

Early Studies

Our first attempts at hosts were based on 2,6-diaminoanthracene (**24**), made from the reduction of commercially available 2,6-diaminoanthraquinone.[115] (See Scheme 5.1.) The electron-rich π-system of **24** would be well suited for a Diels-Alder reaction except that the nucleophilic amines react quickly with most active dienophiles in a Michael-type addition. Protecting groups that mask the nucleophilicity of the amine often mask the electron-donating ability of the amine, as well thereby deactivating the anthracene as a diene. Compound **24** is easily N-tosylated,[116] yielding *N,N'*-ditosyl-2,6-diaminoanthracene (**25**). DMAD does react with **25** yielding the Diels-Alder adduct (**26**), but this molecule does not survive any of the rather severe conditions (e.g., 48% HBr, phenol at reflux) known for removing N-tosyl groups.[116-118] Compound **25** can be combined

Scheme 5.1:

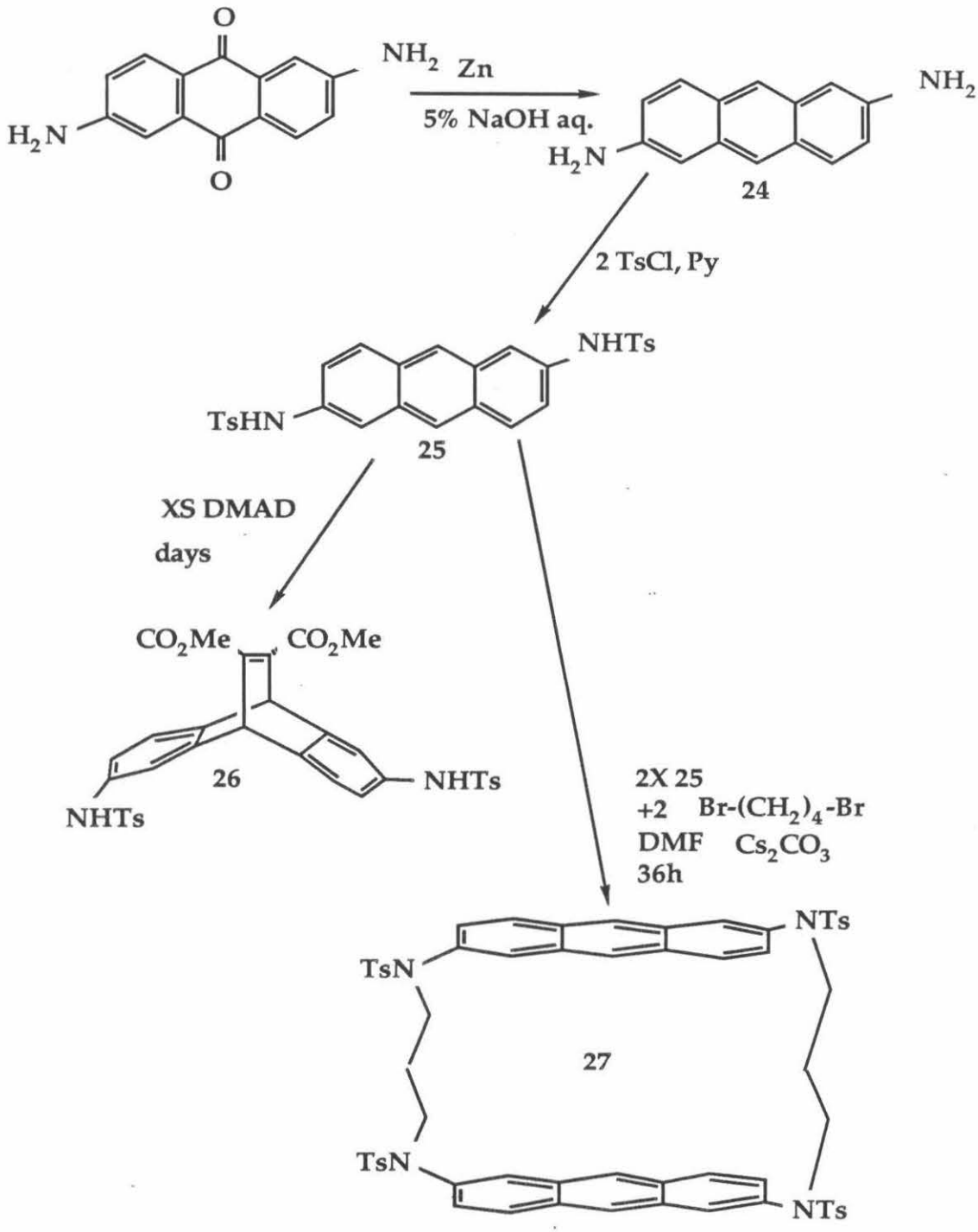
O
NH2 Zn
5% NaOH aq.
H2N
NH2
H2N
O
24
2 TsCl, Py
NHTs
TsHN
25
XS DMAD
days
CO2Me
CO2Me
26
NHTs
NHTs
2X 25
+2 Br-(CH2)4-Br
DMF Cs2CO3
36h
NTs
TsN
27
TsN
NTs

with 1,4-dibromobutane, in the presence of cesium carbonate,[119,120] forming an anthracenophane **27**, but all our attempts at a double Diels-Alder reaction on the insoluble and unreactive **27** are unsuccessful. We have not built a water-soluble aminoanthracene-based host.

With great effort, and often forcing conditions, we probably could have made a series of aminoanthracene-based macrocycles. Unfortunately, the attributes of this system are not consistent with our original goal of an efficient, flexible synthesis. We felt more information would come from a more easily constructed set of molecules, and so proceeded with the hydroxyanthracene-based macrocycles discussed in Chapters 2 and 3.

Another reaction, worth recording here as a potential large-scale anthracene preparation, is the aluminum cyclohexanoxide reduction of 2,6-dibenzyloxyanthraquinone. For similar reactions in the literature see References.124,125. Though the yields of these reductions are not high, no undesired reduction to dihydroanthracene derivatives is observed. An example of one of these reductions is given in the experimental section, Chapter 6.

CHAPTER 6

Experimentals

Uncorrected melting points were recorded on a Thomas-Hoover melting point apparatus. Infrared and ultraviolet spectra were recorded on a Perkin Elmer 1310 infrared spectrometer and a Hewlett Packard 8451 Diode Array Ultraviolet spectrometer respectively. Optical rotations were recorded on a Jasco DIP-181 Digital Polarimeter at 295 ± 2 °C. HPLC was performed on a Perkin Elmer Series 2 liquid chromatograph. Chromatographic eluants are reported as volume-to-volume ratios (v/v). Mass spectra: electron impact (EI MS), Fast Atom Bombardment (FAB MS), and High Resolution (HRMS) were recorded by the University of California at Riverside staff.

Solvents were distilled from drying agents: methylene chloride, CaH_2; toluene, sodium metal; ethereal solvents, sodium benzophenone ketyl. Dimethylformamide was vacuum distilled from calcined CaO, and stored over at least two succesive batches of activated 4Å sieves. All reactions were stirred magnetically under inert atmospheres unless otherwise mentioned.

NMR spectra were recorded on Varian EM-390, XL-200, Jeol JNM GX-400 or Bruker WM-500 spectrometers. Routine spectra were referenced to the residual proton and carbon signals of the solvents, and are reported in ppm downfield of 0.0 as δ values. Binding event spectra were referenced to

external TSP (0.00ppm) in a coaxial reference tube. *J*-coupling is reported in Hz, and peak assignments (when made) are reported in italics before the multiplicity, integration, and coupling constants for each signal.

Host and guest stock solutions for the NMR binding experiments were made up with a standard 10mM deuterated cesium borate buffer at pD ≈ 9. This buffer is referred to in text as borate-d.[123] The buffer was made by dissolving 31.3 mg of boric oxide[124] in 100g D_2O, then adding 467 μL of 1M CsOD in D_2O and mixing thoroughly. All volumetric measurements of these solutions were made with adjustable volumetric pipets. The concentrations of these solutions were quantified by NMR integrations against a primary standard solution of known concentration. All pulse delays for the integration experiments were at least five times the measured T_1 for the species involved.

We determined the solubilities of certain guests in borate-d by first determining the guest ultraviolet absorption values from the stock solutions of known concentration (as quantified by NMR). We then made a saturated solution of the guest in the buffer, passed this solution through a 0.22μm filter and centrifuged the filtrate (13000g, 10min). Ultraviolet spectra were

recorded for known dilutions of the filtrate, and quantified with the absorption values determined earlier.

2,6-Dihydroxyanthracene (2)

We prepared 2,6-Dihydroxyanthracene by a modified procedure of Perkin and Hall[78]. Compound **1** (50g, 0.20mol, 1eq), ethanol (400mL), water (900mL) and ammonium hydroxide (200mL sat.aq.) were placed in a 3L flask fitted with a thermometer, a mechanical stirrer and an argon inlet. Aluminum amalgam, made from granular Al (109g, 4mol, 20eq) dipped in 1.5% aqueous mercuric chloride for 30s was added to the reaction in several portions and the reaction slowly heated to 60-65 °C. The stirring remained vigorous throughout the reaction. This reaction temperature was maintained for 2h by intermittent use of a cool water bath. **Caution** : the reaction can get out of control; higher temperatures lead to over-reduction with the 9,10-dihydroanthracene derivative being formed. After 2h the yellow slurry is cooled to 0 °C, and decanted away from the amalgam onto 1L of ice stirring with 200mL 37% HCl. Any excess acid is destroyed with solid

$NaHCO_3$ (to pH 4-5), and the entire reaction frozen solid and lyophilized. The lyophilized brown solid was slurried with 3x1L of acetone and filtered through a celite pad. The yellow (green fluorescent) anthracene in the filtrate is isolated by evaporating the acetone. The anthracene is stored in the dark at <0 °C. Total recovered, 33g, 78%. This compound can be recrystallized from ethanol. ^1H NMR (acetone-*d*6): δ 7.28 (dd, 2H, *J* =7.5, 1.5), 7.38 (d, 2H, *J* = 1.5), 7.98 (d, 2H, *J* = 7.5), 8.28 (s, 2H), 8.68 (s, 2H, xch. with D_2O). ^{13}C NMR (acetone-*d*6): δ 154.58, 132.29, 130.18, 124.23, 120.98, 107.92.

2,6-Bis(*t*-butyldimethylsiloxy)anthracene (8)

Compound **2** (10.0g, 0.048 mol, 1eq) and *t*-butyldimethylsilyl chloride (21.5g, 0.142 mol, 3eq) were dissolved in 500 mL DMF. Triethylamine (14.4g, 0.142 mol, eq) was added, and the reaction turned black immediately. The reaction is stirred at 35 °C for 8h and cooled to room temperature. The DMF is removed under vacuum, yielding 40g of an orange-black semisolid that is suspended in 100mL petroleum ether/ether (9/1), placed on a 100g flash silica pad and eluted with pet. ether/ether (9/1). The yellow (blue fluorescent)

band was collected and evaporated, yielding **8** which is 95% pure. Pure material was obtained by recrystallizing **8** from hot petroleum ether (35-60 °C) yielding 17.5g of yellow plates (83%), m.p. 111-115°C. ^{1}H NMR ($CDCl_3$): δ 8.17 (*9,10*, s, 2H), 7.82 (*4,8*, d, 2H, *J* = 8), 7.25 (*1,5*, d, 2H, *J* = 2), 7.07 (*3,7*, dd, 2H, *J* = 2, 8), 1.02 (*t-butyl*, s, 18H), 0.26 (CH_3, s, 12H). ^{13}C NMR ($CDCl_3$ at 77.00ppm) δ 151.82, 131.26, 128.98, 128.60, 123.93, 123.17, 113.21, 26.04, 18.56, -3.88. EI MS: 438 (M^+), 381 (M–*t*-butyl). HRMS: 438.2425, calculated for $C_{26}H_{38}O_2Si_2$ 438.2410.

(9 *S*,10 *S*,11 *R*,12 *R*)- and (9 *R*,10 *R*,11 *R*,12 *R*)-2,6-Bis(*t*-butyldimethyl-siloxy)-9,10-dihydro-11,12-dicarboxyethanoanthracene bis-(+)-menthylester (9 and 10)

Di(+)menthylfumarate **(+7)** (1.79g, 4.56 mmol, 1 eq., 4.56mL of a 1 M solution in toluene) was added to a 100mL flask fitted with a thermometer and an argon inlet. The reaction was then cooled to -45 °C in a dry ice/acetonitrile bath. Diethylaluminum chloride (3.3g, 27 mmol, 6eq., 15.2 mL of a 1.8M toluene solution) was then added over two minutes to the

cooled solution, which became orange. After the temperature reequilibrated, **8** (2.00g, 4.56 mmol, 1 eq., 11.2 mL of 0.41 M solution in toluene) was added in a stream over 10 minutes keeping the temperature below -30 °C at all times. Some material precipitated at this temperature. After 15 hours at -45 °C the dienophile reacted and the reaction was warmed to 0 °C. The reaction was carefully poured cold onto 30 mL chilled toluene stirring over 100 mL chilled saturated aqueous sodium potassium tartrate (sat. aq.). (**CAUTION: gas evolution!**) The organic layer and two further toluene extractions of the water were combined, dried ($MgSO_4$),concentrated and chromatographed over 100g flash silica (3-5% Et_2O in hexane). The fractions containing starting material **8** (600mg, 30%, R_f = 0.64), mixed fractions of **9** (R_f = 0.21) and **10** (R_f = 0.29), as well as fractions of pure **10** were collected. The mixture of **9** and **10** was dissolved in 17 mL of pentane at room temperature and chilled slowly to -100 °C. Pure **9** (923mg, 24%, 34% based on recovered starting material) crystallized from solution. The mother liquors contain mostly **10**, and some **9** which can be separated by flash chromatography. The total yield

of Diels-Alder adducts equals 62% (39% **9** and 23% **10**), 89% based on recovered starting material (56% **9** and 33% **10**). Compound **10**: ^{1}H NMR ($CDCl_3$): δ 6.99 (*4,8*, d, 2H, *J* = 8); 6.82 (*1,5*, d, 2H, *J* = 2); 6.50 (*3,7*, dd, 2H, *J* = 2, 8); 4.55 (*O-CH*, td, 2H); 4.51 (*Bridgehead*, s, 2H); 3.30 (*Bridge*, s, 2H); 1.92 (*i-Pr C-H*, d-septets, 2H); 1.77, 1.64, 1.36 (*menthyl CH & CH_2*, m's, 16H); 0.83 (*CH_3*, d, 6H, *J* = 7); 0.92, 0.69 (*i-Pr CH_3's*, 2d's, 12H, *J* = 7); 0.95 (*t-butyl*, s, 18H); 0.15 (*CH_3-Si*, 2s, 12H). ^{13}C NMR ($CDCl_3$, at 77.0ppm): δ 171.31, 153.55, 143.93, 132.43, 125.14, 116.46, 115.40, 74.80, 48.48, 47.06, 46.49, 40.87, 34.38, 31.49, 26.17, 25.87, 23.31, 22.17, 21.20, 18.34, 16.30, -4.04. $[\alpha]_D$ =+58° (c = 2.0, $CHCl_3$), +57° (c = 0.2 , $CHCl_3$). EI MS: 831 (M^+), 438 (compound **8**). HRMS: 830.5326, calculated for $C_{50}H_{78}O_6Si_2$ 830.5337. Compound **9**: ^{1}H NMR ($CDCl_3$): δ 7.13 (*4,8*, d, 2H, *J* = 8); 6.67 (*1,5*, d, 2H, *J* = 2); 6.52 (*3,7*, dd, 2H, *J* = 2, 8); 4.51 (*O-CH*, td, 2H); 4.49 (*Bridgehead*, s, 2H); 3.27 (*Bridge*, s, 2H); 1.96 (*i-Pr CH*, d-septets, 2H); 1.68, 1.64, 1.37(*menthyl CH & CH_2*, m's, 16H); 0.93, 0.82, 0.72 (*CH_3's*, 3d's, 18H, *J* = 7); 0.93 (*t-butyl*, s, 18H); 0.12, 0.11 (*CH_3-Si*, 2s, 12H). ^{13}C NMR ($CDCl_3$, at 77.00 ppm): δ

171.18, 153.36, 141.42, 134.89, 123.63, 116.90, 116.42, 74.84, 48.52, 47.00, 46.49, 40.77, 34.37, 31.43, 26.24, 25.81, 23.32, 22.13, 21.15, 18.23, 16.28, -4.12, -4.15. $[\alpha]_D$ = +13° (c = 0.4 and 0.2, $CHCl_3$). EI MS: 831 (M^+), 438 (compound **8**). HRMS: 830.5358, calculated for $C_{50}H_{78}O_6Si_2$ 830.5337.

(9 *S*,10 *S*)- or (9 *R*,10 *R*)-2,6-Dihydroxy-9,10-dihydro-11,12-dicarboxy-ethenoanthracene bis(+)menthylester (13 or 14)

Diels-Alder adduct **9** or **10** (920 mg, 1.11 mmol, 1 eq) and diphenyl diselenide (553 mg, 1.77 mmol, 1.6 eq) were placed in a flask, and were dissolved in 25mL of toluene. Potassium t-butoxide (348 mg, 3.10 mmol, 2.8 eq, 2.5 mL of a 1.25 M solution in tetrahydrofuran) was added at once, and the yellow solution deposited a tan precipitate. After 5min isopropanol (130 mL) was added to the reaction, and all solids dissolved. HCl (37% aq., 8 mL) was then added, forming a white precipitate. After stirring 18 h, the reaction finished (according to TLC, 1/1 iC_8/EtOAc). Ethyl acetate (250 mL) and $NaHCO_3$ (300 mL sat. aq.), then 1 M potassium phosphate buffer (100 mL, pH = 7) were added to the reaction. The organic layer and another ethyl acetate

extraction of the aqueous layer were combined, dried ($MgSO_4$) and chromatographed (150g flash silica, isooctane/ethyl acetate, 1.2/1). With routine air exposure during the extraction procedure the diphenyl diselenide was quantitatively recovered ($R_f = 0.70$). Clean fractions of the desired product were collected (R_f = 0.36) yielding 650 mg (98%) of off-white solid. Compound **13** (from **9**): ^1H NMR (CD_3CN): δ 7.15 (*4,8*, d, 2H, *J* = 8); 6.88 (*1,5*, d, 2H, *J* = 2); 6.87 (*OH*, s, 2H); 6.42 (*3,7*, dd, 2H, *J* = 2, 8); 5.28 (*Bridgehead*, s, 2H); 4.75 (*O-CH*, td, 2H); 1.98, 1.81, 1.55, 1.38, 1.31, 0.96 (*menthyl CH & CH_2*, m's, 18H); 0.89, 0.88, 0.78 (*3 CH_3's*, 2d's, 18H, *J* = 7). ^{13}C NMR (CD_3CN, at 1.3ppm): δ 165.17, 154.91, 147.05, 146.80, 135.55, 124.65, 112.15, 111.16, 76.14, 52.14, 47.60, 41.39, 34.77, 32.06, 26.89, 24.00, 22.26, 20.92, 16.63. $[\alpha]_D$ = +35.4° (c = 3.4 in CH_3CN). EI MS: 600 (M^+), 280, 235, 210 (compound **2**). HRMS: 600.3427, calculated for $C_{38}H_{48}O_6$ 600.3451. Compound **14** (from **10**): ^1H NMR (CD_3CN): δ 7.17 (*4,8*, d, 2H, *J* = 8); 6.89 (*OH*, s, 2H,); 6.85 (*1,5*, d, 2H, *J* = 2); 6.42 (*3,7*, dd, 2H, *J* = 2, 8); 5.28 (*Bridgehead*, s, 2H); 4.75 (*O-CH*, td, 2H); 2.02, 1.68,

1.49, 1.40 (*menthyl CH's &CH2's*, m's, 18H); 0.89, 0.88, 0.78(3 *CH3's*, 3d's, 18H, *J* = 7). ^{13}C NMR (CD_3CN at 1.30ppm): δ 165.17, 154.90, 146.95, 146.73, 135.54, 124.67, 112.09, 111.11, 76.10, 52.09, 47.57, 41.38, 34.74, 32.04, 26.83, 23.92, 22.25, 20.93, 16.56. $[\alpha]_D$ = +65.2° (c = 2.2, CH_3CN). EI MS: 600 (M^+), 280, 210 (compound **2**). HRMS: 600.3439, calculated for $C_{38}H_{48}O_6$ 600.3451.

(9 *S*,10 *S*)- or (9 *R*,10 *R*)-2,6-Dihydroxy-9,10-dihydro-9,10-etheno-11,12-dicarbomethoxyanthracene (3 *R* or 3 *S*)

Compound **13** or **14** (105mg, 0.175mmol) was dissolved in methanol (5mL). Methanesulfonic acid (0.25 mL) was added dropwise and the reaction brought to reflux. The progress of the ester exchange was followed by TLC (Et_2O). After 40h at reflux, the reaction was cooled to room temperature and mixed with ethyl acetate and 1 M pH7 potassium phosphate buffer (10mL each). The organic layer and another ethyl acetate extraction of the aqueous layer were combined, dried ($MgSO_4$) and concentrated to yield crude product plus menthol. Product could be isolated by crystallization from $CHCl_3$ in

several crops or by flash chromatography (15% pet. ether in ether $R_f = 0.35$). Yield (chromatography) 57mg, 93%. ^1H NMR (CD_3CN): δ 7.17 (*4,8*, d, 2H, *J* = 8), 6.86 (*OH*, s, 2H), 6.84 (*1,5*, d, 2H, *J* = 2), 6.41 (*3,7*, dd, 2H, *J* = 2, 8), 5.32 (*Bridgehead*, s, 2H), 3.71 (*O-CH3*, s, 6H). ^{13}C NMR (CD_3CN at 1.3ppm): δ 166.13, 154.86, 147.64, 146.76, 135.55, 124.74, 112.20, 111.15, 52.76, 51.89. $[\alpha]_D$ = -60° (c = 0.76 CH_3CN). EI MS: 352 (M^+), 293 (M-CO_2Me), 210 (compound **2**). HRMS: 352.0939, calculated for $C_{20}H_{16}O_6$ 352.0947.

2,6-Diethoxy-9,10-dihydro-11,12-dicarbomethoxyethenoanthracene (22)

Ethyl iodide (1.1 g, 7.1 mmol, 568 μL) and ±3 (250 mg, 0.71 mmol) were dissolved in 20 mL of acetonitrile in a dry flask. Cesium carbonate (925 mg, 2.8 mmol) was added and the reaction held at 50 °C for 2h. The reaction was then filtered, concentrated and chromatographed yielding 270 mg of white foam (93%, R_f = 0.28, 2/1 isooctane/ethyl acetate) . ^1H NMR ($CDCl_3$): δ 7.20 (*4,8*, d, 2H), 6.90 (*1,5*, d, 2H), 6.45 (*3,7*, dd, 9H), 5.30 (*bridgehead*, s, 2H), 3.90

(CH_3, s, 6H). ^{13}C NMR ($CDCl_3$ at 77.00ppm): δ 165.99, 156.82, 147.20, 145.79, 135.51, 124.11, 111.49, 109.75, 63.65, 52.34, 51.77, 14.84.

Macrocyclizations:

1. Macrocyclization with racemic bis phenol and benzylic dibromides

(±)Phenol **3** (250mg, 0.7mmol, 2eq) and Cs_2CO_3 (2.8g, 7mmol, 10eq) were placed in an oven-dried 1L flask, and 700 mL DMF was added by cannula. Xylene-α-α'-dibromide (185mg, 0.7mmol, 2eq) was added and the reaction strirred in the dark for 3 days. The solution yellowed slightly, and a fine precipitate formed (CsBr). Acetic acid (1 mL) and flash silica gel (15 mL) were added to the reaction and the solvent stripped on a rotary evaporator. The coated silica was placed on a column of 100 g flash silica, and eluted with 15/1 – 10/1 chloroform/ether. The two dimer macrocycle diastereomers elute together at $R_f = 0.45$. Higher oligomers follow at lower R_f. The *meso* and *d,l* diastereomers were separated and isolated by HPLC on a 1" X 25cm

Vydac 101HS1022 regular phase silica column, eluting with 5-10% acetonitrile in toluene. Yields are for the combined *meso* and *d,l* diastereomers isolated after flash chromatography.

meso -*o*-Xylyl-linked dimer macrocycle, tetramethylester (4a)

^{1}H NMR ($CDCl_3$): δ 7.46, 7.38 (*linker*, AA' BB', 8H), 7.14 (*4,8*, d, 4H, *J* = 8), 6.94 (*1,5*, d, 4H, *J* = 2), 6.55 (*3,7*, dd, 4H, *J* = 2, 8), 5.26 (*bridgehead*, s, 4H), 4.93 (*O-CH*$_2$, AB, *J* = 10.4 Δν = 41.2Hz, 8H), 3.76 (*O-CH*$_3$, s, 12H). ^{13}C NMR ($CDCl_3$): δ 165.94, 156.70, 146.84, 145.72, 136.26, 135.52, 130.38, 128.96, 123.97, 112.19, 110.54, 69.06, 52.38, 51,67. FAB-MS m/e: 909, M+1; 877, M-OCH_3; 849, M-CO_2Me; 766, M-DMAD; 613; 395; 309; 155; 119. HRMS: 908.2801, calculated for $C_{56}H_{44}O_{12}$ 908.2833.

_d,l_ -*o*-Xylyl-linked dimer macrocycle, tetramethylester (4a)

^{1}H NMR ($CDCl_3$): δ 7.46, 7.39 (*linker*, AA' BB', 8H), 7.14 (*4,8*, d, 4H, *J* = 8), 6.96 (*1,5*, d, 4H, *J* = 2), 6.51 (*3,7*, dd, 4H, *J* = 2, 8), 5.26 (*bridgehead*, s, 4H), 4.91

(*O-CH*$_2$, AB, J = 10.2 δν = 48.2Hz, 8H), 3.76 (*O-CH*$_3$, s, 12H). ^{13}C NMR ($CDCl_3$): δ 165.92, 156.74, 146.84, 145.72, 136.30, 135.51, 130.50, 128.99, 124.18, 111.92, 111.04, 69.10, 52.38, 51.68. FAB-MS m/e: 909, M+1; 877, M-OCH_3; 849, M-CO_2Me; 766, M-DMAD; 613; 395; 309; 155; 119. HRMS: 908.2792, calculated for $C_{56}H_{44}O_{12}$ 908.2833.

Combined yield of the two *o*-xylyl diastereomers = 24%.

***meso -m* -Xylyl-linked dimer macrocycle, tetramethylester (5a)**

^{1}H NMR ($CDCl_3$): δ 7.38-7.20 (*linker*, m, 8H), 7.10 (*4,8*, d, 4H, J = 8), 6.93 (*1,5*, d, 4H, J = 2), 6.35 (*3,7*, dd, 4H, J = 2, 8), 5.24 (*bridgehead*, s, 4H), 4.91 (*O-CH*$_2$, AB, J = 11.2, Δν = 68.3Hz, 8H), 3.75 (*O-CH*$_3$, s, 12H). ^{13}C NMR ($CDCl_3$): δ 165.95, 156.52, 147.03, 145.71, 137.63, 135.81, 128.72, 126.08, 125.11, 124.07, 112.11, 109.36, 69.93, 52.36, 51.61. FAB-MS: 909, M+1; 877, M-OCH_3; 849, M-CO_2Me; 817; 766, M-DMAD; 309, 275, 155, 119. HRMS: 908.2784, calculated for $C_{56}H_{44}O_{12}$ 908.2833.

***d,l* -*m* -Xylyl-linked dimer macrocycle, tetramethylester (5b)**

^{1}H NMR ($CDCl_3$): δ 7.37-7.16 (*linker*, m, 8H), 7.08 (*4,8*, d, 4H, *J* = 8), 6.95 (*1,5*, d, 4H, *J* = 2), 6.37 (*3,7*, dd, 4H, *J* = 2, 8), 5.27 (*bridgehead*, s, 4H), 4.99 (*O-CH*$_2$, s, 8H; in benzene-d_6 *O-CH*$_2$, δ = 4.47; AB, *J* = 14.3, Δν + 59.3Hz), 3.77 (*O-CH*$_3$, s, 12H). ^{13}C NMR ($CDCl_3$): δ 165.97, 156.50, 147.09, 145.78, 137.70, 135.92, 128.67, 126.20, 125.53, 124.15, 111.60, 110.50, 69.88, 52.35, 51.67. FAB-MS m/e: 909, M+1; 877, M-OCH_3; 849, M-CO_2Me; 817; 766, M-DMAD; 309; 155; 119. HRMS: 908.2810, calculated for $C_{56}H_{44}O_{12}$ 908.2833.

Combined yield of the two *m*-xylyl diastereomers = 36%.

***meso* -*p*-Xylyl-linked dimer macrocycle, tetramethylester (6a)**

^{1}H NMR ($CDCl_3$): δ 7.28 (*linker*, m, 8H), 7.14 (*4,8*, d, 4H, *J* = 8), 6.96 (*1,5*, d, 4H, *J* = 2), 6.45 (*3,7*, dd, 4H, *J* = 2, 8), 5.27 (*bridgehead*, s, 4H), 4.97 (*O-CH*$_2$, AB, *J* = 12.6, Δν = 28.2Hz, 8H), 3.75 (*O-CH*$_3$, s, 12H). ^{13}C NMR ($CDCl_3$): δ 165.94, 156.33, 146.99, 145.66, 136.96, 135.78, 126.43, 123.95, 112.65, 109.80, 69.72, 52.36, 51.57. FAB-MS m/e: 909, M+1; 877, M-OCH_3; 849, M-CO_2Me; 766, M-DMAD,

309; 155; 119. HRMS: 908.2853, calculated for $C_{56}H_{44}O_{12}$ 908.2833.

***d,l* -*p*-Xylyl-linked dimer macrocycle, tetramethylester (6b)**

^{1}H NMR ($CDCl_3$): δ 7.19 (*linker*, s, 8H), 7.04 (*4,8*, d, 4H, *J* = 8), 6.94 (*1,5*, d, 4H, *J* = 2), 6.42 (*3,7*, dd, 4H, *J* = 2, 8), 5.22 (*bridgehead*, s, 4H), 5.09 (*O-CH*$_2$, AB, *J* = 13.6, Δν = 58.2Hz, 8H), 3.76 (*O-CH*$_3$, s, 12H). ^{13}C NMR ($CDCl_3$): δ 165.95, 156.24, 146.97, 145.66, 136.84, 135.76, 126.71, 123.92, 112.44, 109.92, 69.62, 52.35, 51.56. FAB-MS m/e: 909, M+1; 877, M-OCH_3; 849, M-CO_2Me; 766, M-DMAD, 309; 155; 119. HRMS: 908.2766, calculated for $C_{56}H_{44}O_{12}$ 908.2833.

Combined yield of the two *p*-xylyl diastereomers = 18%.

2. Syringe-pump procedure:

***p*-Xylyl-linked dimer (15 and 16) and trimer (19) macrocycles, per -methyl esters**

Compounds **3***S* or **3***R* (100mg, 0.28mmol. 1eq) and α-α'*p*-xylenedibromide (75 mg, 0.284 mmol, 1eq) were placed in a dried 100 mL flask and dissolved in 10 mL anhydrous DMF. This solution, along with two 5 mL rinsings of the

flask were drawn into a 30 mL syringe, and the syringe was placed in a syringe pump so that the solution would be added to the flask at ≈ 0.45 mL/h (total addition time, 45 h). Cesium carbonate (0.46 g, 1.42 mmol, 5 eq), and more DMF (20 mL) were added to the flask, and the syringe pump was turned on. This reaction was run in the dark. Eight hours after the addition was finished, the syringe was rinsed with a small amount of the reaction mixture. Twelve hours after this, the reaction was filtered and the DMF evaporated. The crude product that remained was chromatographed (20 g flash silica, 5%EtOAc/$CHCl_3$) and the dimer macrocycle (R_f = 0.24, 15 mg, 12%yield) collected. The trimer macrocycle (R_f= 0.16, 12 mg, 10%yield) was also collected, as well as higher oligomers at lower R_f.

Dimer macrocycle (15 or 16)

^{1}H NMR ($CDCl_3$): δ 7.19 (linker, s, 8H), 7.06 (4,8, d, 4H, *J* = 8), 6.88 (1,5, d, 4H, *J* = 2), 6.37 (3,7, dd, 4H, *J* = 2, 8), 5.21 (*Bridgehead*, s, 4H), 5.06 (CH_2, AB, 8H, *J* = 13.6, Δν = 53.5Hz), 3.75 (CH_3, s, 12H). ^{13}C NMR ($CDCl_3$ at 77.00ppm): δ 165.51,

155.88, 146.64, 145.36, 136.58, 135.51, 126.48, 123.70, 112.19, 109.80, 69.67, 52.43, 51.72ppm. $[\alpha]_D$ = +119° (c = 1.1, $CHCl_3$), $[\alpha]_D$ = +144° (c = 1.1 , CH_3CN). FAB MS: M+ 1=909, 878, 849, 766.

Trimer macrocycle (19)

^1H NMR ($CDCl_3$): δ 7.28 (*linker*, s, 12H), 7.14 (*4,8*, d, 6H, *J* = 8), 6.96 (*1,5*, d, 6H, *J* = 2), 6.45 (*3,7*, dd, 6H, *J* = 2, 8), 5.27 (*Bridgehead*, s, 6H), 4.98 (CH_2, AB, 12H, *J* = 12.4, Δν = 27.6Hz), 3.75 (CH_3, s, 18H). ^{13}C NMR ($CDCl_3$ at 77.00ppm) δ 165.48, 156.06, 146.74, 145.46, 136.43, 135.63, 127.07, 123.89, 111.86, 109.92, 69.77, 52.44, 51.86. $[\alpha]_D$ = +17.7° (c = 0.4 , CH_3CN), +15.9° (c = 0.4 , $CHCl_3$) +15.0° (c = 0.2 , $CHCl_3$). FAB MS: M+ 1=1363, 1299, 1220.

The syringe pump procedure was also used to make the *m*-xylyl-linked macrocycles **17**,**18**,**20** and **21**. Flash chromatography used 4% EtOAc/$CHCl_3$ as eluant.

Dimer macrocycles (17 and 18)

R_f = 0.29; yield = 25%; ^1H NMR ($CDCl_3$): δ 7.37 (*linker*, t, 2H), 7.24 (*linker*, d, 4H), 7.08 (*linker*, s, 2H), 7.10 (*4,8*, d, 4H, *J* = 8), 6.93 (*1,5*, d, 4H, *J* = 2), 6.35 (*3,7*, dd, 4H, *J* = 2, 8), 5.25 (*bridgehead*, s, 4H), 5.00 (*O-CH*$_2$, AB, *J* = 13, Δν = 78Hz, 8H), 3.75 (*O-CH*$_3$, s, 12H). ^{13}C NMR ($CDCl_3$ at 77.00ppm): δ 165.45, 156.15, 146.65, 145.38, 137.33, 135.53, 128.41, 125.81, 124.88, 123.80, 111.93, 109.26, 69.97, 52.39, 51.75; $[\alpha]_D$ = -51° (c = 3.2, CH_3CN), $[\alpha]_D$ = -48° (c = 1.6 ,CH_3CN).

Trimer macrocycle (20)

R_f = 0.22; yield = 14%; ^1H NMR ($CDCl_3$): δ 7.36 -7.27 (*linker*, m, 12H), 7.18 (*4,8*, d, 6H, *J* = 8), 7.00 (*1,5*, d, 6H, *J* = 2), 6.50 (*3,7*, dd, 6H, *J* = 2, 8), 5.29 (*bridgehead*, s, 6H), 4.94 (*O-CH*$_2$, s, 12H), 3.75 (*O-CH*$_3$, s, 18H). ^{13}C NMR ($CDCl_3$ at 77.00ppm): δ 165.46, 156.34, 146.72, 145.51, 137.14, 135.75, 128.49, 126.77, 126.40, 123.92, 111.85, 110.00, 70.28, 52.41, 51.91; $[\alpha]_D$ = +19° (c = 1.7, CH_3CN), $[\alpha]_D$ = +18° (c = 0.85 ,CH_3CN).

Tetramer macrocycle (21)

R_f = 0.15; yield = 7%; ^1H NMR ($CDCl_3$): δ 7.42-7.35 (*linker*, m, 16H), 7.25 (*4,8*, d, 8H, *J* = 8), 7.08 (*1,5*, d, 8H, *J* = 2), 6.58 (*3,7*, dd, 8H, *J* = 2, 8), 5.36 (*bridgehead*, s, 8H), 5.02 (*O-CH*$_2$, s, 16H), 3.81 (*O-CH*$_3$, s, 24H). ^{13}C NMR ($CDCl_3$ at 77.00ppm): δ 165.44, 156.31, 146.76, 145.49, 137.33, 135.72, 128.49, 126.54, 125.90, 123.92, 111.82, 110.01, 70.15, 52.40, 51.90; $[\alpha]_D$ =+66° (c = 1.0, CH_3CN). FAB MS: M+ 3=1819, 1742, 1679, 1518.

Methyl ester saponification to macrocycle cesium carboxylates

Macrocycle permethyl ester (10^{-5} mol) was dissolved in 1 mL dimethylsulfoxide, then CsOH (20 mg, 10^{-4} mol, 10 eq) and water (25 mL) were added and the reaction stirred overnight at 35 °C in the dark. The dimethylsulfoxide was washed away from the precipitated product with several successive ether washes. The remaining precipitate was dissolved in 0.5 mL water and passed down a column of Dowex 50X4 (NH_4^+ form). The UV active fractions of the eluant were lyophilized. The resulting white foam

(characterized below) was dissolved in 10mM cesium borate buffer (borate-d, 5-15 mL) and treated with 1 M CsOD in D_2O (20 ml, 20 mmol, 2 eq). These host stock solutions were filtered through a 0.22 μm filter and quantified by NMR integration. Typical yields were 75-95%.

These solutions pick up atmospheric moisture readily upon repeated handling in the open air. Known volumes can be lyophilized and regenerated quantitatively with fresh D_2O.

Spectral data are reported for the *meso* compounds and the racemates. Only the optical rotations are reported for the enantiomerically pure compounds.

O*meso*

^1H NMR(D_2O; external TSP-*d4* at 0.00ppm): δ 7.43, 7.30 (*linker*, AA'BB', 8H); 7.01 (*4,8*, d, 4H, *J* = 8); 6.98 (*1,5*, d, 4H, *J* = 2); 6.57 (*3,7*, dd, 4H, *J* = 2, 8); 5.73 (*bridgehead*, s, 4H); 4.94 (*O-CH2*, AB, *J* = 11.1, Δν = 16.2Hz, 8H). ^{13}C NMR (D_2O; external TSP-*d4* at 0.00ppm): δ 165.27, 155.43, 149.10, 146.58, 137.13,

135.42, 129.25, 127.94, 123.32, 111.57, 109.56, 68.50, 52.35.

±O

^{1}H NMR (D_2O; external TSP-*d4* at 0.00ppm): δ 7.57(*linker*, AA'BB', 8H), 7.19(*4,8*, d, 4H, *J* = 8), 7.16(*1,5*, d, 4H, *J* = 2), 6.59(*3,7*, dd, 4H, *J* = 2, 8), 5.20(*bridgehead*, s, 4H), 5.10(*O-CH2*, AB, *J* = 11, Δν = 113Hz, 8H).

M*meso*

^{1}H NMR (D_2O; external TSP-*d4* at 0.00ppm): δ 6.72 and 5.76 (*linker*, s and br s, 8H), 7.14(*4,8*, d, 4H, *J* = 8), 6.77(*1,5*, d, 4H, *J* = 2), 6.11(*3,7*, dd, 4H, *J* = 2, 8), 5.15(*bridgehead*, s, 4H), 3.96(*O-CH2*, AB, *J* =14, Δν = 99Hz, 8H). ^{13}C NMR (D_2O; external TSP-*d4* at 0.00ppm): δ 174.62, 155.09, 147.75, 147.29, 138.86, 136.80, 128.50, 125.31, 124.03, 123.52, 112.83, 111.59, 70.05, 52.92.

±M , M*R*, and M*S*

^{1}H NMR(borate-d; external TSP-*d4* at 0.00ppm): δ 7.02 (*linker*, s + br s, 8H), 7.26(*4,8*, d, 4H, *J* = 8), 6.97(*1,5*, d, 4H, *J* = 2), 6.44(*3,7*, dd, 4H, *J* = 2, 8),

5.26(*bridgehead*, s, 4H), 4.9(*O-CH*$_2$, AB, *J* =15, 8H). ^{13}C NMR (D_2O; external TSP-*d4* at 0.00ppm): δ 175.38, 155.56, 148.27, 147.66, 139.42, 137.29, 128.95, 125.81, 124.46, 124.19, 113.26, 112.13, 70.33, 52.97. $[\alpha]_D$ (M_R) -37° (c = 0.051 in borate-d). $[\alpha]_D$ (M_S) +37° (c = 0.036 in borate-d).

P*meso*

^{1}H NMR (D_2O; external TSP-*d4* at 0.00ppm): δ 7.14 (*linker*, s, 8H), 7.13 (*4,8*, d, 4H, *J* = 8), 7.04 (*1,5*, d, 4H, *J* = 2), 6.38 (*3,7*, dd, 4H, *J* = 2, 8), 5.19 (*bridgehead*, s, 4H), 5.02 (*O-CH*$_2$, AB, 8H). ^{13}C NMR (D_2O; external TSP-*d4* at 0.00ppm): δ 174.64, 155.00, 147.65, 146.96, 139.08, 136.57, 127.59, 123.88, 113.77, 112.01, 71.69, 52.73.

±P, **P**$_R$, and **P**$_S$.

^{1}H NMR (D_2O; external TSP-*d4* at 0.00ppm): δ 7.21 (*linker*, s, 8H), 7.04 (*4,8*, d, 4H, *J* = 8), 6.84 (*1,5*, d, 4H, *J* = 2), 6.40 (*3,7*, dd, 4H, *J* = 2, 8), 5.60 (*bridgehead*, s, 4H), 5.02 (*O-CH*$_2$, AB, *J* = 13.5, Δν = 39.3Hz, 8H). ^{13}C NMR

(D_2O; external TSP-*d4* at 0.00ppm): δ 176.08, 154.49, 148.59, 146.75, 136.86, 136.29, 126.60, 123.09, 111.69, 109.04, 68.43, 52.34. $[\alpha]_D$ (P_R) -364° (c = 0.021 in borate-d). $[\alpha]_D$ (P_S) +358° (c = 0.058 in borate-d).

2,6-Diethoxy-9,10-dihydro-9,10-ethenoanthracene-11,12 -dicarboxylate dicesium salt (23)

^1H NMR (D_2O; external TSP-*d4* at 0.00ppm): δ 7.05(*4,8*, d, 4H, *J* = 8), 6.77(*1,5*, d, 4H, *J* = 2), 6.20(*3,7*, dd, 4H, *J* = 2, 8), 5.09 (*bridgehead*, s, 4H), 3.57(*O-CH2*, m; decouple at 1.01ppm, AB, *J* = 9, Δν = 15Hz, 8H). ^{13}C NMR (D_2O; external TSP-*d4* at 0.00ppm): δ 171.70, 152.67, 144.95, 144.41, 135.53, 121.33, 108.78, 107.79, 62.36, 49.99, 11.92.

Guest syntheses

Guests **G1–G9**, **G17**, and **G21** were obtained from commercial sources. We synthesized the trimethylammonium (TMA) guests that were not commercially available by exhaustively methylating (5 eq CH_3I) in DMF or acetonitrile solution of the precursor amine (1 M) overnight, at room

temperature. Excess potassium carbonate was added to react with liberated acid when necessary. The reactions were filtered and concentrated. Chloroform was added to dissolve the product and to precipitate inorganics. The chloroform solution was filtered, and ether was added to the filtrate, precipitating the product. The TMA salts were recrystallized from acetonitrile, unless other solvents are mentioned.

(–)-*S* -1-(1)-Naphthylethyltrimethylammonium iodide ((–)-G18)

Plates from toluene/acetonitrile. ^{1}H NMR (D_2O): δ 1.74 (*C-CH*$_3$, d, 3H), 2.91 (*N-CH*$_3$, s, 9H), 5.54 (*CH*, q, 1H), 7.72 (#2, d, 1H), 7.51 (#3, t, 1H), 7.92 (#4, d, 1H), 7.88 (#5, d, 1H), 7.58, 7.49 (#6,#7, 2t, 1H ea.), 8.17 (#8, d, 1H). ^{13}C NMR ($CDCl_3$ at 77.00ppm): δ 132.27, 131.25, 130.37, 128.12, 127.78, 127.35, 126.96, 125.43, 123.97, 123.00, 66.92, 51.45, 16.54. $[\alpha]_D$ = -47°, (c = 0.16 in borate-d).

(+)-*R* -1-(1)-Naphthylethyltrimethylammonium iodide ((–)-G18)

Plates from toluene/acetonitrile. ^{1}H NMR (D_2O): δ 1.74 (*C-CH*$_3$, d, 3H), 2.91 (*N-CH*$_3$, s, 9H), 5.54 (*CH*, q, 1H), 7.71 (#2, d, 1H), 7.50 (#3, t, 1H), 7.92 (#4, d,

1H), 7.87 (#5, d, 1H), 7.57, 7.49 (#6,#7, 2t, 1H ea.), 8.17 (#8, d, 1H). ^{13}C NMR ($CDCl_3$ at 77.00ppm): δ 133.42, 131.88, 131.07, 128.72, 128.32, 127.79, 127.71, 126.12, 124.46, 123.63, 67.57, 52.05, 17.10. $[\alpha]_D$ = +44°, (c = 0.11 in borate-d).

S-(cis)-Myrtanyl-TMA (G16)

^1H NMR ($CDCl_3$): δ 3.78 (*1/2N-CH2*, dd, 1H); 3.56 (*1/2N-CH2*, br d, 1H); 3.22 (*N-CH3, s*, 9H); 2.59 ,2.43, 1.86, 1.10 (*CH, CH2*, m's, 11H); 1.86, 0.94(*C-CH3's*, s, 3H ea.). ^{13}C NMR ($CDCl_3$ at 77.00ppm): δ 76.68, 53.94, 53.82, 47.74, 40.39, 38.30, 35.77, 27.40, 25.75, 23.82, 23.39. $[\alpha]_D$ = +23°, (c = 0.10 in borate-d).

R-α-trimethylammoniummethyl-3,4-dimethoxybenzylalcohol iodide salt (Tetramethylepinephrine) (G20)

Cesium carbonate was used instead of K_2CO_3 for the alkylation reaction. ^1H NMR (borate-d; external TSP-*d4* at 0.00ppm): δ 7.09 (*Arom*, m, 3H); 5.36 (*C-H*, d, 1H); 3.96 (*O-CH3*, s, 3H); 3.88 (*O-CH3*, s, 3H); 3.69, 3.51(*CH2*, 2dd, 2H); 3.29 (*N-CH3*, s, 9H). ^{13}C NMR (CD_3CN at 1.3ppm): δ 141.24, 132.93,

118.63, 114.65, 111.83, 110.26, 71.04 68.45, 53.66, 56.11, 54.97. $[\alpha]_D$ = +33°, (c = 0.15 in borate-d).

(1S,2R)-(1-methyl-2-phenyl-2-hydroxy)ethyltrimethylammonium iodide. ((–)-Dimethylephedrine) (G19)

^{1}H NMR (D_2O): δ 7.45 (*o-Aromatic*, d, 2H), 7.39 (*m-Aromatic*, t, 2H), 7.31 (*p-Aromatic*, t, 1H), 5.62 (*OH*, d, 1H), 4.43 (*Benzylic C-H*, d, 1H), 3.60 (*N-CH*, q, 1H), 3.24 (*N-CH$_3$*, s, 9H), 1.16 (*C-CH$_3$*, dt 1:1:1, 3H). ^{13}C NMR (CD_3CN at 1.3ppm): δ 141.47, 128.80, 128.19, 126.29, 75.22, 69.39, 53.23 (1:1:1 t, *J* =4.4), 7.65. $[\alpha]_D$ = -22°, (c = 0.12 in borate-d).

(–)-Bornyltrimethylammonium iodide (G15).

^{1}H NMR (borate-d): δ 3.61 (*N-CH*, dd, 1 H); 3.05 (*N-CH$_3$*, dd, 9 H); 2.21, 1.77, 1.71, 1.46, 1.21 (*CH and CH$_2$*, m's, 7 H); 1.01, 0.90, 0.86 (3·*CH$_3$*, 3s, 3 H ea.). ^{13}C NMR ($CDCl_3$ at 77.00ppm): δ 82.01, 54.71, 52.35, 51.60, 43.27, 31.58, 28.47,

27.89, 19.83, 19.60, 17.48. $[\alpha]_D$ = -8.0°, (c = 0.075 in borate-d).

Adamantyltrimethylammonium iodide (ATMA) (G14)

^{1}H NMR (borate-d; external TSP-*d4* at 0.00ppm): δ 2.99 (*N-CH*$_3$, s, 9H), (*CH*$_2$, s, 6H, 2.07ppm), 2.31 (*CH*, s, 3H), 1.70 (*CH*$_2$, AB, 6H, *J* =14, Δν = 31.8Hz). ^{13}C NMR ($CDCl_3$ at 77.00ppm): δ 73.16, 48.85, 35.29, 35.14, 30.21.

Other guests:

N-ethyl-5-nitroisoquinolinium iodide (G12).

5-Nitroisoquinoline (250 mg, 1.4 mmol, 1 eq), ethyl iodide (9.6 g, 0.06 mol, 43 eq, 5 mL) and a small piece of copper wire were placed in a flask, and refluxed overnight. The clear yellow solution deposited a yellow precipitate within an hour. After 15 hours the reaction was filtered and the yellow precipitate extensively washed with ether. This crude precipitate was recrystallized from (2% water in acetone)/ether yielding 275 mg of olive

needles (60%). ^{1}H NMR (DMSO-d_6): δ 10.33 (*#1*, s, 1H), 9.04 (*#6*, d 1H), 9.03, 8.95 (*#3&4*, 2d, 2H), 8.86 (*#8*, d, 1H), 8.24 (*#7*, t, 1H), 4.80 (CH_2, q, 2H), 1.65 (CH_3, t, 3H). ^{13}C NMR (DMSO-d_6 at 39.5 ppm): δ 150.13, 143.42, 136.94, 136.81, 133.47, 129.95, 128.58, 127.63, 121.04, 56.41, 15.62.

N-ethylisoquinolinium iodide (G11).

G11 was synthesized according to the procedure for **G12**, and crystallized as yellow micro-crystals from acetone. ^{1}H NMR ($CDCl_3$): δ 10.76 (*#1*, s, 1H); 8.84 (dd, 1H); 8.60 (d, 1H); 8.37 (d, 1H); 8.11 (d, 1H); 8.03, 7.84 (*#'s 6&7*, 2dt, 2H); 5.01 (CH_2, q, 2H); 1.69 (CH_3, t, 3H). ^{13}C NMR ($CDCl_3$ at 77.00ppm): δ 148.47, 136.94, 136.56, 133.94, 130.79, 127.75, 126.72, 126.06, 56.74, 17.22.

8,8'-Biquinoline

8,8'-Biquinoline was synthesized in a similar fashion to other isomeric biquinolines in the literature.[125] Instead of a chromatographic work up, alternate acidic and basic extractions were used to isolate the crude product,

which was crystallized from ethanol. Yield = 19% tan prisms. ^{1}H NMR ($CDCl_3$): δ 8.79 (#*2,2'*, dd, 2H, J = 2, 4), 8.20 (#*4,4'*, dd, 2H, *J* = 2, 8), 7.90 (#*5,5*, dd, 2H, *J* = 1, 8), 7.81 (#*7,7'*, dd, 2H, *J* = 1, 8), 7.67 (#*6,6'*, t, 2H, *J* = 8), 7.35 (#*3,3'*, dd, 2H, *J* = 4, 8). ^{13}C NMR ($CDCl_3$ at 77.00ppm): δ 150.02, 147.29, 139.31, 136.08, 131.61, 128.53, 127.80, 125.88, 120.74. m.p. 207-209 °C; lit[86] m.p. 205-207 °C. EI MS: 256 (M^+), 255 (M–1). HRMS: 256.10005, calculated for $C_{18}H_{12}N_2$ 256.10005.

N,N'-Dimethyl-8,8'-biquinolinium bis(tetrafluoroborate) (G13)

8,8'-Biquinoline (265 mg, 1 mM), trimethyloxonium tetrafluoroborate (570mg, 4.5mM) and 2,6-di-*t*-butylpyridine were placed in a dried 250 mL flask, and were suspended in 125 mL CH_2Cl_2 and stirred for 60 hours. Tan precipitate slowly formed. Methanol (1 mL), then ether (100 mL), was added and the reaction filtered through a medium porosity frit. The precipitate was crystallized from boiling 1/1 ethyl acetate/acetonitrile, with a hot filtration yielding 280 mg (61%) of tan leaflets. ^{1}H NMR (CD_3CN): δ 9.27 (*dd*, 2H, *J* = 2,

9), 9.03 (*dd*, 2H, *J* = 1, 6), 8.58 (*dd*, 2H, *J* = 3, 7), 8.12 (*dd*, 2H, *J* = 6, 8), 8.07 (m, 4H), 8.07 (*m*, 4H), 3.89 (s, 6H). ^{13}C NMR (CD_3CN at 1.3ppm): δ 154.64, 150.82, 142.18, 138.10, 134.43, 132.20, 131.42, 130.19, 123.85, 53.39.

N-Methylisoquinolinium iodide (G10)

Isoquinoline was added to an excess of methyl iodide. The solid that resulted after stirring the two reactants together for 10 min was dried at the pump and crystallized as needles from acetone/water. ^1H NMR (CD_3CN): δ 9.95 (*#1*, s, 1 H), 8.76-8.34 (*Arom.atic*, m's, 6 H), 5.10 (*CH_3*, s, 3 H). ^{13}C NMR ($CDCl_3$ at 77.00ppm): δ 150.25, 137.30, 137.08, 135.32, 131.42, 130.78, 127.10, 126.10, 48.97.

Compounds from Chapter 5:

2,6-Diaminoanthracene (24)

Compound **24** was prepared by a literature procedure.[119] Yield 27%, m.p. 299-301 °C dec. ^1H NMR (DMSO-*d6*): δ 7.87 (s, 2 H), 7.62 (d, 2 H, *J* = 9), 6.90 (dd, 2 H, *J* = 9, 2), 6.79 (d, 2 H, *J* = 2), 5.15 (br s, 4 H). ^{13}C NMR (DMSO-*d6*):

δ 160.61, 143.94, 127.88, 127.17, 121.32, 120.41, 103.71. IR (KBr) 3460, 3400, 1530, 1260, 930, 840 cm^{-1}.

N,N'-Ditosyl-2,6-diaminoanthracene (25)

Tosyl chloride (1.88 g, 9.8 mmol) and **24** (1.0 g, 4.8 mmol) were dissolved in 50 mL pyridine and stirred together 30 min at 45 °C. The pink-orange solution was poured warm into 100 mL of 50% aqueous ethanol and after 1 min the entire reaction was poured into 0.5 L ice water. The tan precipitate that formed was filtered off and recrystallized from 2/1 acetonitrile/ethanol yielding 2.0 g (81%) of tan needles. ^1H NMR (DMSO-*d6*): δ 10.50 (s, 2 H), 8.25 (s, 2 H), 7.69 (d, 2 H, *J* = 9), 7.61 (d, 2 H, *J*=2), 7.26 (dd, 2 H, *J* = 9, 2), 7.70 (d, 4 H, *J* = 5), 7.23 (d, 4 H, *J* = 5), 2.22 (s, 6 H). IR (KBr) 3440 b, 3260 sh, 1650, 1170, 1090, 570, 550, cm^{-1}; m.p. 266-269 °C.

N,N'-Ditosyl-2,6-diamino-9,10-dihydro-11,12-dicarbomethoxy-ethenoanthracene (26)

DMAD (66 mg, 0.47 mmol) was added to a suspension of **25** (0.2 g, 0.39 mmol) in 50 mL dioxane. The reaction was heated to reflux, the solid

dissolved, and a purple fluorescence appeared. Five additional equivalents of DMAD (275 mg, 1.95 mmol) were added daily to the reaction for one week, then the reaction was cooled and evaporated in the presence of 5 g flash silica. The residue was chromatographed and re-chromatographed over 50 g flash silica to remove extensive DMAD polymers (eluent 4/1 benzene/acetonitrile) yielding 35 mg adduct (14%). ^{1}H NMR (DMSO-*d6*): δ 10.25 (s, 2 H), 7.61 (d, s H, *J* = 8), 7.26 (d, 8 H, *J* = 6), 7.13 (d, 2 H, *J* = 2), 6.71 (dd, 2 H, *J* = 8, 2), 5.45 (s, 2 H), 3.66 (s, 2 H), 2.26 (s, 6 H). ^{13}C NMR (DMSO-*d6*): δ 165.11, 150.20, 146.51, 144.98, 143.30, 138.82, 136.64, 135.10, 124.69, 124.28, 115.87, 115.55, 52.44, 50.20, 20.94.

N,N',N",N"'-Tetratosyl-1,6,15,20-tetraaza-[6,6]-(2,6-anthracenophane) (27)

A solution of **26** (1.5 g, 2.5 mmol) and 1,4-dibromobutane (0.63 g, 2.9 mmol) in 25 mL DMF was placed in a 30 mL syringe and cyclized with cesium carbonate (3.30 g, 10.2 mmol) using the syringe-pump procedure mentioned above. The reaction was run at 100 °C for 36 h. When finished,

the reaction had become yellow with purple fluorescence. The reaction was cooled and poured into 0.5 L water. HCl (5 M aq.) was added to the suspension until the solution became acidic and gas evolution ceased. This suspension was extracted with ethyl acetate (3 X 300 mL). The combined organic layers were washed with water, dried ($MgSO_4$) and concentrated. The residue was chromatographed (eluant 5/1 benzene/acetonitrile) and the purple fluorescent fraction at R_f = 0.4 was collected yielding 263 mg (16%) of a tan powder. ^1H NMR (DMSO-*d6*): δ 8.10 (s, 4 H), 7.89 (d, 4 H, *J* = 8), 7.39 (d, 4 H, *J* = 2), 7.32 (d, 16 H, *J* = 5), 6.93 (dd, 4 H, *J* = 8, 2), 3.54 (m, 8 H), 2.34 (s, 12 H), 1.43 (m, 8 H). ^{13}C NMR (DMSO-*d6*): δ 143.4, 135.0, 129.7, 128.5, 128.3, 128.2, 127.2, 125.9, 125.0, 124.5, 118.1, 30.7, 21.0, 11.1.

2,6-Dibenzyloxyanthracene

2,6-Dibenzyloxyanthraquinone (2.6 g, 62 mmol: made from **1**, and benzyl chloride with cesium carbonate in DMF) was placed in a 100 mL round-bottomed flask along with 25 g, aluminum cyclohexanoxide[124] in cyclohexanol (2 M). Cyclohexanol (15 mL) was added and the reaction

refluxed for 24 h. The reaction was cooled to ≈ 45 °C and product precipitated. The reaction was filtered warm with the aid of a heat gun, and the precipitate was collected and recrystallized from toluene, yielding 510 mg (21%) light yellow (blue fluorescent) needles. More product is available from the mother liquors and from extractions of the reaction filtrate. ^{1}H NMR ($CDCl_3$): δ 8.18 (#*9, 10*, s, 2 H), 7.84 (#*4, 8*, d, 2 H, *J* = 9), 7.3-7.5 (*1,5 and benzyl,* m's, 12H), 7.21 (#3, *7*, dd, 2 H, *J* = 9, 2).

CHAPTER 7

References

1. For reviews on the subject see this reference and Reference 2. *Topics in Current Chemistry 98*; Vögtle, F., Ed.; Springer-Verlag: Berlin, 1981.

2. *Topics in Current Chemistry 101*; Vögtle, F., Ed.; Springer-Verlag: Berlin, 1982.

3. Franke, J.; Vögtle, F. *Topics in Current Chemistry* **1986**, *132*, 135-170.

4. Breslow, R. *Science* **1982**, *218*, 532-537.

5. Cram, D. J.; Cram, J. M. *Science (Washington D. C.)*, **1974**, *183*, 803-809.

6. Cram, D. J. *Science (Washington D. C.)*, **1983**, *219*, 1177-1183.

7. Saenger. W. *Angew. Chem. Int. Ed. Engl.* **1980**, *19*, 344-362.

8. Breslow, R.; Hammond, M.; Lauer, M. *J. Am. Chem. Soc.* **1980**, *102*, 421-422.

9. Emert, J.; Breslow, R. *J. Am. Chem. Soc.* **1975**, *97*, 670-672.

10. Tabushi, I. *Pure Appl. Chem.* **1986**, *58*, 1529-1534.

11. Diederich, F.; Lutter, H. *Angew. Chem. Int. Ed. Engl.* **1986**, *25*, 1125-1127.

12. Croft, A. P.; Bartsch, R. A. *Tetrahedron* **1983**, *39*, 1417-1474.

13. Odashima, K.; Itai, A.; Iitaka, Y.; Koga, K. *J. Am. Chem. Soc.* **1980**, *102*, 2504-2505.

14. Vögtle, F.; Muller, W. M.; Puff, H.; Friedrichs, E. *Chem. Ber.* **1983**, *116*, 2344-2354.

15. Andreetti, G. D.; Pochini, A.; Ungaro, R. *J. Chem. Soc., Perkin Trans. 1* **1983**, 1773-1779.

16. Tabushi, I.; Yamamura, K.; Nonoguchi, H.; Hirotsu, K.; Higuchi, T. *J. Am. Chem. Soc.* **1984**, *106*, 2621-2625.

17. Diederich, F.; Krieger, C. *Chem. Ber.* **1985**, *118*, 3620-3631.

18. Soga, T.; Odashima, K.; Koga, K. *Tetrahedron Lett.* **1980**, *21*, 4351-4354.

19. Odashima, K.; Koga, K. *Heterocycles* **1981**, *15*, 1151-1154.

20. Odashima, K.; Soga, T.; Koga, K. *Tetrahedron Lett.* **1981**, *22*, 5311-5314.

21. Odashima, K.; Itai, A.; Iitaka, Y.; Arata, Y.; Koga, K. *Tetrahedron Lett.* **1980** , *21*, 4347-4350.

22. Takahashi, I.; Odashima, K.; Koga, K. *Tetrahedron Lett.* **1974** , 973-976.

23. Tabushi, I.; Sasaki, H.; Kuroda, Y. *J. Am. Chem. Soc.* **1976** , *98*, 5727-5728.

24. Tabushi, I.; Kuroda, Y.; Kimura, Y. *Tetrahedron Lett.* **1976** , 3327-3330.

25. Tabushi, I.; Kimura, Y.; Yamamura, K. *J. Am. Chem. Soc.* **1978** , *100*, 1304-1306.

26. Tabushi, I.; Kimura, Y.; Yamamura, K. *J. Am. Chem. Soc.* **1981** , *103*, 6486-6492.

27. Benesi, H. A.; Hildebrand, J. H. *J. Am. Chem. Soc.* **1949** , *71*, 2703-2707.

28. Diederich, F.; Dick, K. *J. Am. Chem. Soc.* **1984** , *106*, 8024-8036.

29. Diederich, F.; Griebel, D. *J. Am. Chem. Soc.* **1984** , *106*, 8037-8046.

30. Diederich, F.; Dick, K. *Tetrahedron Lett.* **1982** , *23*, 3167-3170.

31. Diederich, F.; Dick, K. *Angew. Chem. Suppl.* **1983** , 957-972.

32. Diederich, F.; Dick, K.; Griebel, D. *Chem. Ber.* **1985** , *118*, 3588-3619.

33. Diederich, F.; Dick, K. *Chem. Ber.* **1985** , *118*, 3817-3829.

34. Diederich, F.; Dick, K.; Griebel, D. *J. Am. Chem. Soc.* **1986** , *108*, 2273-2286.

35.Diederich, F.; Ferguson, S. *Angew. Chem. Int. Ed. Engl.* **1986** , *25*, 1127-1129.

36. Petti, M. A.; Shepodd, T. J.; Barrans, R. E. Jr.; Dougherty, D. A. Submitted for publication.

37. Diederich, F.; Schurmann, G. *Tetrahedron Lett.* **1986** , *27*, 4249-4252.

38. Rubin, Y.; Dick, K.; Diederich, F.; Georgiadis, T. M. *J. Org. Chem.* **1986** , *151*, 3270-3278.

39. Dharanipragada, R.; Diederich, F. *Tetrahedron Lett.* **1987** , *28*, 2443-2446.

40. Vögtle, F.; Löhr, H.; Franke, J.; Worsch, D. *Angew. Chem. Int. Ed. Engl.* **1985** , *24*, 727-742.

41. Vögtle, F.; Muller, W. M. *Angew. Chem. Int. Ed. Engl.* **1984** , *23*, 712-714.

42. Vögtle, F.; Merz, T.; Wirtz, H. *Angew. Chem. Int. Ed. Engl.* **1985** , *24*, 221-222.

43. Dhaenens, M.; Lacombe, L.; Lehn, J. M.; Vigneron, J. P. *J. Chem. Soc., Chem. Commun.* **1984** , 1097-1099.

44. Dietrich, B.; Hosseini, M. W.; Lehn, J. M.; Sessions, R. B. *J. Am. Chem. Soc.* **1981** , *103*, 1282-1283.

45. Rebek, J. *Science (Washington D. C.)* **1987** , *235*, 1478-1484.

46. Rebek, J.; Costello, T.; Marshall, L.; Wattley, R.; Gadwood, R. C.; Onan, K. *J. Am. Chem. Soc.* **1985** , *107*, 7481-7487.

47. Rebek, J.; Costello, T.; Wattley, R. *J. Am. Chem. Soc.* **1985** , *107*, 7487-7493.

48. Rebek, J.; Askew, B.; Islam, N.; Killoran, M.; Nemeth, D.; Wolak R. *J. Am. Chem. Soc.* **1985** , *107*, 6736-6738.

49. Rebek, J.; Nemeth, D. *J. Am. Chem. Soc.* **1985** , *107*, 6738-6739.

50. Rebek, J.; Askew, B.; Kiloran, M.; Nemeth, D.; Lin, F. T. *J. Am. Chem. Soc.* **1987** , *109*, 2426-2431.

51. Rebek, J.; Askew, B.; Ballester, P.; Doa, M. *J. Am. Chem. Soc.* **1987** , *109*, 4119-4120.

52. Rebek, J.; Askew, B.; Ballester, P.; Baur, C.; Jones, S.; Nemeth, D.; Williams, K. *J. Am. Chem. Soc.* **1987** , *109*, 5033-5035.

53. Rebek, J.; Askew, B.; Ballester, P.; Baur, C.; Costero, A.; Jones, S.; Williams, K. *J. Am. Chem. Soc.* **1987** , *109*, 6866-6867.

54. Hamilton, A. D.; Van Engen, D. *J. Am. Chem. Soc.* **1987** , *109*, 5035-5036.

55. Diederich, F.; Dick, K. *Angew. Chem. Int. Ed. Engl.* **1984** , *23*, 810-812.

56. Jarvi, E. T.; Whitlock, H. W. *J. Am. Chem. Soc.* **1982** , *104*, 7196-7204.

57. Whitlock, B. J.; Whitlock, H. W. *J. Am. Chem. Soc.* **1983** , *105*, 838-844.

58. Adams, S. P.; Whitlock, H. W. *J. Org. Chem.* **1981** , *46*, 3474-3478.

59. Slawin, A. M. Z.; Spencer, N.; Stoddart, J. F.; Williams, D. J. *J. Chem Soc., Chem. Commun.* **1987** , 1070-1072.

60. Colquhoun, H. M.; Stoddart, J. F.; Williams, D. J.; Wolstenholme, J. B.; Zarzycki, R. *Isr. J. Chem.* **1985** , *25*, 15-26.

61. Colquhoun, H. M.; Doughty, S. M.; Maud, J. M.; Stoddart, J. F.; Williams, D. J.; Wolstenholme, J. B. *Angew. Chem. Int. Ed. Engl.* **1981** , *20*, 1051-1053.

62. Allwood, B. L.; Colquhoun, H. M.; Doughty, S. M.; Kohnke, F. H.; Slawin, A. M. Z.; Stoddart, J. F.; Williams, D. J.; Zarzycki, R. *J. Chem Soc., Chem. Commun.* **1987** , 1054-1058.

63. Allwood, B. L.; Shahriari-Zavareh, H.; Stoddart, J. F.; Williams, D. J. *J. Chem Soc., Chem. Commun.* **1987** , 1058-1061.

64. Allwood, B. L.; Spencer, N.; Shahriari-Zavareh, H.; Stoddart, J. F.; Williams, D. J. *J. Chem Soc., Chem. Commun.* **1987** , 1061-1064.

65. Allwood, B. L.; Spencer, N.; Shahriari-Zavareh, H.; Stoddart, J. F.; Williams, D. J. *J. Chem Soc., Chem. Commun.* **1987** , 1064-1066.

66. Ashton, P. R.; Slawin, A. M. Z.; Spencer, N.; Stoddart, J. F.; Williams, D. J. *J. Chem Soc., Chem. Commun.* **1987** , 1066-1069.

67. Canceill, J.; Lacombe, L.; Collet, A. *J. Chem Soc., Chem. Commun.* **1987** , 219-221.

68. Canceill, J.; Lacombe, L.; Collet, A. *J. Am. Chem. Soc.* **1985** , *107*, 6993-6996.

69. Murakami, Y.; Aoyama, Y.; Dobashi, K.; Kida, M. *Bull. Chem. Soc. Jpn.* **1976** , *49*, 3633-3636.

70. Murakami, Y.; Nakano, A.; Miyata, R.; Matsuda, Y. *J. Chem. Soc., Perkin Trans. 1* **1979,** 1669-1676.

71. Murakami, Y.; Nakano, A.; Akiyoshi, K.; Fukuya, K. *J. Chem. Soc., Perkin Trans. 1* **1981** , 2800-2808.

72. Cram. D. J. *Angew. Chem. Int. Ed. Engl.* **1986** , *25*, 1039-1134.

73. For examples of studies with functionalized hosts see References 4, 8-11.

74. Mislow, K.; Bickart, P. *Isr. J. Chem.* **1976/77** , *15*, 1-6.

75. Mislow, K.; Siegel, J. *J. Am. Chem. Soc.* **1984** , *106*, 3319-3328.

76 2,6-Diamino-, dihydroxy- (anthraflavic acid), and disulfonyl-anthraquinone are commercially available. For the preparation of several other 2,6-disubstituted anthraquinones see: Josephy, E.; Radt, F. *Elsevier Encyclopedia of Organic Chemistry*; Elsevier: New York, 1946, Vol. 13, Series III. For some modern characterizations of some of these molecules see: Berger, Y.; Berger-Deguee, M.; Castonguay, A. *Org. Mag. Resonance* **1981** , *15*, 244-247.

77. For a potential synthesis of cationic hosts based on our macrocycles, see: Petti, M. A. Ph.D. Thesis, California Institute of Technology, 1988.

78. Hall, J.; Perkin, A. G. *J. Chem. Soc.* **1923** , *125*, 2029-2037.

79. Compound **2** can also be synthesized by a two-step procedure *via* 2,6-dihydroxyanthrone: Goodall, F. L.; Perkin, A. G. *J. Chem. Soc.* **1923** , *125*, 470-476.

79. Cristol, S. J.; Bly, R. K. *J. Am. Chem. Soc.* **1960** , *82*, 6155-6162.

80. Pioneering work with this system was done by Michael Petti in our group. Petti showed that the racemic Diels-Alder adduct ±**3** was directly available from **2** and dimethyl acetylenedicarboxylate.

81. The di-π-methane rearrangement has been extensively studied in other systems, see: Paddick, R. G.; Richards, K. E.; Wright, G. J. *Aust. J. Chem.* **1976** , *29*, 1005-1015; Ciganek, E. *J. Am. Chem. Soc.* **1966** , *88*, 2882-2883; Zimmerman, H. E.; Grunewald, G. L. *J. Am. Chem. Soc.* **1966** , *88*, 183-184; Rabideau, P. W.; Hamilton, J. B.; Friedman, L. *J. Am. Chem. Soc.* **1968** , *90*, 4465-4466.

82. Kruizinga, W. H.; Kellog, R. M. *J. Org. Chem.* **1987** , *52*, 4230-4234.

83. Walborsky, H. M.; Barash, L.; Davis, T.C. *Tetrahedron* **1963** , *19*, 2233-2351.

84. Dijkstra, G.; Kruizinga, W. H.; Kellog, R. M. *J. Am. Chem. Soc.* **1981** , *103*, 5183-5189.

85. Petti, M. A.; Shepodd, T. J.; Dougherty, D. A. *Tetrahedron Lett.* **1986** , *27*, 807-810.

86. *CRC Handbook of Chemistry and Physics*; Weast, R. C., Ed.; The Chemical Rubber Company: Cleveland, OH, 1974.

87. Shepodd, T. J.; Petti, M. A.; Dougherty, D. A. *J. Am. Chem. Soc.* **1986** , *108*, 6085-6087.

88. Many classical resolutions were attempted with a variety of chiral derivatives of **5**, including resolutions of acids with alkaloid bases, and crystallographic separation of diastereomeric imide and ether derivatives. These procedures are tedious and give low yields of partially enriched materials.

90. Oppolzer, W. *Angew. Chem. Int. Ed. Engl.* **1984** , *23*, 876-889.

91. Helmchen, G.; Karge, R.; Weetman, J. In *Modern Synthetic Methods Vol. 4*; Scheffold R., Ed.; Springer Verlag: Berlin, **1986** ; 261-306.

92. Walborsky, H. M.; Barash, L.; Davis, T. C. *J. Org. Chem.* **1961** , *26*, 4778 -4779.

92. Paquette, L. A. In *Asymmetric Synthesis*; Morrison, J. D., Ed; Academic Press: New York, 1984; Vol. 3, Part B, Chapter 7.

94. Helmchen, G.; Schmierer, R. *Angew. Chem. Int. Ed. Engl.* **1981** , *20*, 205-207.

93. Furuta, K.; Iwanaga, K.; Yamamoto, H. *Tetrahedron Lett.* **1986** , *27*, 4507-4510.

95. Hagishita, S.; Kuriama, K. *Tetrahedron* **1972** , *28*, 1435-1467.

96. For an example of side reactions in Diels-Alder-adduct ester hydrolysis see: Takeda, K.; Hagishita, S.; Sugiura, M.; Kitahonoki, K.; Ban, I.; Miyazaki, S.; Kuriama, K.; *Tetrahedron* **1970** , *26*, 1435-1451.

97. Pavelich W. A.; Taft, R. W. *J. Am. Chem. Soc.* **1957** , *79*, 4935-4940.

98. When **±3** is used in our macrocyclization procedures, we always get a 1:1 *meso:d,l* diastereomer ratio. Only for the *o*-xylyl-linked macrocycles, **4a** and **4b**, is the *meso* compound formed in a 1.5:1 excess. We interpret this as a result of difficulty involved with cyclizing the highly strained **4b** .

99. Shaeiwitz, J. A.; Chan, A., F.; Cussler, E. L.; Evans, D. F. *J. Colloid and Interface Sci.* **1981** , *84*, 47-56.

100. Inoue, H.; Nakagawa, T. *J. Phys. Chem.* **1966** , *70*, 1108-1113.

101. Fendler, E. J.; Constien, V. G.; Fendler, J. H. *J. Phys. Chem.* **1975** , *79*, 917-926.

102. For some examples of related "half-molecule" studies in the field see References 18-21,23,24,28.

103. All the flat aromatic guests **G1–G12** have C_s symmetry.

104. Petti, M. A. Ph.D. Thesis, California Institute of Technology, 1988.

105. The majority of chemical shift changes in donor-acceptor or charge transfer complexes are caused by the anisotropy of the adjacent (host or guest) species, not by charge transfer. See: Foster, R. *Organic Charge-Transfer Complexes*; Academic: London, 1969, p 113.

106. Petsko, G. A.; Burley, S. K. *FEBS Lett.* **1986** , 139-143.

107. Deakyne, C. A.; Meot-Ner, M. *J. Am. Chem. Soc.* **1985** , *107*, 474-479.

108. Cromwell, W. C.; Byström, B.; Eftink, M. R. *J. Phys. Chem.* **1984** , *89*, 326-332.

109. Gelb, R. I.; Schwartz, L. M.; Laufer, D. A. *J. Chem. Soc., Perkin Trans. 1* **1984** , 15-21.

110. See the Experimental section (Chapter 6) for the details of our concentration determinations.

111. Wolfenden, R. *Science (Washington D. C.)* **1983** , *222*, 1087-1093.

112. Foster, R.; Fyfe, C. A. *Prog. Nucl. Mag. Reson.* **1969** , *4*, 1-89.

113. Shepodd, T. J.; Petti, M. A.; Dougherty, D. A. Submitted for publication.

114. Polyaromatic hydrocarbon water solubilities are determined by different methods in the literature. The values that we determined for the guest solubilities in our weak buffers are similar to published solubility values in pure water. Davis, W. W.; Parke, T. V. *J. Am. Chem. Soc.* **1942** , *64*, 101-107. Davis, W. W.; Krahl, M. E.; Clowes, G. H. A. *J. Am. Chem. Soc.* **1942** , *64*, 108-110.

115. Ruggli, P.; Henzi, E. *Helv. Chem. Acta.* **1930** , *13*, 409-437.

116. Stetter, H. *Chem. Ber.* **1953** , *86*, 380-383.

117. Searles, S.; Nukina, S. *Chem. Rev.* **1959** , *59*, 1077-1103.

118. Snyder, H. R.; Heckert, R. E. *J. Am. Chem. Soc.* **1952** , *74*, 2006-2009.

119. Vögtle, F.; Kliesser, B. *Synthesis* **1982** , 294-296.

120. Vriesema, B. K.; Buter, J.; Kellog, R. M. *J. Org. Chem.* **1984** , *49*, 110-113.

121. Coffey, S.; Boyd, V. *J. Chem. Soc.* **1954** , 2468-2470.

122. Hinshaw, J. C. *Org. Prep. and Proc. Int.* **1972** , *4*, 211-213.

123. We refer to borate-d loosely as a cesium borate buffer. Actually, aqueous borate chemistry is complex, and a number of different borate species are present. See, *Supplement to Mellor's Comprehensive Treatise on Inorganic and Theoretical Chemistry*; Longman: London, **1980** , Vol. 5, pp 321-426.

124. We wish to thank Bryan Hamel and the scientific staff at the U.S. Borax Co. for advice about borate chemistry and for samples of high purity boric oxide.

125. Tiecco, M.; Testaferri, L.; Tingoli, M.; Chianelli, D. *Synthesis*, **1984** , 736-738.

Chapter 8

D-values.

This chapter contains the calculated D-values for the chiral-host-guest pairs discussed in the previous chapters. The values are reported in ppm and are placed next to the position of the guest proton in question in the figures that follow. Positive values refer to upfield shifts upon complexation. The host (or hosts) for each figure is listed above the guests. Where the exact proton assignment for a given D-value is unclear both possible values are listed.

The relative D-value magnitudes for the different protons of a given guest are how we measure the local influence of the highly anisotropic environment of our host receptors upon binding. The error bars that we report for the binding affinities (± 0.2 kcal/mol) can correspond to large variations in the D-values, so comparisons among the values for different guests have limited value.

The host-guest pairs are listed below.

Figure 8.1: D-values for the host-guest pairs indicated.

Host M

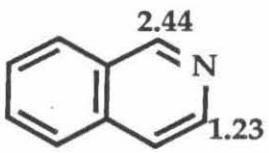

G6

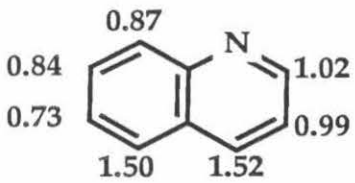

G3

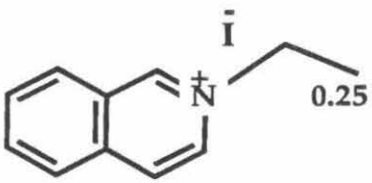

G11

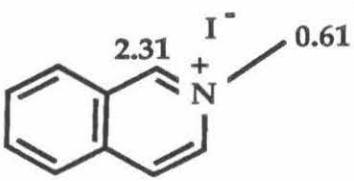

G10

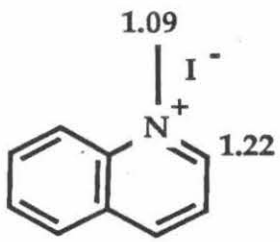

G9

Figure 8.2: D-values for the host-guest pairs indicated.

Host M

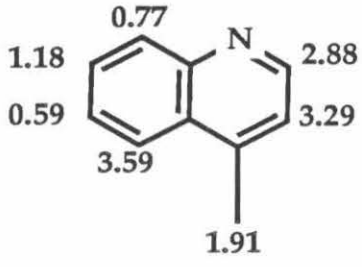

G5

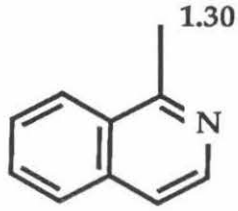

G7

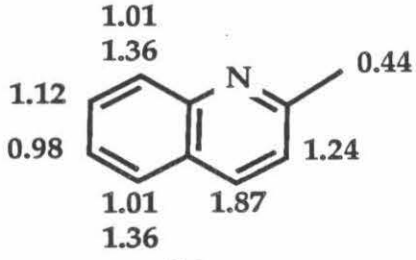

G4

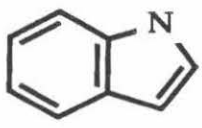

No Significant Complexation Observed.

G1

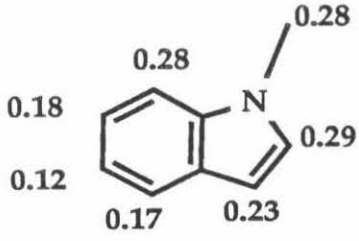

G2

Figure 8.3: D-values for the host-guest pairs indicated.

Host M

G21

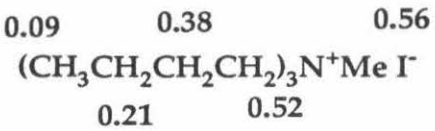

G17

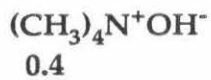

M_S

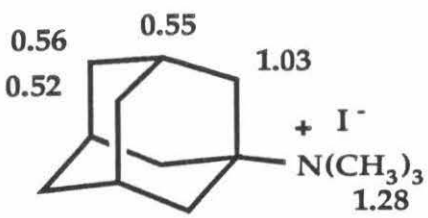

G14

M_R

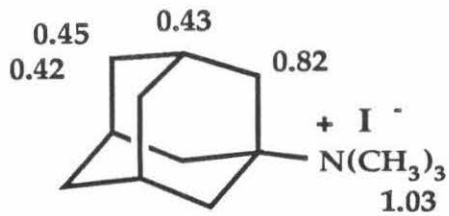

G14

Figure 8.4: D-values for the host-guest pairs indicated.

M_S M_R

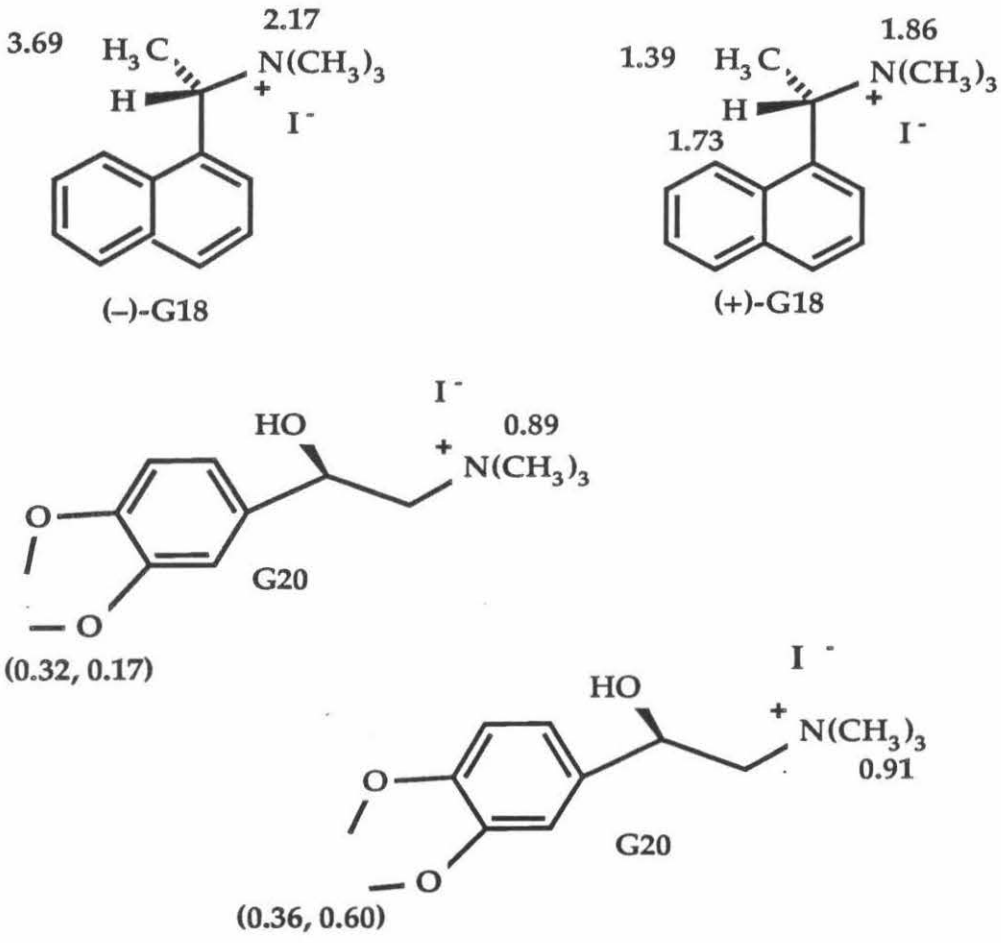

Figure 8.5: D-values for the host-guest pairs indicated.

M_S M_R

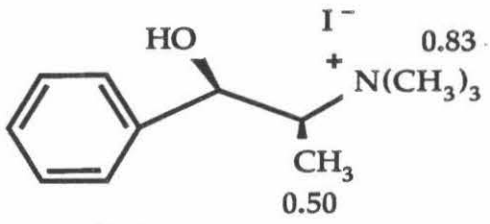

G19

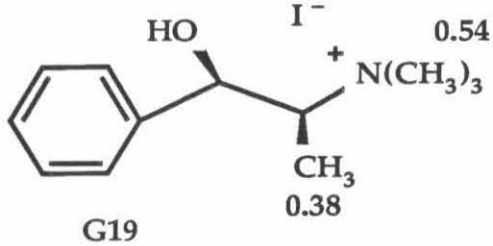

G19

FIGURE 8.6: D-values for the host-guest pairs indicated.

M_S

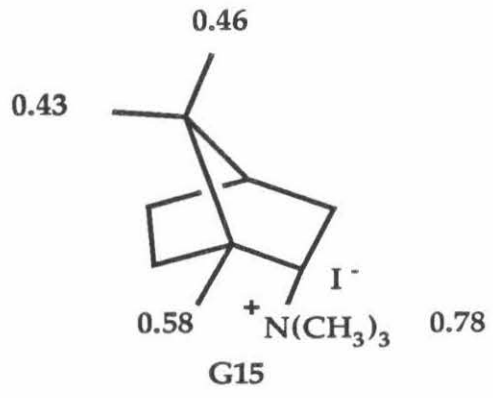

G15

M_R

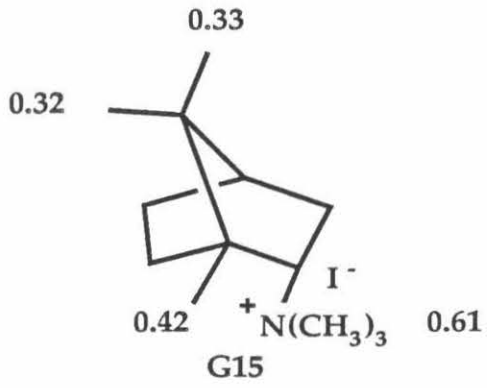

G15

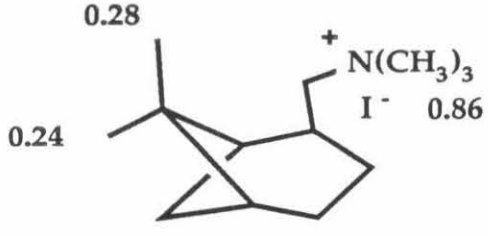

G16

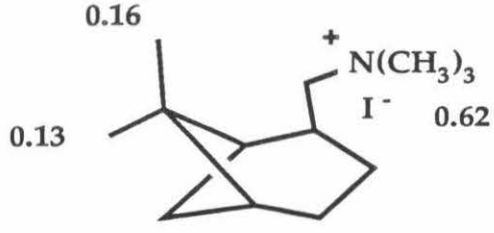

G16

Figure 8.7: D-values for the host-guest pairs indicated.

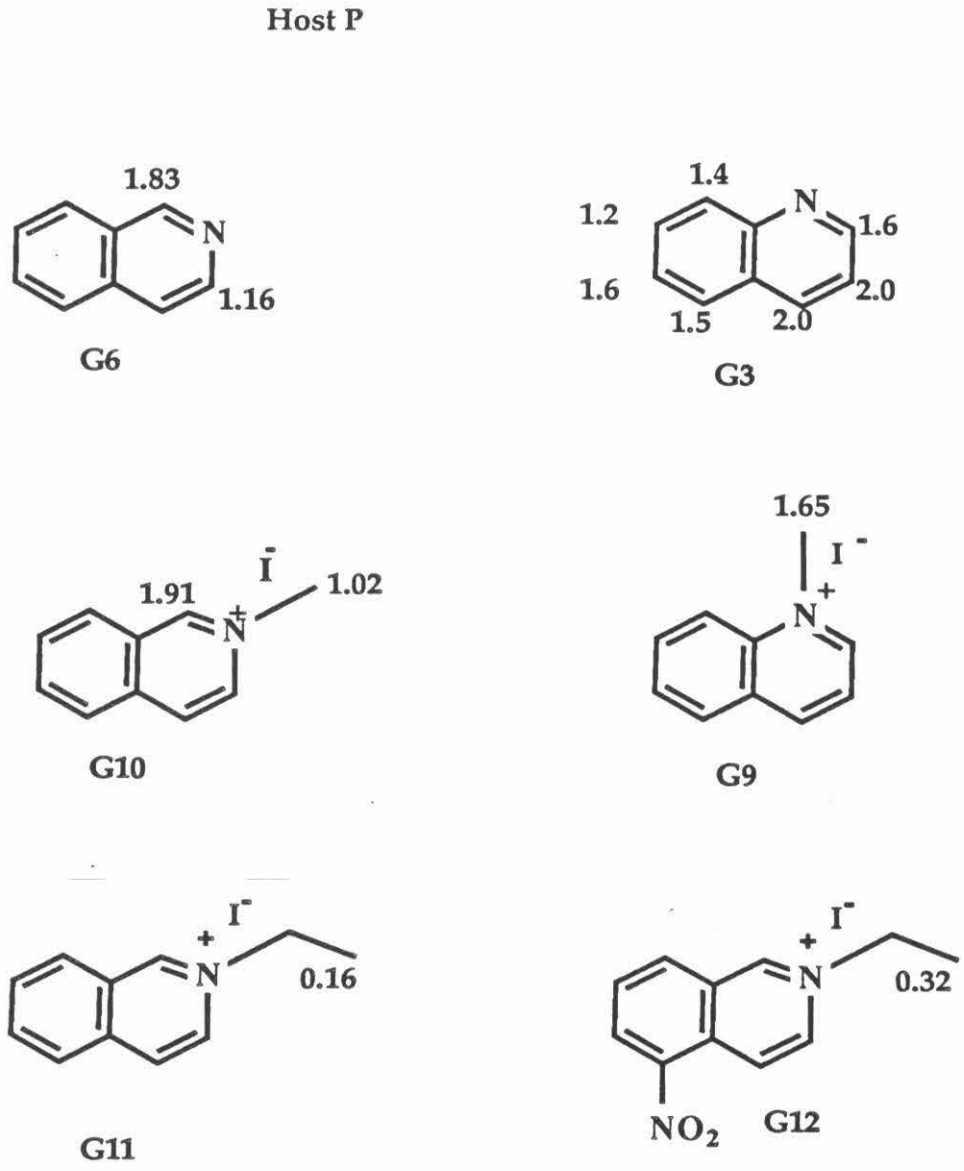

Figure 8.8: D-values for the host-guest pairs indicated.

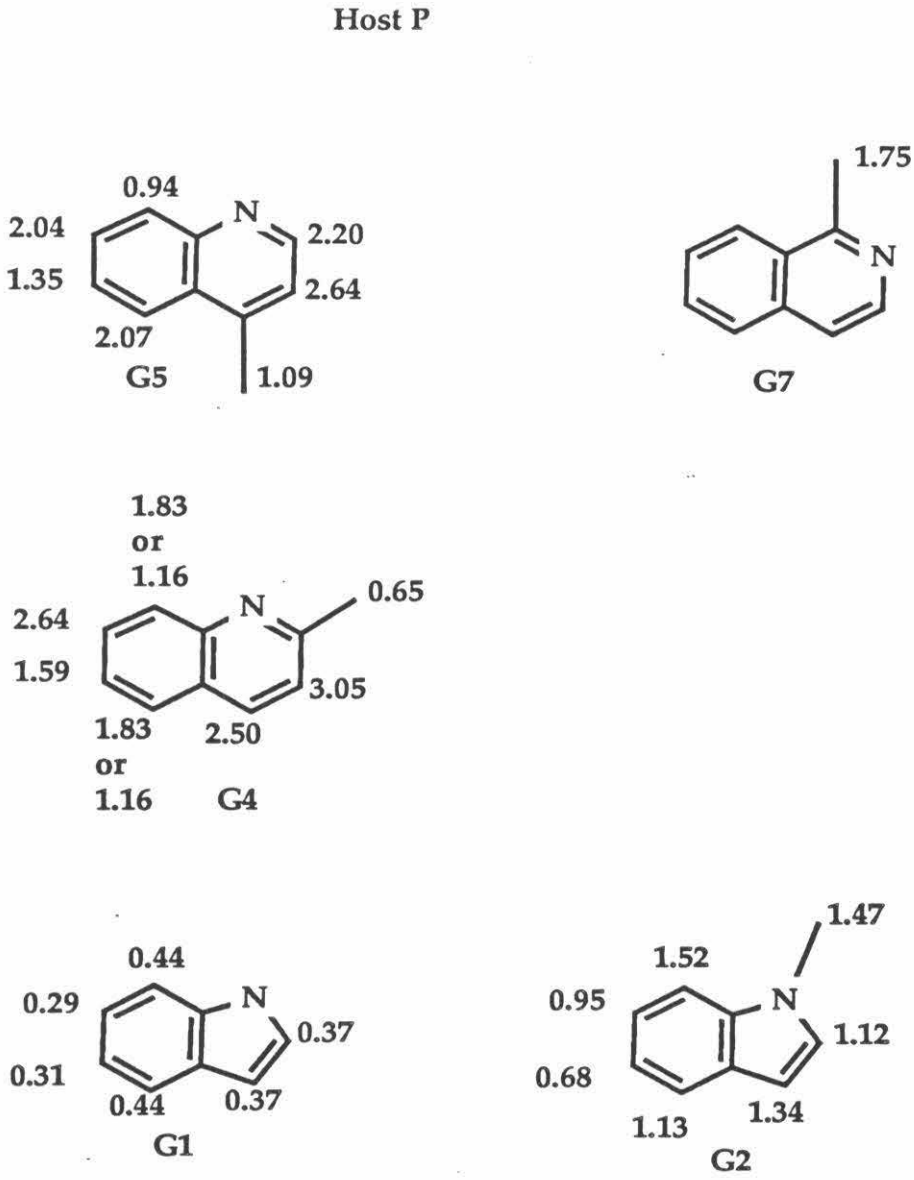

Figure 8.9: D-values for the host-guest pairs indicated.

Host P

G21

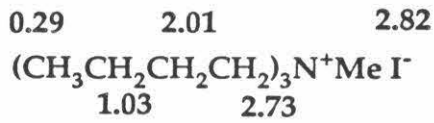

G17

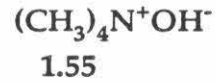

P_S

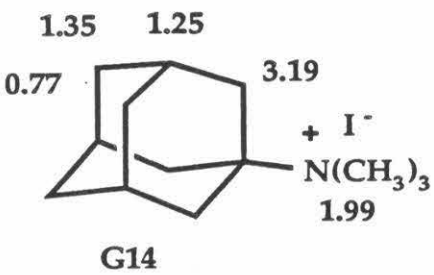

G14

P_R

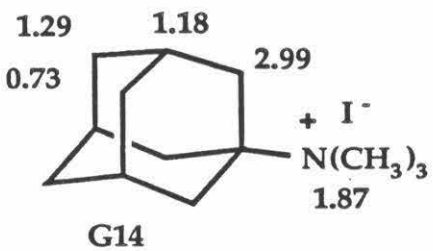

G14

Figure 8.10: D-values for the host-guest pairs indicated.

P_S P_R

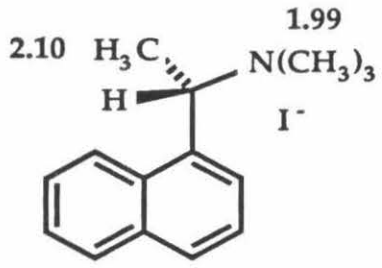

(–)-G18

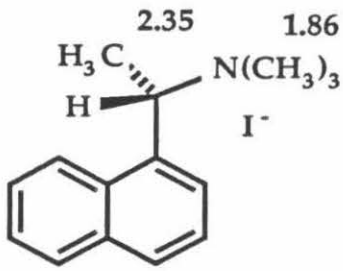

(+)-G18

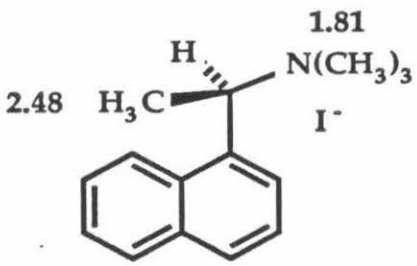

(–)-G18

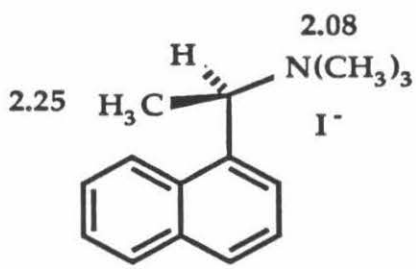

(+)-G18

Figure 8.11: D-values for the host-guest pairs indicated.

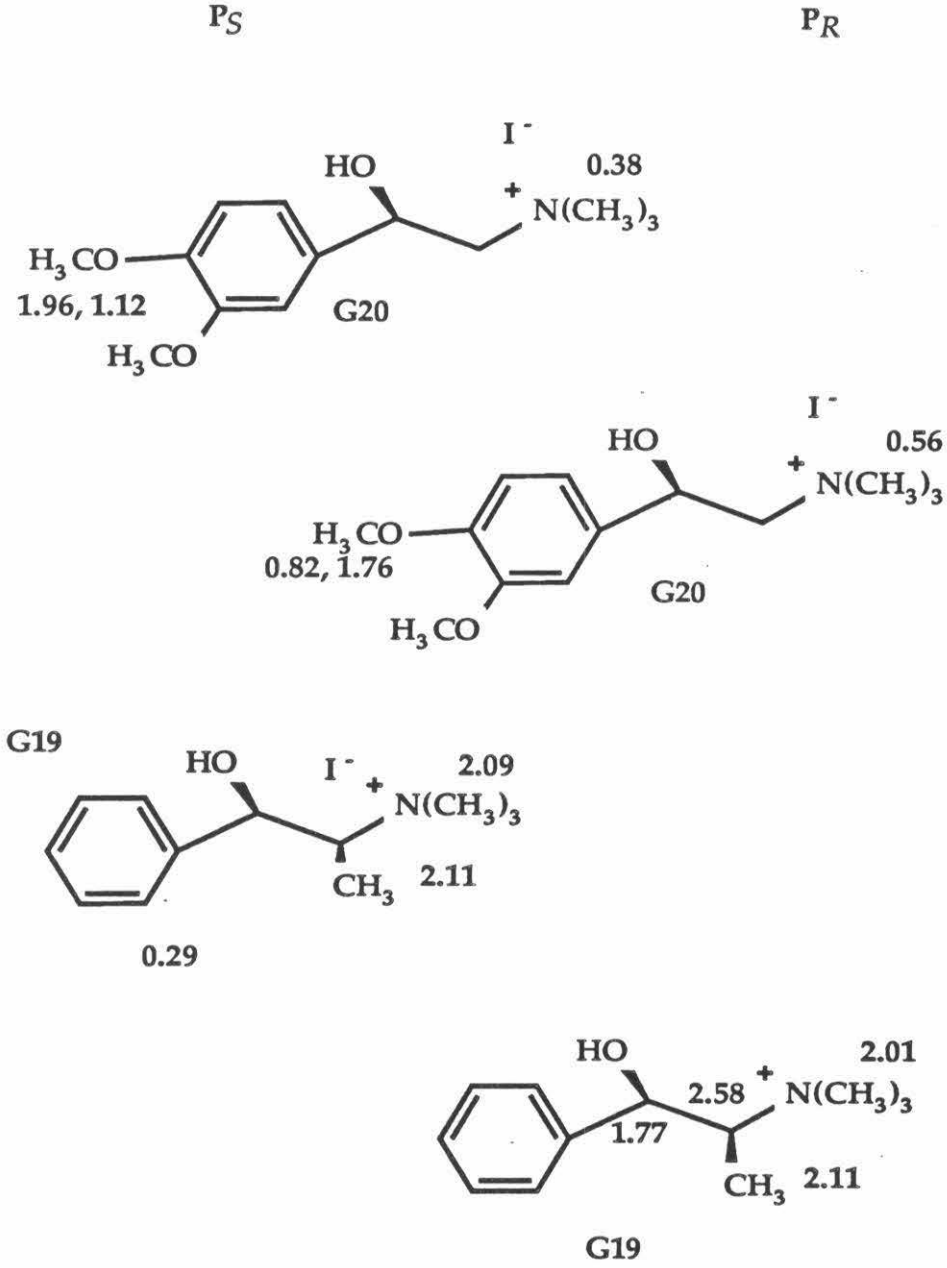

Figure 8.12: D-values for the host-guest pairs indicated.